DTU Environment
Department of Environmental Engineering

# Black Carbon at a High Arctic Location, Station Nord, North-East Greenland

## *- An Important Contributor to Climate Change*

**Master Thesis**

Ditte Kristensen (s071478) & Ingeborg Elbæk Nielsen (s072364)

August 2013

**Supervisors**

Professor Henrik Skov - Department of Environmental Science, AU
Associate Professor Charlotte Scheutz - Department of Environmental Science, DTU

**Co-supervisors**

Senior Researcher Andreas Massling, AU
Senior Researcher Jacob Klenø Nøjgaard, AU
Professor Emeritus Jens-Christian Tjell, DTU
External Consultant Kåre Press-Kristensen, DTU

AARHUS UNIVERSITY
DEPARTMENT OF ENVIRONMENTAL SCIENCE

# Abstract

Recent studies have found that black carbon (BC), also known as soot, is the second biggest contributor to the present temperature increase, only exceeded by $CO_2$. BC, which is a short lived climate forcer, exerts an overall warming effect on the climate and may affect the energy balance of the Earth in three ways: by direct absorption of solar radiation in the atmosphere, by changing the snow/ice albedo and by cloud formation. The Arctic is due to the positive snow-albedo feedback very sensitive to temperature changes. Measurements and observations of BC in the Arctic are thus important in order to improve the understanding of the characteristics of BC and identify source origins by applying receptor models. This information is needed to develop and validate climate and transport models, improve emission inventories, and formulate strategies to reduce further warming of the Arctic through mitigation actions.

The BC air concentrations at Station Nord from August 2008 to April 2013 have been estimated using two different analyses; the thermal-optical OC-EC analysis and the light absorption method, the Particle Soot Absorption Photometer (PSAP). EC concentrations determined by the OC-EC analysis vary between 1 ng/m$^3$ (November 2009) and 145 ng/m$^3$ (January 2011). A specific absorption coefficient of 6.2 m$^2$/g ($R^2$ = 0.4), based on measurements from the entire period, is determined from the EC concentrations and the absorption coefficients measured by the PSAP. The BC concentrations vary between -1 ng/m$^3$ (May 2012) and 161 ng/m$^3$ (March 2009) based on a specific absorption coefficient of 5.5 m$^2$/g. Comparison of the average monthly measured BC and EC concentrations in air and BC concentrations modelled using the Danish Eularian Hemispheric Model (DEHM) show concentrations in the same order of magnitude, following the same seasonal patterns, with high concentrations during winter and spring and lower concentrations during summer and autumn. The EC concentration in the upper 5 cm snow at Station Nord has been measured in April 2013 using the OC-EC analyser, resulting in an average concentration of 525 ± 441 ng/l.

BC source apportionment was modelled applying the receptor model Positive Matrix Factorisation (PMF). For the period, March 2008 to February 2010, five sources were identified: a *Soil, Marine, Combustion, Cu/Ni* and *Zn* source, comprising 0%, 17 %, 57 %, 9 % and 17 % of the total BC, respectively. The analysis for January 2011 to December 2012 also resulted in five sources: a *Soil, Marine, Combustion, Cu* and *Ni/Cr* source, comprising 0 %, 21 %, 7 %, 9 % and 64 % of the total BC, respectively.

# Resumé

Nye studier har vist, at black carbon (BC), også kaldet sod, er den anden største bidragyder til klimaændringer næstefter $CO_2$. BC, som er en kortlivet klimakomponent, har overordnet set en varmende effekt på klimaet og påvirker jordens energibalance på tre måder: ved direkte absorption af sollys i atmosfæren, ved ændring af albedoen for sne og is og ved skydannelse. Arktis er på grund af den positive albedo feedback meget sårbar over for temperaturændringer. Målinger og observationer af BC i Arktis er derfor vigtige for at forbedre forståelsen af BC og for at identificere kilder ved hjælp af receptormodeller. Denne information er nødvendig for at udvikle og validere klima- og transportmodeller, forbedre emissionsopgørelser og udforme strategier med henblik på at reducere yderligere opvarmning i Arktis.

BC koncentrationer på Station Nord fra august 2008 til april 2013 er blevet estimeret ved hjælp af to forskellige metoder; en termisk-optisk metode kaldet OC-EC analyse og en absorptionsmetode, hvor et *Particle Soot Absorption Photometer* (PSAP) er blevet anvendt. EC koncentrationer bestemt ved hjælp af OC-EC analysen varierer mellem 1 ng/m$^3$ (november 2009) og 145 ng/m$^3$ (januar 2011). En specifik absorptionskoefficient på 6.2 m$^2$/g ($R^2$ = 0.4), baseret på målinger fra hele perioden, er blevet bestemt fra EC koncentrationerne og absorptionskoefficienterne målt med PSAP. BC koncentrationerne varierer mellem -1 ng/m$^3$ (maj 2012) og 161 ng/m$^3$ (marts 2009) baseret på en specifik absorptionskoefficient på 5.5 m$^2$/g. Sammenligning af de gennemsnitlige, månedlige BC og EC koncentrationer i luft med BC koncentrationer modellerede ved hjælp af den Danske Eulerske Hemisfæriske Model (DEHM) viser, at koncentrationerne ligger i den samme størrelsesorden. Desuden følger koncentrationerne de samme sæsonmønstrer med høje koncentrationer om vinteren og foråret og lavere koncentrationer om sommeren og efteråret. EC koncentrationen i de fem øverste centimeter sne på Station Nord er blevet målt i april 2013 ved hjælp af OC-EC analysen og har vist en gennemsnitlig koncentration på 525 ± 441 ng/l.

Kildefordelingen af BC blev modelleret ved brug af receptormodellen *Positive Matrix Factorisation* (PMF). Fem kilder er identificeret i perioden fra marts 2008 til februar 2010: en *Jord-*, *Marin-*, *Forbrændings-*, *Kobber/Nikkel-* og *Zink* kilde, som hver især indeholder 0 %, 17 %, 57 %, 9 % og 17 % af den totale mængde BC. Analysen af perioden fra januar 2011 til december 2012 resulterer også i fem kilder: en *Jord-*, *Marin-*, *Forbrændings-*, *Kobber-* og *Nikkel/Krom* kilde, som hver især indeholder 0 %, 21 %, 7 %, 9 % and 64 % af den totale mængde BC.

# Preface

This project is a 30 ECTS master thesis from the Department of Environmental Engineering (ENV), Technical University of Denmark (DTU) conducted in association with Department of Environmental Science (ENVS), Aarhus University (AU). The report is written in the period February 2013 to August 2013 and is based on fieldwork conducted at Station Nord, N.E. Greenland in April 2013 and laboratory work at ENVS, AU. The main supervisors are Associate Professor Charlotte Scheutz, ENV, DTU and Professor Henrik Skov, ENVS, AU. Several co-supervisors have contributed with assistance and guidance throughout the whole project period: Professor Emeritus Jens-Christian Tjell, ENV, DTU; Senior Researcher Andreas Massling, ENVS, AU; Senior Researcher Jacob Klenø Nøjgaard, ENVS, AU and External Consultant Kåre Press-Kristensen, ENVS, DTU. The workload has been divided equally between the two group members, as shown in the table on the following page. In the back of the report a fold-out list of abbreviations and a dvd with appendices 6 to 10 can be found.

_____

Ditte Kristensen s071478
16 August 2013

_____

Ingeborg Elbæk Nielsen s072364
16 August 2013

| Section | Ingeborg | Ditte |
|---|---|---|
| **Abstract** | 1, 2 | 1, 2 |
| **1 Introduction** | 1, 2 | 1, 2 |
| **2 Black Carbon – A Major Climate Forcer** | 1, 2 | 1, 2 |
| 2.1 Properties of Black Carbon | 1 | 2 |
| 2.2 Impacts of Black Carbon on Human Health | 1 | 2 |
| 2.3 Impacts of Black Carbon on Climate | 1 | 2 |
| 2.4 Black Carbon in the Arctic | 2 | 1 |
| 2.5 Black Carbon Emission Sources | 2 | 1 |
| **3 Methods** | 1, 2 | 1, 2 |
| 3.1 Measurement site - Station Nord | 1 | 2 |
| 3.2 Sampling Overview | 2 | 1 |
| 3.3 Sampling of EC and OC in Air | 2 | 1 |
| 3.4 Sampling of EC in Snow | 1 | 2 |
| 3.5 OC-EC analyser | 2 | 1 |
| 3.6 Sampling of BC in Air by PSAP | 1 | 2 |
| 3.7 DEHM – A Transport Model | 2 | 1 |
| 3.8 PMF Source Apportionment | 2 | 1 |
| **4 Results** | 1, 2 | 1, 2 |
| 4.1 Measured EC and OC Concentrations | 2 | 1 |
| 4.2 Measured BC Concentrations in air | 1 | 2 |
| 4.3 Modelled BC Concentrations at Station Nord | 2 | 1 |
| 4.5 PMF Analysis | 1 | 2 |
| **5 Discussion** | 1, 2 | 1, 2 |
| 5.1 Measured and modelled concentrations of BC | 2 | 1 |
| 5.2 Source Apportionment | 1 | 2 |
| **6 Conclusion** | 1, 2 | 1, 2 |

*1 = Main author - responsible for first draft; 2 = Second author - responsible for quality control

# Acknowledgements

The authors would like to thank Professor Henrik Skov, Associate Professor Charlotte Scheutz, Senior Researcher Andreas Massling, Senior Researcher Jacob Klenø Nøjgaard, Professor Emeritus Jens-Christian Tjell and External Consultant Kåre Press-Kristensen for excellent supervision throughout the whole project period. Gratitude is also shown to Professor Johan Ström for his essential comments and suggestions. The authors thank the Department of Environmental Science at Aarhus University for always being so kind and helpful and the staff at Station Nord for their hospitality and support during the field work. Finally, a very special thanks goes to our friend, Laboratory Technician Bjarne Jensen for technical assistance and several memorable experiences in Greenland.

# Contents

**1 Introduction** ..... **1**

**1.1 Objectives** ..... **2**

**2 Black Carbon – A Major Climate Forcer** ..... **4**

**2.1 Properties of Black Carbon** ..... **4**
**2.2 Impacts of Black Carbon on Human Health** ..... **6**
**2.3 Impacts of Black Carbon on Climate** ..... **8**
2.3.1 Radiative Forcing ..... 10
2.3.2 Global Warming Potential and Global Temperature Change Potential ..... 12
**2.4 Black Carbon in the Arctic** ..... **13**
2.4.1 Transport of Black Carbon to the Arctic ..... 15
2.4.2 Black Carbon Concentrations in the Arctic ..... 18
**2.5 Black Carbon Emission Sources** ..... **19**
2.5.1 Arctic Council Nations ..... 22

**3 Methods** ..... **25**

**3.1 Measurement Site - Station Nord** ..... **25**
**3.2 Sampling Overview** ..... **27**
**3.3 Sampling of EC and OC in Air** ..... **28**
**3.4 Sampling of EC in Snow** ..... **28**
**3.5 OC-EC analyser** ..... **30**
3.5.1 Procedure ..... 31
3.5.2 Data Processing ..... 33
3.5.3 Uncertainty ..... 33
3.5.4 Quality Control ..... 33
3.5.5 Air Samples ..... 34
3.5.6 Snow Samples ..... 34
**3.6 Sampling of BC in Air by PSAP** ..... **35**
3.6.1 Quality Control of PSAP data ..... 36
3.6.2 Calculation of BC concentration ..... 36
**3.7 DEHM – A Transport Model** ..... **38**
**3.8 PMF Source Apportionment** ..... **39**
3.8.1 Filter Pack Sampler ..... 41

**4 Results ..... 42**

**4.1 Measured EC and OC Concentrations ..... 42**
4.1.1 EC and OC Concentrations in Air ..... 42
4.1.2 EC Concentrations in Snow ..... 47
**4.2 Measured BC Concentrations in Air ..... 48**
4.2.1 Quality Control ..... 48
4.2.2 Absorption Coefficient ..... 49
4.2.3 Specific Absorption Coefficient ..... 50
4.2.4 BC Concentrations ..... 53
**4.3 Modelled BC Concentrations at Station Nord ..... 55**
**4.4 PMF Analysis ..... 57**
4.4.1 Input Matrices ..... 57
4.4.2 PMF from 2008 to 2010 ..... 58
4.4.3 PMF from 2011 to 2012 ..... 61

**5 Discussion ..... 65**

**5.1 Measured and Modelled Concentrations of BC ..... 65**
5.1.1 BC Concentrations in Snow ..... 68
**5.2 Source Apportionment ..... 69**

**6 Conclusion ..... 75**

**7 References ..... 78**

**Appendices ..... I**

# List of Figures

**Figure 2.1** Absorption of solar radiation (UV, visible and infrared light) by BC, BrC and light-absorbing OC (U.S. EPA, 2012). **5**

**Figure 2.2** Measurement approaches for carbonaceous components of particles. The light-absorption classification is applied for BC, BrC and light-absorbing carbon, whereas the thermal-optical classification approach is used for EC and OC (U.S. EPA, 2012). **6**

**Figure 2.3** The effects of BC on climate compared to effects from GHGs. (1) Reflection of solar radiation by white surfaces; (2) reflection or scattering of solar radiation by clean clouds and particles with no light-absorbing capacity; (3) absorption by BC in the atmosphere; (4) absorption of solar radiation by clouds containing BC; (5) absorption of solar radiation by BC deposited on snow and ice-covered surfaces; (6) solar radiation absorbed by the Earth, where part of the energy is reemitted as infrared radiation; (7) absorption of infrared radiation by GHGs. The gases reemit some of the absorbed radiation and send it back to the surface of the Earth, leading to a warming of the lower atmosphere (U.S. EPA, 2012). **9**

**Figure 2.4** The total climate forcing of BC and the forcing from direct effects, cloud indirect effects, and snow and sea ice effects **(**Bond et al., 2013). **12**

**Figure 2.5** Map showing latitudes from 30 ˚N to 90 ˚N (Aquarius.NET, 2013). **14**

**Figure 2.6** Annual and seasonal variation of BC concentrations at Alert (Law & Stohl, 2007). **15**

**Figure 2.7** Nine different processes affecting the transport of BC to the Arctic; 1. Lifting at the Arctic front, leading to BC deposition on snow, 2. Lifting at low latitudes, leading to deposition of BC outside the Arctic, 3. Low level transport, 4. Slow descent into polar dome, 5. Slow mixing into polar dome, 6. Fast transport in the free troposphere with multiple aerosol removal events, 7. Agricultural fires, 8. Pyrocumulonimbus cloud (Pyro-Cb) injection into stratosphere, 9. Top of Greenland does not receive low-level transport (AMAP, 2011). **17**

**Figure 2.8** Comparison of measured BC concentration (blue line) and modelled values from DEHM (red line) at four Arctic stations in 2008 and 2009 (AMAP, 2011). **19**

**Figure 2.9** The anthropogenic emissions of BC in 2000 by latitude and source sector (AMAP, 2011) **21**

**Figure 2.10** Left: Absolute radiative forcing in the Arctic (60˚N to 90˚N) from direct atmospheric BC and OC and from snow deposited BC and OC by sector and geographical region. Right: Normalized radiative forcing in the Arctic (60˚N to 90˚N) from direct atmospheric BC and OC and from snow deposited BC and OC by sector and geographical region. Results are obtained from the Community Climate System Model (AMAP, 2011). **23**

**Figure 2.11** Comparison of Bond, AMAP and GAINS inventories estimating the sectoral distribution of BC in Russia, Canada, United States and the Nordic Countries (Denmark, Finland, Iceland, Norway, Sweden) in 2000 (AMAP, 2011). **23**

**Figure 3.1** Map of Greenland (Walkowiak, 2013), where Station Nord is located on Prinsesse Ingeborg Peninsula on Kronprins Christians Land (Heidam et al., 2004). **26**

**Figure 3.2** Left: The monitoring station, Flyger's Hut, located 2.5 km south-east of Station Nord. Right: The DMI Hut located at the station. **26**

**Figure 3.3** Left: Windrose showing local wind directions at Station Nord from April 2011 to April 2013. Right: 1. The icebergs, 2: Station Nord and the runway, 3: Flyger's Hut, 4: Knuths Fjeld. **27**
**Figure 3.4** The HVS in the DMI Hut at Station Nord. From left: The HVS inlet (1), The pump (3), The HVS with particle separator (2), The HVS filter (4), PUF/XAD (5), Flow meter (6). **28**
**Figure 3.5** From top left: Taking surface snow samples at Station Nord; experimental setup inside Flyger's Hut; filters drying on pins; filter container used in experimental setup. **30**
**Figure 3.6** Conceptual drawing of the OC-EC analyser showing the sample oven, the oxidizer oven, the methanator and the diode laser (Birch & Cary, 1996). **31**
**Figure 3.7** Thermogram showing temperature, transmittance, detector (FID) response and the OC-EC split. The peaks (from left to right) in the detector response curve correspond to OC (organic carbon), CC (carbonate carbon), PC (pyrolytic carbon), EC (elemental carbon) and methane calibration (Birch & Cary, 1996). **31**
**Figure 3.8** Left: Air sample filter punch is inserted into the OC-EC analyser. Right: Filter punch from the snow samples. **34**
**Figure 3.9** Left: The PSAP in Flyger's Hut. Right: Schematic drawing of the cross-section of a PSAP, consisting of a light source and two mirrors (1), a filter (2), two light detectors (3), an amplifier (4) and a pump (5) (Drawing: Bjarne Jensen, AU-ENVS). **35**
**Figure 3.10** Illustration of Beer Lambert's Law showing an exponential decrease in light intensity ($I_1$ to $I_2$) caused by an increase in thickness of the medium ($x_1$ to $x_2$). $I_0$ is incoming light intensity with no medium present. **37**
**Figure 3.11** A FPS that consist of eight channels and a reference channel. **41**
**Figure 4.1** EC concentrations [ng/m$^3$] with instrumental uncertainty at Station Nord from August 2008 to April 2013. The empty space indicates missing data periods. **43**
**Figure 4.2** Monthly average EC concentrations [ng/m$^3$] with standard deviations at Station Nord from 2008 to 2013. **43**
**Figure 4.3** Annual average EC concentrations [ng/m$^3$] at Station Nord from 2008 to 2013. The years 2008 and 2013 (dashed line) only contain data from August to December and January to April, respectively. **44**
**Figure 4.4** OC concentrations [ng/m$^3$] with instrumental uncertainty at Station Nord from August 2008 to April 2013. The empty space indicates missing data periods. **44**
**Figure 4.5** Monthly average OC concentrations [ng/m$^3$] with standard deviations at Station Nord from 2008 to 2013. **45**
**Figure 4.6** Annual average OC concentrations [ng/m$^3$] at Station Nord from 2008 to 2013. The years 2008 and 2013 (dashed line) only contain data from August to December and January to April, respectively. **45**
**Figure 4.7** The ratio between measured EC and OC concentrations at Station Nord from August 2008 to April 2013. The empty space indicates missing data periods. **46**
**Figure 4.8** Monthly average EC/OC ratio with standard deviations at Station Nord from 2008 to 2013. **46**
**Figure 4.9** Annual average EC/OC ratios at Station Nord from 2008 to 2013. The years 2008 and 2013 (dashed line) only contain data from August to December and January to April, respectively. **46**
**Figure 4.10** The signal [V] (black line), the reference signal [V] (grey line) and the flow [ml/min] (dashed line) with a time interval of 15 min. at Station Nord from January to December 2009 before the quality control. **48**
**Figure 4.11** The signal [V] (black line), the reference signal [V] (grey line) and the flow [ml/min] (dashed line) with a time interval of 15 min at Station Nord from January to December 2009 after the quality control. The arrows indicate filter changes. **48**
**Figure 4.12** The flow [ml/min] used by the PSAP instrument from August 2008 to April 2013. **49**
**Figure 4.13** The absorption coefficients [$\mu m^{-1}$] with a time interval of 15 minutes at Station Nord from January to December 2009 before the quality control. **50**

**Figure 4.14** The absorption coefficients [$\mu m^{-1}$] with a time interval of 15 minutes at Station Nord from January to December 2009 after the quality control. **50**
**Figure 4.15** The monthly absorption coefficients [$m^{-1}$] as a function of the monthly EC concentrations [$g/m^3$] at Station Nord from 2008 to 2013. The resulting specific absorption coefficient is 6.2 $m^2/g$ with a coefficient of determination ($R^2$) of 0.4. **51**
**Figure 4.16** The monthly absorption coefficients [$m^{-1}$] as a function of the monthly EC concentrations [$g/m^3$] at Station Nord for 2010. The resulting specific absorption coefficient is 8.7 $m^2/g$ with a coefficient of determination ($R^2$) of 0.6. **51**
**Figure 4.17** The monthly absorption coefficients [$m^{-1}$] as a function of the monthly EC concentrations [$g/m^3$] at Station Nord for the winter months, December to February, from 2008 to 2013. The resulting specific absorption coefficient is 5.7 $m^2/g$ with a coefficient of determination ($R^2$) of 0.4. **52**
**Figure 4.18** The monthly absorption coefficient [$m^{-1}$] as a function of the monthly EC concentration [$g/m^3$] at Station Nord for the summer months, June to August, from 2008 to 2012. **52**
**Figure 4.19** The BC concentrations [$ng/m^3$] with instrumental uncertainties at Station Nord from August 2008 to April 2013 derived from the PSAP instrument applying a specific absorption coefficient of 5.5 $m^2/g$. The empty space indicates missing data periods. **54**
**Figure 4.20** Monthly average BC concentrations [$ng/m^3$] with standard deviations at Station Nord from 2008 to 2013. **54**
**Figure 4.21** Annual average BC concentrations [$ng/m^3$] at Station Nord from 2008 to 2013. 2008 and 2013 (dashed line) only contain data from August to December and January to April, respectively. **55**
**Figure 4.22** Modelled BC concentrations [$ng/m^3$] in air at Station Nord from August 2008 to April 2013. The empty space indicates missing data periods. **56**
**Figure 4.23** Monthly average modelled BC concentrations [$ng/m^3$] with standard deviations at Station Nord from 2008 to 2013. **56**
**Figure 4.24** Annual average modelled BC concentrations [$ng/m^3$] at Station Nord from 2008 to 2013. The years 2008 and 2013 (dashed line) only contain data from August to December and January to April, respectively. **56**
**Figure 4.25** Source 1 from the PMF analysis based on measurements taken at Station Nord from March 2008 to February 2010. Upper: The columns represent the concentration of the species, where the magnitude is read on the primary y-axis and the squares indicate the percentage of the species that is apportioned to this source which is read on the secondary y-axis. Lower: Time profile showing the source strength, where the average concentration is normalised to 1. **59**
**Figure 4.26** Source 2 from the PMF analysis based on measurements taken at Station Nord from March 2008 to February 2010. Upper: The columns represent the concentration of the species, where the magnitude is read on the primary y-axis, and the squares indicate the percentage of the species that is apportioned to this source, which is read on the secondary y-axis. Lower: Time profile showing the source strength, where the average concentration is normalised to 1. **59**
**Figure 4.27** Source 3 from the PMF analysis based on measurements taken at Station Nord from March 2008 to February 2010. Upper: The columns represent the concentration of the species, where the magnitude is read on the primary y-axis, and the squares indicate the percentage of the species that is apportioned to this source, which is read on the secondary y-axis. Lower: Time profile showing the source strength, where the average concentration is normalised to 1. **60**
**Figure 4.28** Source 4 from the PMF analysis based on measurements taken at Station Nord from March 2008 to February 2010. Upper: The columns represent the concentration of the species, where the magnitude is read on the primary y-axis, and the squares indicate the percentage of the species that is apportioned to this source, which is read on the secondary y-axis. Lower: Time profile showing the source strength, where the average concentration is normalised to 1. **60**

**Figure 4.29** Source 5 from the PMF analysis based on measurements taken at Station Nord from March 2008 to February 2010. Upper: The columns represent the concentration of the species, where the magnitude is read on the primary y-axis, and the squares indicate the percentage of the species that is apportioned to this source, which is read on the secondary y-axis. Lower: Time profile showing the source strength, where the average concentration is normalised to 1. **61**

**Figure 4.30** Source 1 from the PMF analysis based on measurements taken at Station Nord from January 2011 to December 2012. Upper: The columns represent the concentration of the species, where the magnitude is read on the primary y-axis, and the squares indicate the percentage of the species that is apportioned to this source, which is read on the secondary y-axis. Lower: Time profile showing the source strength, where the average concentration is normalised to 1. **62**

**Figure 4.31** Source 2 from the PMF analysis based on measurements taken at Station Nord from January 2011 to December 2012. Upper: The columns represent the concentration of the species, where the magnitude is read on the primary y-axis, and the squares indicate the percentage of the species that is apportioned to this source, which is read on the secondary y-axis. Lower: Time profile showing the source strength, where the average concentration is normalised to 1. **63**

**Figure 4.32** Source 3 from the PMF analysis based on measurements taken at Station Nord from January 2011 to December 2012. Upper: The columns represent the concentration of the species, where the magnitude is read on the primary y-axis, and the squares indicate the percentage of the species that is apportioned to this source, which is read on the secondary y-axis. Lower: Time profile showing the source strength, where the average concentration is normalised to 1. **63**

**Figure 4.33** Source 4 from the PMF analysis based on measurements taken at Station Nord from January 2011 to December 2012. Upper: The columns represent the concentration of the species, where the magnitude is read on the primary y-axis, and the squares indicate the percentage of the species that is apportioned to this source, which is read on the secondary y-axis. Lower: Time profile showing the source strength, where the average concentration is normalised to 1. **64**

**Figure 4.34** Source 5 from the PMF analysis based on measurements taken at Station Nord from January 2011 to December 2012. Upper: The columns represent the concentration of the species, where the magnitude is read on the primary y-axis, and the squares indicate the percentage of the species that is apportioned to this source, which is read on the secondary y-axis. Lower: Time profile showing the source strength, where the average concentration is normalised to 1. **64**

**Figure 5.1** Measured EC (grey line) and BC (black line) concentrations in air using a specific absorption coefficient of 5.5 $m^2/g$ at Station Nord from August 2008 to April 2013 compared to BC concentrations modelled by DEHM (dashed line). Empty space indicates missing data periods. **67**

**Figure 5.2** Measured EC (grey line) and BC (black line) concentrations using a specific absorption coefficient of 6.2 $m^2/g$ at Station Nord from August 2008 to April 2013 compared to BC concentrations modelled by DEHM (dashed line). Empty space indicates missing data periods. **67**

**Figure 5.3** Source origins of chemical species apportioned by PMF analysis conducted with data from Station Nord in the period from March 2008 to February 2010. The columns indicate the percentage of the species that is apportioned to the five different sources: *Soil, Marine, Cu/Ni, Zn* and *Combustion.* **70**

**Figure 5.4** Source origins of chemical species apportioned by PMF analysis conducted with data from Station Nord in the period from January 2011 to December 2012. The columns indicate the percentage of the species that is apportioned to the five different sources: *Soil, Marine, Cu, Ni/Cr* and *Combustion.* **70**

**Figure 5.5** The apportionment of BC on the five sources obtained from the PMF analysis of the period from 2008 to 2010 (left side) and from 2011 to 2012 (right side). **73**

# List of Tables

**Table 2.1** Causal determinations for exposure to $PM_{2.5}$ (U.S. EPA, 2009). **7**
**Table 2.2** Specific absorption coefficients for BC found in the literature **9**
**Table 2.3** The GWP for BC with time horizons of 20, 100 and 500 years and the GTP for BC with time horizons of 20, 50 and 100 years. The uncertainties for the GWP and GTP are (-90 to +100%) and (-90 to +165%) respectively. All values are relative to $CO_2$ (Bond et al., 2013). **13**
**Table 2.4** Concentrations of BC in snow for ten different Arctic locations during 2005 and 2009 (Doherty et al., 2010). According to Doherty et al. (2010) the definition of the estimated BC concentration ($CBCest$) is the estimated true mass of BC per mass of snow, derived by separating the spectrally-resolved total light absorption into BC and non-BC fractions. **19**
**Table 3.1** Measurement instrument, analysis method, sampling frequency, sampling period, total sample quantity and location for each compound measured at Station Nord in the period from August 2008 to April 2013. **27**
**Table 3.2** Airflow ranges in the OC-EC analyser. **32**
**Table 4.1** The EC concentrations in snow at Flyger's Hut, the icebergs, Knuths Fjeld and the runway. The concentrations are given in ng EC/ l melt water. **47**
**Table 4.2** Average EC concentrations [ng/l] and standard deviations for snow samples taken at Flyger's Hut, the icebergs, Knuths Fjeld, and the Runway. The average EC blind concentration [ng/l] and standard deviation is also stated. For each sample location and the blind, the concentration range [ng/l], the number of samples and the sample depth [cm] are given. **47**
**Table 4.3** The minimum and maximum signal [V], reference signal [V] and absorption [$\mu m^{-1}$] at Station Nord for 2008 to 2013. **50**
**Table 4.4** Compounds, analytical methods, time resolutions and uncertainties used in the PMF analysis based on measurements at Station Nord from January 2008 to February 2010 (Nguyen et al., 2013). **57**
**Table 4.5** Compounds, analytical methods, time resolutions and uncertainties used in the PMF analysis based on measurements at Station Nord from January 2011 to December 2012. **58**

# 1 Introduction

Since the industrial revolution in the 18th century, increases in anthropogenic emissions of aerosols and greenhouse gases (GHGs) have altered the energy balance of the climate system, resulting in climate changes. The global surface temperature has increased with 0.74 °C (0.56 to 0.8 °C) from 1906 to 2006. Together with the warming of the earth an increase in sea level has also been observed. During the period from 1961 to 2003 the global average sea level rose at a rate of 1.8 mm (1.3 to 2.3 mm) per year and from 1993 to 2003 at an annual average rate of 3.1 mm (2.4 to 3.9 mm). The impacts of climate changes are multiple and will affect ecosystems, water availability, food supply, coastal areas and human health (IPCC, 2007).

In the Arctic the average temperature has increased almost twice as fast as the global rate during the past 100 years (IPCC, 2007). Arctic warming has led to a longer melt season resulting in accelerating thawing of the permafrost, mass loss of the Greenland Ice Sheet (GIS) (Lenton, 2012) and a severely decrease of the extent of Arctic sea ice (Stroeve et al., 2007). Since satellite observations began in 1978 the annual average extent of Arctic sea ice has declined by 2.7 % (2.1 to 3.3 %) per decade, while an even greater decrease per decade of 7.4 % (5.0 to 9.8 %) is observed during summer (IPCC, 2007). From 2007 to 2012 the six lowest amounts of Arctic sea ice were recorded, with the minimum extent observed in 2012 (Perovich et al., 2012).

The Arctic sea ice and the GIS have been identified as climate subsystems that may exhibit abrupt and irreversible transition triggered by small temperature changes. When the sun rises in the spring, sea ice starts melting, eventually exposing the surface of the dark ocean. This leads to an increased absorption of solar radiation and finally further warming. The Arctic is due to this positive snow-albedo feedback very sensitive to temperature changes (Lenton, 2012). Furthermore, reduction of the GIS will impact the entire world through global rise in sea level, weakening of the thermohaline circulation and negative impacts on human society and biodiversity. Reducing global warming will reduce Arctic warming and melting of the Arctic sea ice and GIS (AMAP, 2011).

The biggest contributor to climate change and the most important anthropogenic GHG is $CO_2$ for which the annual emission has increased around 80 % between 1970 to 2004, from 21 to 38 gigatonnes (IPCC, 2007). Climate change mitigation strategies therefore need to include a great reduction of $CO_2$ emissions. However, $CO_2$ has a long lifetime in the atmosphere, thus a big present-day reduction may not be in time to prevent the

irreversible thawing of the Arctic. Mitigation of Arctic melting could instead be achieved by additionally focussing on short-lived climate forcers (SLCFs) (AMAP, 2011) also known as short-lived climate pollutants. SLCFs include black carbon (BC), methane, ozone and hydro fluorocarbons; compounds, which are characterised by having a relatively short atmospheric lifetime compared to $CO_2$ and exerting a warming effect on the climate (IGSD, 2013). BC, also known as soot, is the most effective atmospheric aerosol at absorbing solar radiation (AMAP, 2011) and recent studies have found that BC is the second biggest contributor to the present temperature increase, only exceeded by $CO_2$ (e.g. Bond et al., 2013). BC exerts an overall warming effect on the climate and may affect the energy balance in three ways: by direct absorption of solar radiation in the atmosphere, by changing the snow/ice albedo and by cloud formation (U.S. EPA, 2012). Furthermore emissions of BC can result in adverse effects on human health, which will briefly be described. However, the overall focus in this study is put on the climate impacts (WHO, 2012).

Currently there is great uncertainty related to climate modelling of BC especially in the Arctic, which generates uncertainty to the estimated climate forcing and hence to the corresponding temperature increase (e.g. Forster et al., 2007; Bond et al., 2013). Monitoring of BC in the Arctic is hence central in order to improve the understanding of the climate impacts of BC. There are, however, limited long-term observations in the Arctic with focus on BC and only a few atmospheric monitoring sites have provided the majority of the existing long-term observations. These sites include: Summit (78 °N) and Station Nord (81.4 °N) in Greenland, Alert (82.46 °N) in Canada, Zeppelin (79 °N) on Svalbard, and Barrow (71.3 °N) in Alaska (AMAP, 2011). It is hence important to continuously expand and improve the knowledge on BC in the Arctic through measurements, observations and modelling.

## 1.1 Objectives

Measurements and observations of BC in the Arctic are important in order to improve the understanding of the characteristics of BC and identify source origins by applying receptor models. This information is needed to develop and validate transport and climate models, improve emission inventories, and formulate strategies to reduce further warming of the Arctic through mitigation actions. The overall objective of this thesis is hence to expand the current knowledge on BC at a high Arctic location, Station Nord, including determination of mass concentrations, source apportionment and effectiveness of the absorption of solar radiation. In this study the following tasks are conducted:

- Mass concentrations of BC in air at Station Nord are determined by using two different methods: a Particle Soot Absorption Photometer (PSAP) and an OC-EC analyser. The measurements are compared to concentrations at other Arctic locations and to concentrations modelled by J. Christensen using the Danish Eularian Hemispheric Model (DEHM). Furthermore, the mass concentrations of organic carbon (OC) in air are determined and the ratio between BC and OC is analysed.

- Estimation of the specific absorption coefficient for BC at Station Nord is improved. The specific absorption coefficient expresses the effectiveness of absorption of solar radiation (Chýlek et al., 1995) and is used to calculate BC mass concentrations from the PSAP data. Furthermore it is examined if and how the specific absorption coefficient varies seasonally and annually at Station Nord.
- Mass concentrations of BC in snow at Station Nord are determined by using an OC-EC analyser and compared with concentrations at other Arctic locations.
- BC source apportionment at Station Nord is modelled, applying Positive Matrix Factorization (PMF) using measured BC concentrations in air as model input parameter.

The BC mass concentrations are determined on the basis of snow samples from April 2013 and air samples collected from August 2008 to April 2013. The air samples are compared to BC air concentrations modelled by DEHM in the period from August 2008 to April 2013. The modelling by PMF covers the period from March 2008 to December 2012.

# 2 Black Carbon – A Major Climate Forcer

This chapter will explain the properties of BC and its effect on both health and climate. Also the specific effects of BC in the Arctic will be described, including the transport of BC to the Arctic and the current concentrations at different Arctic locations. Finally the emission sources of BC will be presented with a special focus on the Arctic Council Nations.

## 2.1 Properties of Black Carbon

Carbonaceous particulate matter is the carbon-based part of particles containing both OC and BC, which together comprise the total amount of carbon. BC, which is an aerosol, is produced during incomplete combustion of carbon-based fuels meaning that there is not sufficient oxygen available during the combustion to convert all fuel into $CO_2$ and water (Bond et al., 2004). BC is a primary PM since it is emitted directly from the source. BC can, per unit mass, absorb a million times more energy compared to $CO_2$ and is contrary to other aerosols an important climate warming pollutant (U.S. EPA, 2012). Despite the fact that numerous definitions of BC have been published in scientific literature, no generally accepted definition currently exists (Han et al., 2010). According to the U.S. EPA (2012) BC can be defined as *"a solid form of mostly pure carbon that absorbs solar radiation (light) at all wavelengths. BC is the most effective form of PM* (Particulate Matter)*, by mass, at absorbing solar energy"*.

BC is also termed elemental carbon (EC), where the two terms depend on the measurement techniques. Measurements based on thermal-optical classification are referred to as EC whereas measurements based on light absorption/optical methods are referred to as BC (illustrated in Figure 2.2) (Han et al., 2010). These different types of methods will be described more thoroughly in Chapter 3.

BC particles are emitted as small spherules (U.S. EPA, 2012) with a mass median diameter in the nanometre size range depending on the type of combustion source. Pure BC particles are seldom found in the atmosphere, since BC rapidly upon emission coagulates and reacts with other particles and gases from the combustion and the surrounding atmosphere (AMAP, 2011). Relatively fast after emission the BC hence forms larger particles with a size of 0.1 to 1 μm (U.S. EPA, 2012), which increases its atmospheric lifetime. Particles with a diameter within this range, 0.1 to 1.0 μm, have the lowest deposition velocity (Seinfield & Pandis, 2006) and thereby the highest probability

to be transported further. BC is hydrophobic upon emission but within hours it becomes more hydrophilic (or hygroscopic) through the reactions and coagulations with other compounds (EPA, 2012). The change to a more hydrophilic aerosol increases the possibility of being removed from the atmosphere by precipitation or in-cloud scavenging. According to AMAP (2011) "*the ability of an aerosol particle to take up water to the point that it activates and forms a cloud droplet depends on its size and composition (or hygroscopicity) and the supersaturation within the cloud*".

Mixtures of particle bound compounds emitted during incomplete combustion can vary in composition but mainly consist of OC and BC together with sulphates, nitrates, gaseous constituents and metals. For some sources BC and OC make up most of the $PM_{2.5}$ (particulate matter with a diameter < 2.5 μm) (e.g. transport) whereas they for other sources make up less than 50% (e.g. industry), indicating that the emission mixture holds significant amounts of other primary co-pollutants, such as nitrates and sulphates. The emitted BC to OC ratio likewise varies and depends on the type of fuel burned and combustion conditions. Biofuel and biomass burning have relatively low BC to OC ratios of 1:4 and 1:9 respectively. On the other hand combustion of fossil fuels results in high BC to OC ratios, where diesel exhaust is around 1:1. In diesel used for marine vessels BC comprise a smaller fraction of the PM than in diesel used for land transport due to the high content of organics and sulphates. The differences in the fraction of BC in the primary $PM_{2.5}$ emissions and the ratio of BC to OC have important effects on climate, since BC is the most effective component of PM in absorbing light (U.S. EPA, 2012).

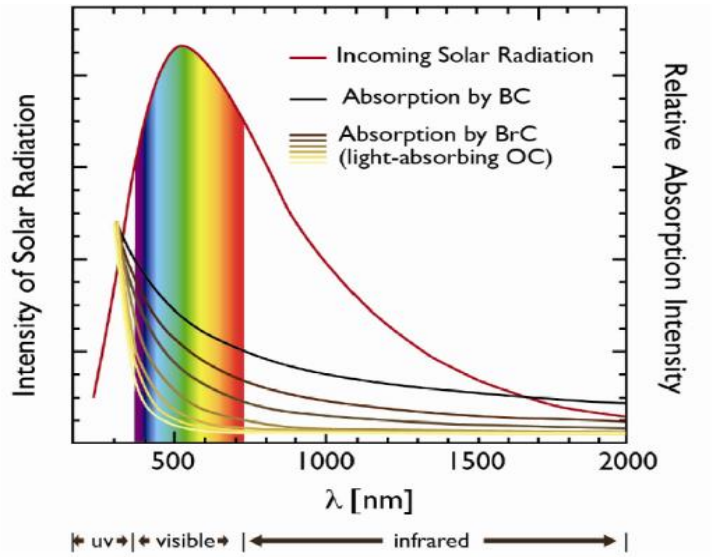


**Figure 2.1** Absorption of solar radiation (UV, visible and infrared light) by BC, BrC and light-absorbing OC (U.S. EPA, 2012).

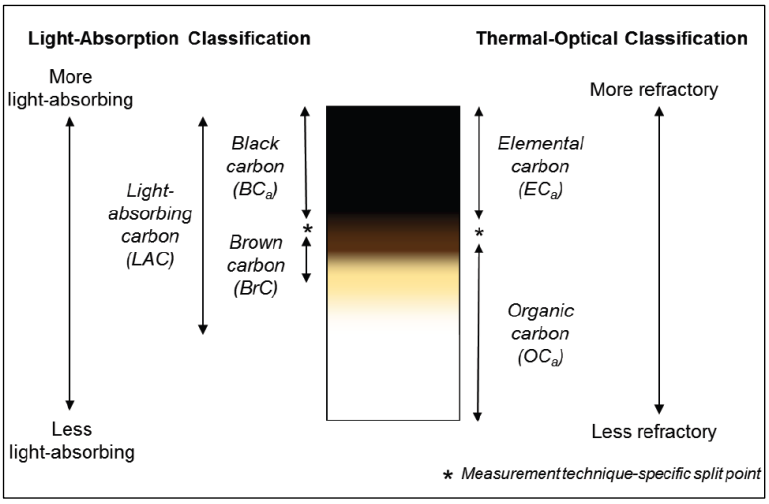


**Figure 2.2** Measurement approaches for carbonaceous components of particles. The light-absorption classification is applied for BC, BrC and light-absorbing carbon, whereas the thermal-optical classification approach is used for EC and OC (U.S. EPA, 2012).

Generally OC refers to a mixture of compounds where carbon is bound with other elements such as oxygen or hydrogen (Bond et al., 2004). OC may be emitted directly from incomplete combustion referred to as primary OC, while it can also be formed through oxidation of volatile organic carbon in the atmosphere, called secondary OC (AMAP, 2011). A dark mixture emitted from incomplete combustion indicates a relatively high BC to OC ratio, whereas OC is the dominating compound in a more brown or yellow mixture. A class of OC compounds are referred to as brown carbon (BrC), which absorbs solar energy to a lesser extent than BC since BrC only absorbs visible and ultraviolet radiation (U.S. EPA, 2012). The darker the mixture is, the more BC it contains and the more effective the mixture is at absorbing solar radiation (Figure 2.1). Figure 2.2 presents the relative light-absorption classification for BC, BrC and OC stating that BC is more light-absorbing than BrC. It furthermore states that BC is more refractory than OC, meaning that BC is more inert at high temperatures compared to OC (U.S. EPA, 2012). This property makes it possible to thermally separate OC and BC.

## 2.2 Impacts of Black Carbon on Human Health

The World Health Organization (WHO) states that ambient air pollution in medium- and high-income countries is among top ten regarding risk factors. This is not the case for low-income countries where other risk factors such as childhood malnutrition and polluted drinking water are relatively more important. Nevertheless it is expected that a higher proportion of the population is dying of ambient $PM_{2.5}$ in developing countries compared to developed regions. Globally the exposure to indoor and ambient $PM_{2.5}$ has been evaluated to cause millions of death worldwide (U.S. EPA, 2012).

In recent decades, scientific evidence has confirmed that exposure to fine particulate matter ($PM_{2.5}$) is connected to multiple health impacts, which among others can lead to premature death. It is not possible to determine a lower adverse $PM_{2.5}$ concentration threshold since scientific studies indicate health effects over the full concentration range

tested (U.S. EPA, 2012). Currently, the human health effects regarding exposure to BC are mainly based on scientific studies, which focus on the effects of BC as part of $PM_{2.5}$. The amount of scientific literature explicitly investigating BC is growing but the U.S. EPA still consider the information to scarce to differentiate between the specific health-effects from $PM_{2.5}$ and BC (U.S. EPA, 2012).

Health effects have been observed for both short-term and long-term exposure, where the duration is days to weeks, and months to years, respectively. The outcome from exposure to $PM_{2.5}$ includes cardiovascular, respiratory, reproductive, and developmental effects together with mortality, cancer, mutagenicity, and genotoxicity (Table 2.1) (U.S. EPA, 2009). There is however not equally weight of evidence for each outcome, which is why the causality determination is presented as a causal, likely to be causal, or suggestive relationship in Table 2.1.

There is strong scientific evidence that concludes a causal relationship between both short- and long-tern exposure to $PM_{2.5}$ and cardiovascular effects, which can range from changes in blood pressure to premature death (U.S. EPA, 2012). There have also been studies conducted with focus on BC, which have generally concluded a consistent evidence of a connection between concentration of BC and cardiovascular effects (e.g. Mordukhovich et al., 2009; Wilker et al., 2010). The effects observed with exposure to BC are generally consistent with the outcomes observed for PM2.5 (U.S. EPA, 2012).

With regard to mortality, scientific papers have determined a causal relationship for both short- and long-term exposure to $PM_{2.5}$. The findings indicate that short-term exposure to $PM_{2.5}$ is linked with cardiovascular- (Ito et al., 2011), respiratory- (Zhou et al., 2011) and all-cause mortality (Cakmak et al., 2011). Long-term exposure is similarly associated with an increased risk of mortality (U.S. EPA, 2009), where the strongest evidence is found for cardiovascular mortality (Ito et al., 2011; U.S. EPA, 2009). Positive associations have been found between $PM_{2.5}$ and respiratory mortality (Zhou et al., 2011) but the evidence is currently more limited (U.S. EPA, 2009).

**Table 2.1** Causal determinations for exposure to $PM_{2.5}$ (U.S. EPA, 2009).

| **Exposure** | **Outcome** | **Causality Determination** |
|---|---|---|
| **Short-term exposure to $PM_{2.5}$** | Cardiovascular effects | Causal |
| | Respiratory effects | Likely to be causal |
| | Mortality | Causal |
| **Long-term exposure to $PM_{2.5}$** | Cardiovascular effects | Causal |
| | Respiratory effects | Likely to be causal |
| | Mortality | Causal |
| | Reproductive and developmental effects | Suggestive |
| | Cancer, mutagenicity, and genotoxicity | Suggestive |

The relationship between both short- and long-term exposure to $PM_{2.5}$ and respiratory effects are likely to be causal (U.S. EPA, 2012). Some studies, with focus on BC, have reported respiratory effects, such as increased respiratory symptoms in asthmatic and non-asthmatic children (e.g. Spira-Cohen et al., 2011), and decreased lung function among women in urban areas (Suglia et al., 2008). However, the scientific evidence is not consistent enough to establish a direct association between the concentration of BC and respiratory effects (U.S. EPA, 2012).

Some scientific studies have reported reproductive and developmental effects such as low birth weight and growth restrictions through long-time exposure to $PM_{2.5}$ (Parker et al., 2005). The scientific evidence is however not consistent; hence the causal determination is suggestive (U.S. EPA, 2009). The same situation is the case for cancer, mutagenicity, and genotoxicity effects. Some epidemiologic studies report association between lung cancer mortality and exposure to $PM_{2.5}$ (e.g. Laden et al., 2006). Other studies have shown that PM from certain combustion sources is mutagenic (De Kok et al., 2005) and genotoxic (e.g. Chakra et al., 2007). Again the evidence is currently too limited, which leads to categorization as suggestive of a causal relationship between the exposure of $PM_{2.5}$ and cancer, mutagenicity, and genotoxicity (U.S. EPA, 2009).

Some scientific studies especially looking on exposure to BC suspect that BC may be more toxic than other finer particles. Especially studies on BC derived from traffic have indicated that BC may be more toxic than $PM_{2.5}$ in general (UNEP and WMO, 2011). The WHO (2012), on the other hand, investigated all available toxicological studies and found that *"BC (measured as EC) may not be a major directly toxic component of fine PM, but it may operate as a universal carrier of a wide variety of, especially, combustion-derived chemical constituents of varying toxicity to sensitive targets in the human body…"*. On the basis of the limited and inconsistent literature it is hence generally recommended to consider all particles as equally toxic since the necessary evidence is presently not sufficient (UNEP and WMO, 2011).

In addition to the above mentioned health impacts $PM_{2.5}$ is linked to visibility impairment and decreasing agricultural crop yield, which can have indirect impact on human health (U.S. EPA, 2012). It must furthermore be emphasized that emission of BC can lead to indirect effects on health through climate change. These could include death caused by changing weather patterns, such as increased frequencies of flooding, heat waves and other extreme events (Confalonieri et al., 2007).

## 2.3 Impacts of Black Carbon on Climate

In recent years it has become generally accepted that BC contributes to climate change on both a regional and global scale. Like GHG, BC directly absorbs solar radiation when present in the atmosphere leading to a warming effect in the atmosphere. BC also has an effect on the albedo of snow and ice and an indirect effect, which is associated with cloud interaction (U.S. EPA, 2012). The different ways BC affect the climate compared to GHG is presented in Figure 2.3 (1 to 7). When solar radiation reaches the surface of the Earth it is reflected by white surfaces, such as surfaces covered with snow and ice (1). Also clean

clouds and particles with no light-absorbing capacity reflect or scatter incoming solar radiation (2). However, when BC is present in the atmosphere it absorbs the radiation at all wavelengths leading to a direct warming effect in the atmosphere (3). BC absorbs both incoming and outgoing solar radiation, contrary to GHGs, which only absorb outgoing infrared radiation. BC-cloud interactions as mentioned have an indirect effect on climate but the net effect is highly uncertain (4). When BC is deposited on snow and ice-covered surfaces it has an albedo effect because it absorbs part of the radiation, which would usually have been reflected to the atmosphere, thus increasing the degree of melting (5). Part of the incoming solar energy is transformed into infrared radiation, which is transmitted back to the atmosphere and space (6). Some of the infrared radiation is absorbed by GHGs and reemitted to the surface, which warms the atmosphere and the Earth's surface (7) (U.S. EPA, 2012).

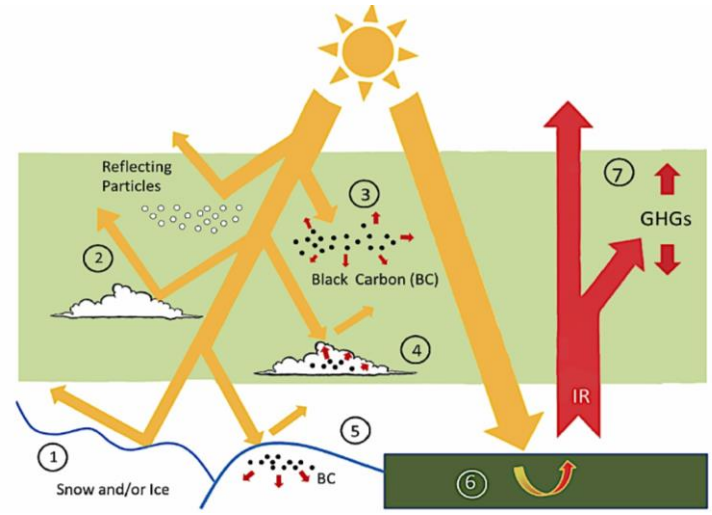


**Figure 2.3** The effects of BC on climate compared to effects from GHGs. (1) Reflection of solar radiation by white surfaces; (2) reflection or scattering of solar radiation by clean clouds and particles with no light-absorbing capacity; (3) absorption by BC in the atmosphere; (4) absorption of solar radiation by clouds containing BC; (5) absorption of solar radiation by BC deposited on snow and ice-covered surfaces; (6) solar radiation absorbed by the Earth, where part of the energy is reemitted as infrared radiation; (7) absorption of infrared radiation by GHGs. The gases reemit some of the absorbed radiation and send it back to the surface of the Earth, leading to a warming of the lower atmosphere (U.S. EPA, 2012).

**Table 2.2** Specific absorption coefficients for BC found in the literature

| Reference | Specific absorption coefficient | Notes |
|---|---|---|
| Hegg et al., 2011; J. Ström, Professor, Stockholm University, pers. comm., June 2013 | 5.5 $m^2/g$ | Found on Svalbard |
| Bond and Bergstrom, 2006 | 7.5 $m^2/g$ | Fresh BC for a variety of sources |
| Sharma et al., 2002 | 10 $m^2/g$ | |

As mentioned earlier BC is the most effective aerosol in absorbing solar radiation. The effectiveness of this absorption is referred to as the specific absorption coefficient and is defined as "*the absorption cross section of a given carbon particle divided by its mass"*, thus having the units [$m^2$/g] (Chýlek et al., 1995). According to Chýlek et al. (1995) the effectiveness of absorption of solar radiation by BC depends on *"the BC refractive index, the size and shape of the carbon particle, and the medium in which the particle is embedded"*. Coagulation with other particles thus plays an important role. Different studies have documented the specific absorption coefficient to be site - and seasonally dependent. This dependency is mostly based on different ageing of the BC from location to location and on the diverse source origins, which may change seasonally. Freshly emitted BC is assumed to have a higher specific absorption coefficient compared to aged BC, which have undergone transport and transformation through coagulation with other particles. In urban and near-street measuring sites the coefficient is therefore higher compared to rural and remote areas (Petzold et al., 1997). Table 2.2 presents different values from the literature.

### 2.3.1 Radiative Forcing

Currently more energy is entering the atmosphere than leaving. The energy balance of the climate system is hence no longer in equilibrium, which is referred to as radiative forcing (RF) (UNEP and WMO, 2011). RF is a standard measure of how pollutants affect the balance between incoming solar radiation and outgoing infrared radiation. It is calculated as a change relative to preindustrial times, using a 1750 emission-year. A pollutant's net RF since preindustrial conditions can be averaged over the surface of the Earth and is hence often given in watts per square meter ($W/m^2$). When a compound reflects solar energy it results in a negative RF and thereby leads to cooling. Contrary absorption of radiation increases the amount of energy in the climate system resulting in a positive RF and hence warming of the atmosphere (U.S. EPA, 2012). The overall RF of aerosols is negative hence leading to cooling, whereas the overall RF of GHGs is positive resulting in warming (IPCC, 2007).

The total RF from BC includes direct forcing, snow and ice albedo forcing and indirect forcing. As mentioned, direct positive forcing originates from the absorption of solar radiation and reemitted infrared radiation from the earth (U.S. EPA, 2012). In 2007 the Intergovernmental Panel on Climate Change (IPCC) estimated the global average direct RF of BC to +0.34 (±0.25) $W/m^2$ (Forster et al., 2007) but multiple studies conducted since the IPCC report has indicated a higher value. Bond et al. (2013) has in a recent study reported a direct RF from BC of +0.71 (+0.08 to +1.27) $W/m^2$, with a medium level of scientific understanding (LOSU). Snow and ice albedo forcing result from darkening of snow- or ice covered surfaces due to BC. This result in a decrease in the natural albedo effect of snow and ice hence leading to a positive RF. Based on available studies the IPCC (Forster et al., 2007) reported a global average RF of BC on snow and ice of +0.10 (±0.10) $W/m^2$ with a low LOSU, where the more recent study by Bond et al. (2013) has estimated a RF of +0.12 (+0.02 to +0.36) $W/m^2$.

The indirect forcing, which results from BC-cloud interaction, is currently less understood and the uncertainty is high. In general, the aerosols' impacts on clouds have been divided into five different types by IPCC: cloud albedo effect, cloud lifetime effect, glaciation indirect effect, semi-direct effect and thermodynamic effect. These effects are applied to all aerosols and few studies have examined BC's specific influence on the effects. The following description of the effects will be with focus on aerosols in general. Aerosols affect the formation of clouds, since cloud droplets are produced by water vapour condensing onto a particle. Increasing the emission of particles leads to an increase in the formation of smaller cloud droplets, which leads to brighter and more reflective clouds. This is referred to as the cloud albedo, which results in a cooling effect. It should be emphasised that BC in clouds may absorb solar radiation, hence reducing the reflection, but the net effect is highly uncertain. The smaller cloud droplets do not aggregate to form raindrops to the same extent as normal cloud droplets, which change the precipitation patterns and results in clouds with a longer lifetime. This is referred to as the cloud lifetime effect which also has a cooling effect. The glaciation indirect effect happens in super-cooled liquid water clouds where aerosols, such as BC, serve as ice nuclei and activate precipitation. This effect only occurs in some mixed-phase clouds (containing both ice and water), and is thought to have a warming effect (U.S. EPA, 2012).

For the semi-direct and the thermodynamic effects it is not determined whether the consequences are cooling or warming. The semi-direct effect happens when absorbing aerosols heat the troposphere, changing its stability and humidity. This change also results in an effect on the lifetime and formation of clouds. The thermodynamic effect can occur in certain mixed-phase clouds, when the smaller cloud droplets cause a delay in the normal freezing of droplets. This results in a change in the characteristics of the cloud (U.S. EPA, 2012). Bond et al., (2013), is one of the studies estimating the RF from all indirect effects with a value of 0.23 $W/m^2$ (a 90 % uncertainty range of -0.47 to +1.0).

The majority of scientific studies conclude that the total forcing from BC is positive resulting in a warming of the climate. Bond et al., (2013) estimated the total climate forcing of BC to +1.1 (+0.17 to +2.1) $W/m^2$ including both direct and indirect forcing together with snow and ice albedo forcing. This positive RF strongly indicates that BC contributes to a warming of the climate. According to Bond et al., (2013) the strong total RF makes BC the second most important climate forcer in the atmosphere - only exceeded by $CO_2$, with an estimated RF of +1.66 (+1.49 to +1.83) $W/m^2$ (Forster et al., 2007). This contradicts IPCC's conclusion that BC is the third biggest climate forcer, due to its direct and snow/ice albedo forcing of +0.34 and +0.1 $W/m^2$ respectively (Forster et al., 2007). Other studies, such as UNEP and WMO (2011) support the assumption that BC is the second biggest contributor to global warming, but has reported lower total RF for BC, of +0.6 (0.0 to +1.0) $W/m^2$. Figure 2.4 summarizes the total global climate forcing of BC and specifies the forcing from direct effects, cloud indirect effects, and snow and sea ice effects (Bond et al., 2013).

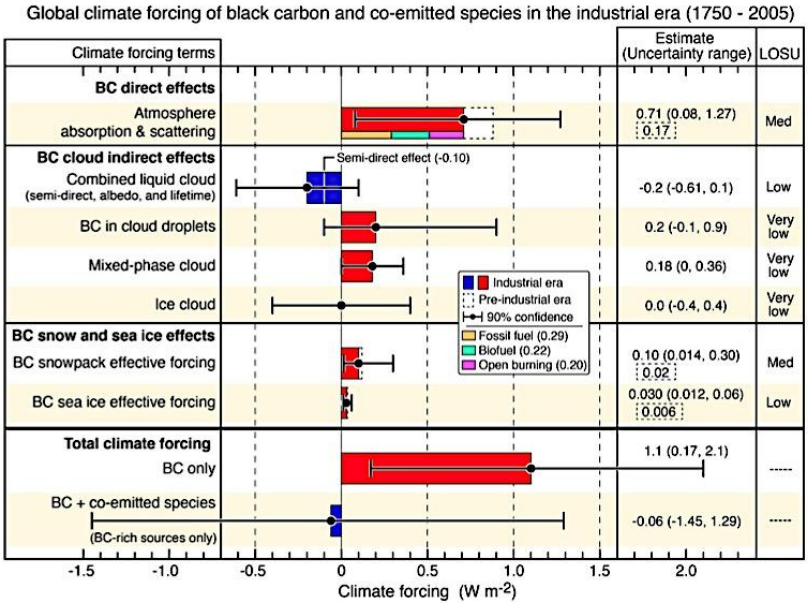


**Figure 2.4** The total climate forcing of BC and the forcing from direct effects, cloud indirect effects, and snow and sea ice effects **(**Bond et al., 2013).

### 2.3.2 Global Warming Potential and Global Temperature Change Potential

To compare climate effects of different compounds it is necessary to use a common scale, where the same metrics are applied. The global warming potential (GWP) is one of the most accepted and well-defined metric. GWP is based on a time-integration of the RF caused by pulse emission of a unit mass of gas. The GWP can be given as an absolute GWP (AGWP) (e.g. in $Wm^{-2}\,kg^{-1}$ year) or as a dimensionless metric where the AGWP is divided with the AGWP of a reference gas, often being $CO_2$. The AGWP of a given compound x is found by equation 2.1 (Fuglestvedt et al., 2010):

$$AGWP^{x}(H) = \int_{0}^{H} A_x e^{-t/a_x} dt \qquad (2.1)$$

Where $A_x$ is the specific RF of the compound x, $a_x$ is the lifetime of the compound and H is the time horizon. As seen from equation 2.1 it is assumed that the compound is removed exponentially from the atmosphere. The GWP is generally calculated using time horizons of 20, 100 and 500 years, which reflect the importance of the compound at different time intervals (Fuglestvedt et al., 2010). Even though GWP is the most frequently used metric, it has been criticised for not taking economic dimensions into consideration (U.S. EPA, 2012).

Another applied metric is the global temperature change potential (GTP), which expresses a global temperature change at a given point in time resulting from an emission. The GTP hence addresses an actual climate response, in this case temperature change, as a response to RF (U.S. EPA, 2012). As for the GWP, the GTP can be given as an absolute GTP (AGTP) (in K/kg) or as a dimensionless metric where the AGTP is divided with the AGTP of a reference gas, often being $CO_2$ (Bond et al., 2013; Fuglestvedt et al., 2010).

**Table 2.3** The GWP for BC with time horizons of 20, 100 and 500 years and the GTP for BC with time horizons of 20, 50 and 100 years. The uncertainties for the GWP and GTP are (-90 to +100%) and (-90 to +165%) respectively. All values are relative to $CO_2$ (Bond et al., 2013).

| | **GWP** | | | **GTP** | | |
|---|---|---|---|---|---|---|
| | **20 years** | **100 years** | **500 years** | **20 years** | **50 years** | **100 years** |
| **BC** | 3200 | 910 | 280 | 925 | 150 | 130 |

The GWP and GTP for BC is presented in Table 2.3, with time horizons of 20, 100 and 500 years and 20, 50 and 100 years, respectively. Both metrics are dimensionless with $CO_2$ used as reference gas. In calculation of the GWP and GTP all effects are taken into consideration including both direct, indirect, and snow and ice effects. The uncertainty for GTP (-90 to +165%) is relatively higher than for GWP (-90 to +100%). BC has a short atmospheric lifetime of days to weeks, which is why the GWP and GTP increase with a decreasing time horizon. The choice of time horizon is thus important when considering SLCF. The effects of reducing BC emissions with a time horizon of 100 to 500 years are much more limited compared to a time horizon of 20 years (Bond et al., 2013). The relative importance of BC compared to $CO_2$ hence relies on the time horizon, where a shorter time horizon makes the relative importance of BC greater (U.S. EPA, 2012). The use of GWP and GTP metrics is largely depending on the overall policy target (Fuglestvedt et al., 2010). Finally, the global impact metrics should be used with caution since BC is a regional pollutant, where the impacts depend on the region and timing of emission (Bond et al., 2013).

## 2.4 Black Carbon in the Arctic

The Arctic, which is defined as the region between 60 ˚N and 90 ˚N (Figure 2.5), is very sensitive to small changes in temperature (AMAP, 2011). There is widespread concern that Arctic warming will lead to significant irreversible effects where tipping points will be reached (Lenton, 2012). According to IPCC (Halsnæs et al. 2007) a tipping point can be defined as: "*when change may accelerate and when environmentally, socially and economically significant effects become irreversible, and the cost and effectiveness of mitigation and adaptation responses are all uncertain, to a greater or lesser extent*".

The Arctic sea ice extent and the GIS have been identified as elements in the Earth system, which could exhibit tipping points where abrupt or irreversible transitions are caused by a small change in temperature. Tipping points may be reached if a strong self-amplification of external forcing exists through positive feedback processes, such as the snow-albedo feedback where dark ocean is exposed when sea-ice melts hence reducing the albedo (Lenton, 2012). The Arctic Ocean is projected to be largely ice-free in summer when the global warming is approximately 0.5-2ºC above present temperature levels (1980-1999) (Lenton et al., 2008). This will, according to some scientists happen already in 2016 ±3 years, but most models have projected this to occur around 2050 (Lenton, 2012). This tipping point will cause increased warming and changes in ecosystems (Lenton et al., 2008) and the decrease in sea ice extent will also open up for increased Arctic shipping, which will amplify the regional BC pollution (Corbett et al., 2010).

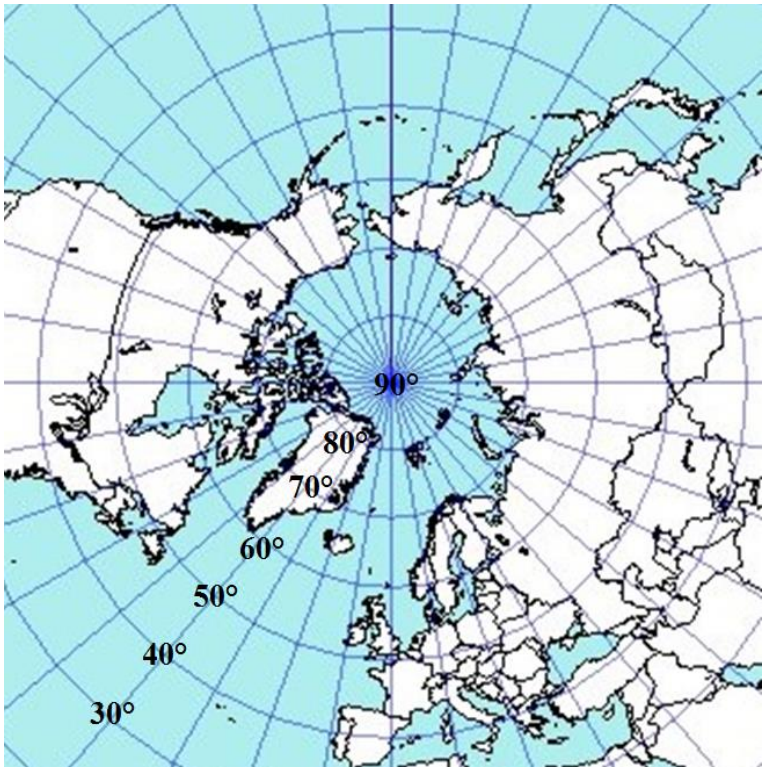


**Figure 2.5** Map showing latitudes from 30 ˚N to 90 ˚N (Aquarius.NET, 2013).

The GIS still has a positive surface mass balance due to more snowfall than melt-off but the overall mass balance is negative due to the big loss flux from calving glaciers. The GIS will be subject to irreversible meltdown if the surface mass-balance becomes negative, due to a positive feedback, where temperature increases as the altitude of the surface declines (Lenton, 2012). This meltdown will result in 2-7 metres higher sea level (Lenton et al., 2008). Two different models have estimated irreversible meltdown of the GIS when the global warming reaches 3 ºC and 6 ºC. However, other scientists have in recent work suggested that this tipping point could be reached much sooner only at 0.7-1.7 ºC further temperature increase. IPCC has put the threshold at 1.9 to 4.6 ºC above preindustrial levels (Lenton, 2012; Lenton et al., 2008; Meehl et al., 2007).

There is a great focus on $CO_2$ in international climate policies and it is by no doubt important to reduce $CO_2$ globally in order to limit the risk of reaching Arctic tipping points in the future. However, according to Lenton (2012) up to 70 % of Arctic warming is currently due to BC together with a reduced amount of reflective sulphate aerosols (Lenton, 2012). As described in section 2.3 BC impact the climate directly, indirectly and by snow and ice albedo effect, but in the Arctic these effects may be stronger. First of all, atmospheric BC absorbs incoming solar radiation and outgoing radiation reflected by ice and snow, which makes the direct absorbing effect of BC larger in the Arctic (Corbett et. al., 2010). Deposition of BC on ice and snow results in a positive snow/ice albedo effect because the albedo decreases and regional climate change intensifies (Lenton, 2012; Arctic council, 2011). Furthermore substances, co-emitted with BC, which may have a cooling effect on the climate in other regions, can similarly cause warming when

deposited in the Arctic because they are darker than ice and snow (Arctic Council, 2011). There is uncertainty related to the indirect effects through BC-cloud interactions but when occurring over snow and ice the net effect is thought to be warming (Arctic Council, 2011). Due to the short lifetime of BC, emission reductions will result in an almost immediate decrease in radiative forcing. Hence BC reduction strategies, such as use of appropriate technologies and air pollution policies would be a fast way to start limiting the radiative forcing in the Arctic (Lenton, 2012) and postpone Arctic tipping points.

### 2.4.1 Transport of Black Carbon to the Arctic

Pollution in the Arctic creates a so called Arctic haze during winter and spring because of greater accessibility to the Arctic air masses during this time of the year. The majority of the mass of BC arrives due to long-range transport from source regions outside the Arctic, which is affected by the polar dome and the Arctic front (AMAP, 2011).

#### 2.4.1.1 Arctic Haze

The remote Arctic atmosphere was believed to be extremely clean until the 1950'ies when pilots flying over the North American Arctic noticed a decreased visibility every winter and spring due to a widespread haze. In the 1970'ies scientists discovered that this Arctic haze was air pollution transported from more southerly regions (Heidam et al., 1999; Heidam et al., 2004; Law & Stohl, 2007; Stohl, 2006). During winter the Arctic surface temperatures become very low and a stable stratification occurs resulting in strong temperature inversions (Stohl, 2006). The stability of the Arctic air results in reduced removal of aerosols and increased atmospheric residence time (Shaw, 1995). The phenomenon takes place because of the greatly reduced amount of sunlight during winter months, and the strong radiative cooling over snow and ice covered surfaces, enhanced by the clear sky and light surface winds (Rasmussen, 2003; Shaw, 1995). Removal of aerosols by dry deposition is reduced due to little turbulent exchange caused by the thermally stable stratification (Stohl, 2006). Wet deposition of particulate pollutants is less dominant in the Arctic winter as precipitation is reduced compared to mid-latitudes because of the relatively small amounts of moisture in the corresponding air masses (Rasmussen, 2003; Shaw, 1995). Removal or modification of aerosols by clouds is also minor because the low vapour pressure results in thin cloudiness (Shaw, 1995).

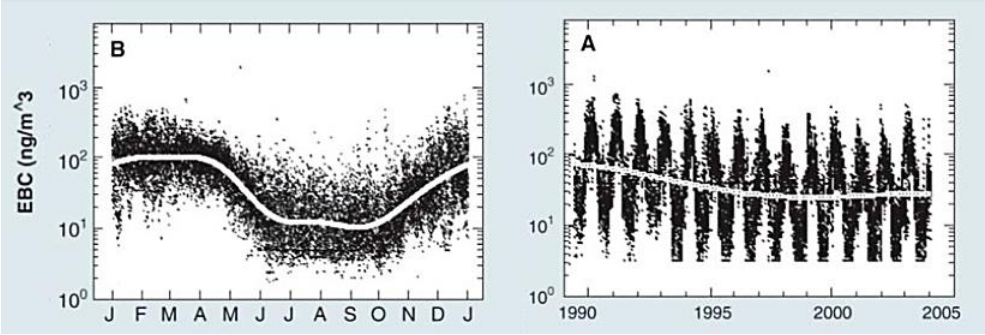


**Figure 2.6** Annual and seasonal variation of BC concentrations at Alert (Law & Stohl, 2007).

The combination of aerosol emissions in the Northern hemisphere and slow aerosol removal processes during winter and spring results in the so-called Arctic haze (Ménégoz, 2011). According to Law and Stohl (2007), Arctic haze is transported from the mid-latitudes and is "*a mixture of sulphate and particulate organic matter and, to a lesser extent, ammonium, nitrate, black carbon (BC) and dust aerosols".* Arctic haze follows a seasonal cycle with highest concentrations in winter and early spring when the atmosphere is dry and stable (Law & Stohl, 2006). This is illustrated in Figure 2.6, which shows the annual and seasonal variations of BC concentrations at Alert. A similar pattern is expected to be observed for the concentrations of BC at Station Nord found in this study.

#### 2.4.1.2 Polar Dome

Due to the low potential temperatures in the Arctic, a polar dome forms over the lower Arctic troposphere during winter and spring (Figure 2.7) (Stohl, 2006; Law & Stohl, 2007; Sodemann, 2011; AMAP, 2011). Inside the polar dome the air mass is highly stratified and very stable with little turbulence and slow vertical exchange resulting in long aerosol residence times (AMAP, 2011; Sodemann, 2011). Furthermore the Arctic troposphere is extremely dry, which reduces the chances of wet deposition and hence leads to long aerosol lifetimes during winter (Stohl, 2006). Towards the southern boundaries of the polar dome a horizontal transport barrier called the Arctic front is created. The Arctic front complicates the transport of aerosols into the Arctic, thus increasing the concentration gradients of air pollution between the mid-latitudes and the Arctic (Sodemann, 2011). The Arctic front is not located at the same latitudes; over the eastern North Atlantic Ocean the front is almost permanently located north of 70˚ while in northern Eurasia the Arctic front can extend as far south as 40˚ in January making this region the major contributor to the Arctic haze (Law & Stohl, 2007; Stohl, 2006).

As described in section 2.6 most of the BC in the Arctic originates from more southerly regions outside the Arctic. In order to identify the specific sources and develop reduction strategies, it is important to identify the main transport pathways (AMAP, 2011). The long-range transport of BC to the Arctic may occur either in the free troposphere or in the lower part of the atmosphere, which is in contact with the Earth's surface, and referred to as the planetary boundary layer (U.S. EPA, 2012). According to Stohl (2006) BC can reach the Arctic along three different pathways; "*low level transport followed by ascent in the Arctic, low level transport alone, and uplift outside the Arctic followed by descent in the Arctic".* During winter pollution originating from Europe can be transported to the Arctic along all three pathways while in summer low level transport alone is not possible. Pollution emitted in North America and Asia is most frequently transported to the Arctic by uplift followed by descent into the polar dome (Stohl, 2006; AMAP, 2011). BC emission in the southern and eastern parts of Asia has increased rapidly during the past decades and is now higher than the total emissions from Europe, North America and Russia. South and East Asia is the most dominant source of BC concentrations in the upper Arctic troposphere, but it is not clear whether this BC can intrude into the polar dome given its short lifetime (Stohl, 2006).

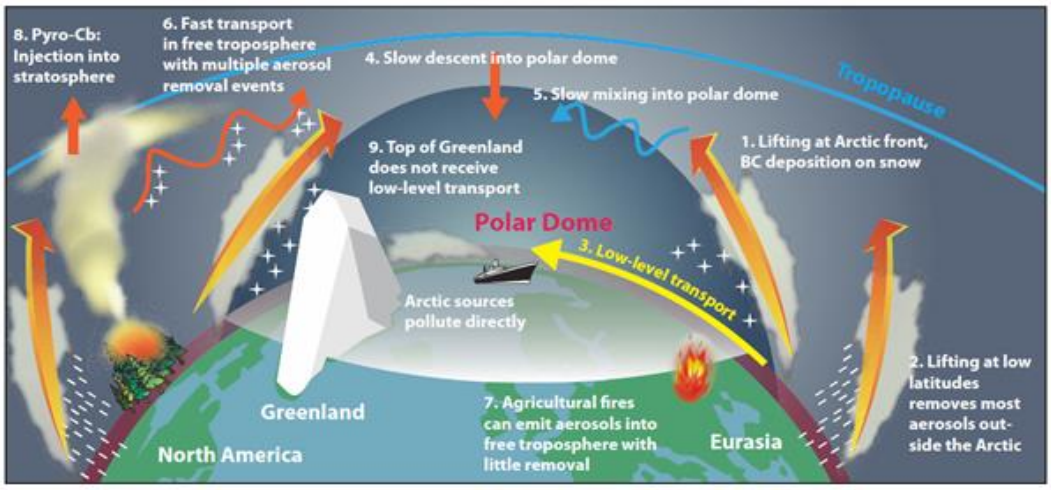


**Figure 2.7** Nine different processes affecting the transport of BC to the Arctic; 1. Lifting at the Arctic front, leading to BC deposition on snow, 2. Lifting at low latitudes, leading to deposition of BC outside the Arctic, 3. Low level transport, 4. Slow descent into polar dome, 5. Slow mixing into polar dome, 6. Fast transport in the free troposphere with multiple aerosol removal events, 7. Agricultural fires, 8. Pyrocumulonimbus cloud (Pyro-Cb) injection into stratosphere, 9. Top of Greenland does not receive low-level transport (AMAP, 2011).

BC emitted in sufficiently cold regions may reach the lower troposphere of the Arctic through low-level transport. This transport pathway is possible from northern Eurasia in winter and early spring where the Arctic front can be located at latitudes as far south as 40˚N and BC may reach the entire Arctic in 10 to 15 days (AMAP, 2011). In summer the Arctic front is located much further north than in winter roughly following the northern coastline of Eurasia. This means that the low altitude transport of BC along this pathway does not occur in summer, which partly explains the much higher BC concentrations in winter (Stohl, 2006; AMAP, 2011).

BC emitted into warm air masses in regions south of the polar dome will be lifted into the middle or upper troposphere above the dome. The lifting will often lead to formation of clouds and precipitation whereby wet deposition of BC in the Arctic may occur. Lifting of air masses from eastern North America and south-eastern Asia will often occur over the North Atlantic or North Pacific storm tracks; hence BC emissions from these regions will often be deposited south of the Arctic (AMAP, 2011). It is more likely that BC emitted in source regions further north (Europe and eastern Asia) will be deposited on snow and ice surfaces, because lifting of these air masses occur at the Arctic front or north of it.

Based on the study by Stohl (2006), AMAP (2011) has identified nine different processes relevant for BC transported to the Arctic (Figure 2.7): 1. lifting at the Arctic front, which may lead to BC deposition on snow and ice; 2. lifting at low latitudes, leading to deposition of BC outside the Arctic; 3. low level transport; 4. slow descent into polar dome; 5. slow mixing into polar dome; 6. fast transport in free troposphere with multiple aerosol removal events; 7. agricultural fires; 8. injection into stratosphere by pyrocumulonimbus cloud (AMAP, 2011). The fires mostly occur in summertime when the BC removal by dry and wet deposition is relatively efficient (Stohl, 2006). 9. Top of

Greenland does not receive low-level transport, due to the high altitude, but is instead connected more directly to transport from lower latitudes.

The transport patterns are affected by the North Atlantic Oscillation (NAO), which should be taken into consideration when looking into the Arctic pollution trends. Transport from both Europe, North America and Asia is enhanced during positive phases of the NAO resulting in higher Arctic pollution levels (Stohl, 2006).

### 2.4.2 Black Carbon Concentrations in the Arctic

Four Arctic stations: Alert, Barrow, Zeppelin and Summit, conduct long-term monitoring of BC concentrations in the Arctic atmosphere. Figure 2.8 presents a comparison of measured and modelled concentrations by DEHM for the four stations in 2008 and 2009. The measured BC concentrations at the four stations are approximately in the range of 0 to 85 ng/m$^3$ with peaking concentrations during winter months. For Alert the model underestimates the concentration in winter 2008 and overestimates the values in winter 2009, while at Barrow the model overestimates the values with up to a factor of six throughout the two years period. The best fit between modelled and measured data is found at Zeppelin (AMAP, 2011). It should be emphasised that the time period is relatively short, which makes it difficult to make any firm conclusion.

Currently there exist no long-term monitoring of BC concentrations in snow but a recent study conducted by Doherty et al. (2010) has investigated the concentration of BC in surface snow in the Arctic during spring and summer from 2005 to 2009. The study is based on individual observations for a specific location and not a time series, hence not reflecting the natural variability of BC. The study comprises 1200 samples from different locations including, Alaska, Canada, Greenland, Svalbard, Norway, Russia and the Arctic Ocean, which were analysed in a spectrophotometer system. The median concentration of BC in surface snow was observed to be in the range of 1 (±1) ng/g in Greenland during summer to 34 (±46) ng/g in Eastern Russia during spring (Table 2.4) (Doherty et al., 2010). The concentrations were converted to ng/l assuming that 1 g of snow corresponds to 1 gram of melt water.

Generally the concentration was found to be lower near the North Pole compared to sites at lower latitudes (Doherty et al., 2010). The eastern Arctic sites (Tromsø, western and eastern Russia) showed concentrations with a factor of two higher than the western Arctic sites (Canadian Arctic). This indicates that emissions from northern parts of Europe and Russia have a stronger influence on reducing the albedo of snow in Arctic compared to emissions from North America (Doherty et al., 2010). The BC concentrations found by Doherty et al., (2010) are lower compared to a survey conducted by Clarke and Noone in 1983 to 1984. It is not clear whether the difference is significant, due to methodological variation and due to a lower sampling size of 60 samples in 1983-1984 (Doherty et al., 2010).

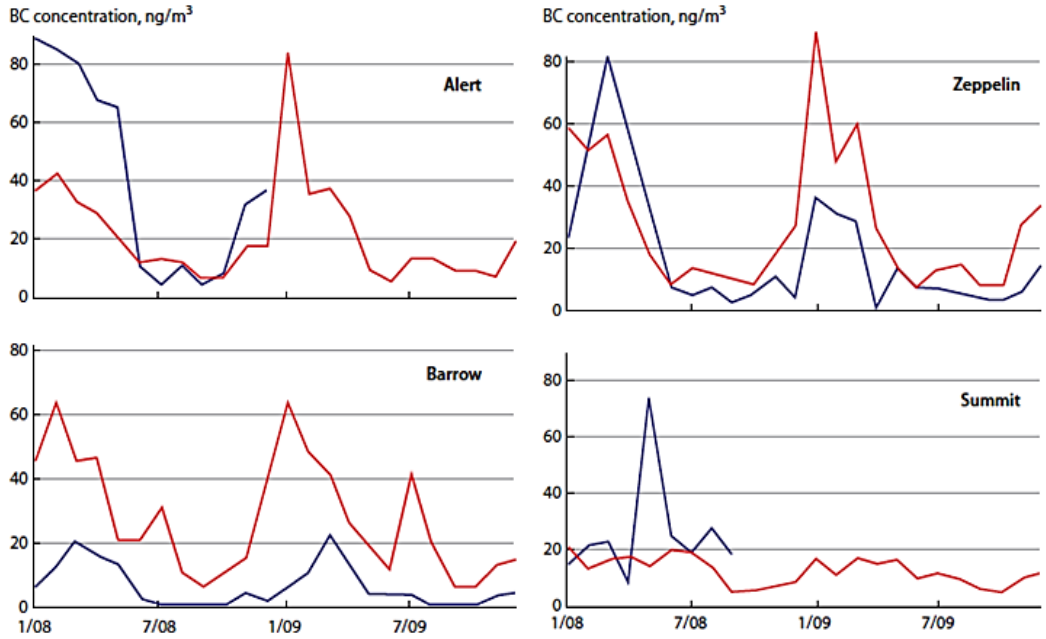


**Figure 2.8** Comparison of measured BC concentration (blue line) and modelled values from DEHM (red line) at four Arctic stations in 2008 and 2009 (AMAP, 2011).

**Table 2.4** Concentrations of BC in snow for ten different Arctic locations during 2005 and 2009 (Doherty et al., 2010). According to Doherty et al. (2010) the definition of the estimated BC concentration ($C_{BC}^{est}$) is the estimated true mass of BC per mass of snow, derived by separating the spectrally-resolved total light absorption into BC and non-BC fractions.

| **Snow samples** | | $C_{BC}^{est}$ **[ng/g]** | $C_{BC}$ **[ng/l]** |
|---|---|---|---|
| **Arctic Ocean, spring** | Median | 7±3 | $7 \cdot 10^3 \pm 3 \cdot 10^3$ |
| **Arctic Ocean, summer** | Median | 8±8 | $8 \cdot 10^3 \pm 8 \cdot 10^3$ |
| **Canadian and Alaskan Arctic** | Median | 8±3 | $8 \cdot 10^3 \pm 3 \cdot 10^3$ |
| **Canadian sub-Arctic** | Median | 14±9 | $14 \cdot 10^3 \pm 9 \cdot 10^3$ |
| **Greenland, spring** | Median | 4±2 | $4 \cdot 10^3 \pm 2 \cdot 10^3$ |
| **Greenland, summer** | Median | 1±1 | $1 \cdot 10^3 \pm 1 \cdot 10^3$ |
| **Western Russia** | Average | 27 | $27 \cdot 10^3$ |
| **Eastern Russia** | Median | 34±46 | $34 \cdot 10^3 \pm 46 \cdot 10^3$ |
| **Svalbard** | Median | 13±9 | $13 \cdot 10^3 \pm 9 \cdot 10^3$ |
| **Tromsø, Norway** | Median | 21±12 | $21 \cdot 10^3 \pm 12 \cdot 10^3$ |

## 2.5 Black Carbon Emission Sources

In order to reduce the climatic impacts of BC by developing reduction strategies, it is important to identify the main sources and geographical regions of emissions that are transported to the Arctic. As previously mentioned Arctic is defined as the region

between 60˚N and 90˚N (AMAP, 2011), hence countries with Arctic territory are the eight Arctic Council nations; Canada, Denmark including Greenland and Faroe Islands, Finland, Iceland, Norway, Russia, Sweden and USA. The total global emission of BC is approximately 8.4 million tons (US EPA, 2009) and the main part of the world's anthropogenic BC emission originates from the northern mid-latitudes and peaks around the 35°N, as illustrated in Figure 2.9 (AMAP, 2011).

BC is produced from incomplete combustion and is emitted from a multiple range of different sources. The emissions originate from the transport sector, shipping sector, domestic sector, and the energy, industrial production and waste treatment sector, together with agricultural burning, biomass burning and gas flaring. Figure 2.9 shows the anthropogenic emissions of BC by latitude and source. Anthropogenic emissions are divided into the aforementioned sectors but do obviously not include natural occurring forest and grass fires. This sectorial aggregation level is sufficient for impact analysis of the different sources but for designing targeted mitigation strategies a finer breakdown is necessary (AMAP, 2011).

The transport sector is one of the biggest contributors to BC production and includes emissions from on- and off-road diesel and gasoline machines and vehicles. In this assessment transport only includes land transport, as shipping is categorized separately and aviation is excluded. The global emissions from aircrafts comprise approximately 0.1% of total emissions. This is a small contribution but future attention on aviation is needed, as some of the major routes go north of 60˚N, where the climatic effects per unit emissions are strong (AMAP, 2011). The BC fraction of diesel $PM_{2.5}$ is around 70-80% whereas for gasoline it is only about 20%. Those fractions vary by operating conditions. The total light absorbing capacity of the emission mixtures in diesel and gasoline exhaust is not known, but several measurements indicate that both kinds of particle emissions are strongly light absorbing (U.S. EPA, 2012). Shipping currently comprises around 4% of the BC emissions north of 60˚N (AMAP, 2011). This is a relatively small amount, but since the emissions occur far north the regional effects on climate are becoming increasingly important (Corbett et al., 2010). Future projections furthermore suggest that in-Arctic shipping will increase if the sea-ice extent and the area of multi-year ice keep decreasing. The Arctic Ocean will become more accessible to shipping and to the potential Arctic resources such as oil, gas and minerals. Shorter sea routes between Asia, Europe and the Pacific may save travel distances of up to 25% and 50% by using the North West Passage and the North East Passage respectively (Corbett et al., 2010).

Emissions from domestic combustion occur due to heating and cooking which mainly include the use of solid fuels like wood and coal. North of 55˚N all domestic combustion is assumed to come from heating, while at lower latitudes cooking is of higher relevance. The combustion is often poor in small domestic heating stoves resulting in high emissions of BC and OC. The domestic heating sector has a higher seasonal variation than other sectors, because heating activities peak during winter in the Northern latitudes. At latitudes between 55˚N and 65˚N, emissions from domestic heating are almost 40 times higher in January than in July, whereas for lower latitude bans the seasonal cycle is less strong (Stohl et al., 2013; AMAP, 2011).

The energy, industrial production and waste sector includes emissions from waste combustion, industrial production and power generation (Stohl et al., 2013; AMAP, 2011). Anthropogenic field burning occurs in areas with high agricultural fire activity where important regions include North America, Eastern Europe, European Russia, Asian Russia, and central and north-eastern Asia (AMAP, 2011). The agricultural burning varies both seasonally and regionally depending on precipitation patterns and different crop conditions (McCarty et al., 2009; AMAP, 2011). Biomass burning includes both natural and anthropogenic grass and forest fires. At Northern latitudes biomass burning is in general considered natural, but anthropogenic burning may be increasing. According to AMAP (2011) flaring, which occurs in the oil and gas industry, is "*a way of discharging and disposing of gaseous and liquid hydrocarbons through combustion at offshore and onshore petroleum prospecting sites, production installations, and refineries."* Several flares are located in the Arctic but there exists no quantitative measure of flaring emissions, which is why gas flaring is not included in Figure 2.9 but (AMAP, 2011).

North of 40˚N and 50˚N anthropogenic BC emissions comprise approximately 24 % and 9 % of the total anthropogenic emissions respectively, while north of 60˚N the fraction of emissions is less than 1 %. Most of the emissions originate from domestic combustion, transport and energy, industrial production and waste. North of 70˚N the emissions are negligible and originate mainly from shipping. The emission data originates from the Representative Concentration Pathways (RCP), which is a source meant to be used as an input for climate and atmospheric chemistry modelling. Different emission models and measurement techniques with unaccounted levels of uncertainty exist and hence differences between results of BC concentrations occur (AMAP, 2011).

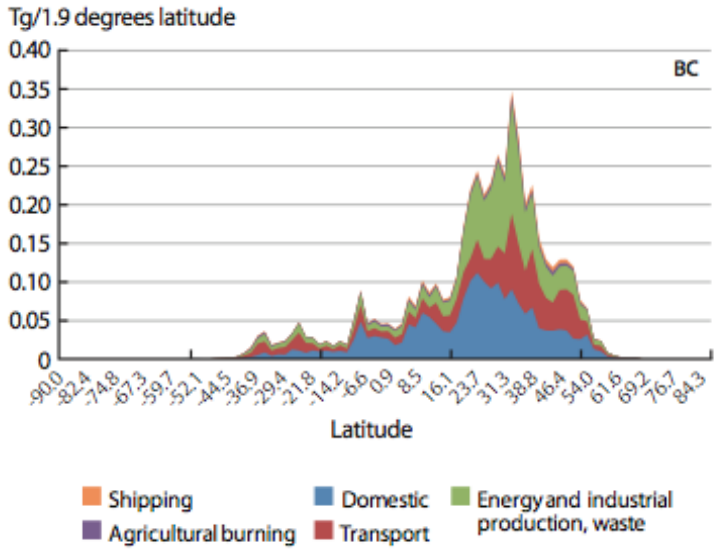


**Figure 2.9** The anthropogenic emissions of BC in 2000 by latitude and source sector (AMAP, 2011)

Most of the BC affecting the Arctic atmosphere is transported there from outside locations, while some is produced within the region, e.g. from shipping (Arctic Council, 2011). Figure 2.10 (left) shows that the absolute radiative forcing in the Arctic is caused mainly by emissions originating from Russia and the rest of the world. This goes for both direct atmospheric forcing and forcing caused by BC and OC deposited on snow and ice. The emission results are obtained from the Community Climate System Model developed by the National Center for Atmospheric Research. Especially grass and forest fires together with domestic combustion, transport, energy, industrial and waste cause high radiative forcing. The quantities of BC emissions in Russia and the rest of the world are much higher than in US, Canada and the Nordic countries (Denmark, Finland, Iceland, Norway, Sweden), and hence cause the largest absolute radiative forcing. In order to develop cost effective mitigation strategies, it is of great interest to look into the radiative forcing caused per unit BC emission (normalized radiative forcing). Figure 2.10 (right) shows that BC emissions occurring in the Nordic countries and from open biomass burning in Canada and Russia yield the highest normalized radiative forcing. That is, BC emitted close to or within the Arctic region has larger effects on climate per unit emission than BC emissions located further away from the Arctic (AMAP, 2011). This can partly be explained by the Arctic front, which isolates the Arctic from the rest of the atmosphere and acts as a transport barrier. The southernmost boundary of the Arctic front is approximately located at 40˚N in January (Law & Stohl, 2007).

Emissions north of 40˚N latitude, which pass over Europe, the United States and Asia, are assumed to affect the Arctic atmosphere significantly due to the short atmospheric lifetime of BC and the Arctic front. The further north the emissions occur, the more dominant is the effect on the radiative forcing per unit emission. BC emissions originating from regions south of 40˚N have less potential of being transported to the Arctic and have a smaller effect on the radiative forcing per mass unit. BC emissions originating from Arctic Council nations only make up 10 % of the total emissions globally, but 40 % of the emissions north of 40˚N, almost 60 % of the emissions north of 50˚N and close to 99 % of the emissions north of 60˚N (Arctic council, 2011). The focus in the following session is therefore put on emission sources in the Arctic council nations, because there is a potential for cost effective mitigation options due to the great normalized forcings (AMAP, 2011).

### 2.5.1 Arctic Council Nations

Data from three different inventories estimating the sectoral distribution of anthropogenic BC emissions in the Arctic Council nations in 2000 are compared (Figure 2.11). The sector called ‘other’ includes cigarette smoking and barbeques, which could not be classified into any of the aforementioned sectors. The inventory ‘Bond’ is a BC and OC inventory as presented in ACTFSLCF (Arctic Council Task Force on Short-Lived Climate Forcers), whereas the ‘AMAP emission inputs’ is data from the RCP database. The ‘GAINS’ emission data (Greenhouse Gas and Air pollution Interactions and Synergies) is calculated with the model from International Institute for Applied Systems Analysis (AMAP, 2011).

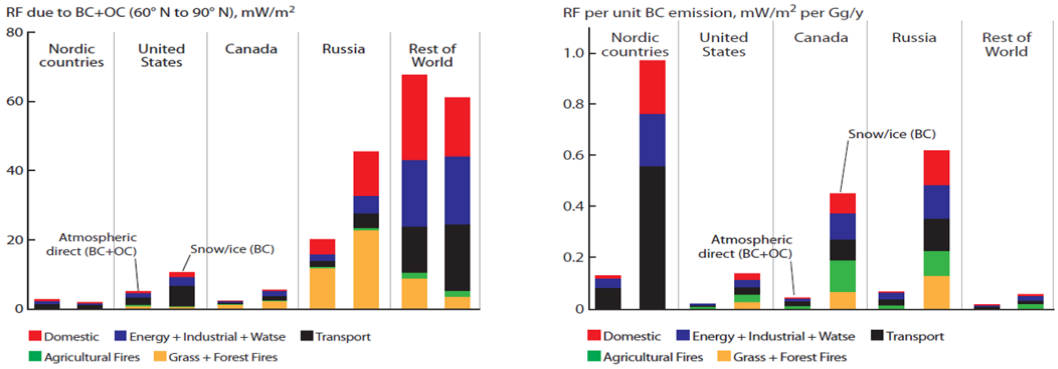


**Figure 2.10 Left:** Absolute radiative forcing in the Arctic (60˚N to 90˚N) from direct atmospheric BC and OC and from snow deposited BC and OC by sector and geographical region. **Right:** Normalized radiative forcing in the Arctic (60˚N to 90˚N) from direct atmospheric BC and OC and from snow deposited BC and OC by sector and geographical region. Results are obtained from the Community Climate System Model (AMAP, 2011).

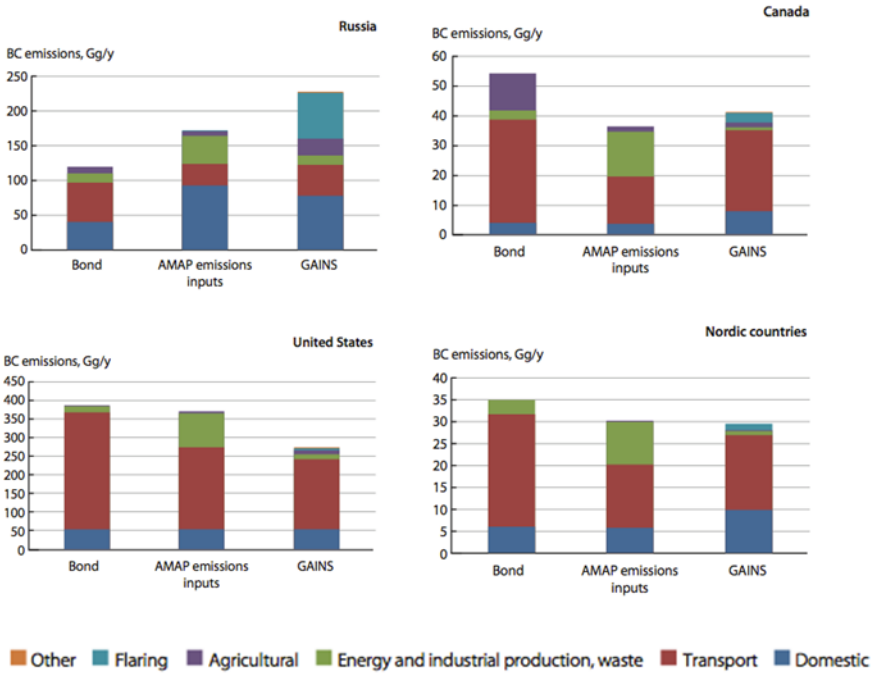


**Figure 2.11** Comparison of Bond, AMAP and GAINS inventories estimating the sectoral distribution of BC in Russia, Canada, United States and the Nordic Countries (Denmark, Finland, Iceland, Norway, Sweden) in 2000 (AMAP, 2011).

Figure 2.11 shows that the United States and Russia are the largest contributors of BC emissions; 61 % and 28 % respectively. It should be kept in mind though, that a big part of the United States is located south of 40˚N and that only 40% of the BC emissions originate from north of this latitude. Canada and the Nordic countries (Denmark, Finland, Iceland, Norway, and Sweden) together emit 11%. There is agreement among the three inventories that in all the countries the most emitting sectors are transport, domestic combustion and energy, industry and waste. Especially in the United States, Canada and the Nordic countries the major emitting sector is transport. There are differences in the

distribution of the sectoral emissions and the total amounts among the inventories. This may be due to differences in background data such as emission factors and fuel use estimates. Also, what is included in the different sectors plays a role. In the RCP database used by AMAP (2011) diesel fuel consumed by tractors and in machinery is included in the industry sector, whereas the two other inventories include this in the transport sector. GAINS is the only inventory, which includes BC emission estimates from gas and oil flaring. Although the data source is limited, the estimate indicates that it is an important sector, especially in Russia, which might contribute up to 12 % of the total BC emissions in the Arctic Council Nations. Agricultural burning is another relatively important emission source in Russia according to GAINS and also in Canada when looking at the Bond estimates (AMAP, 2011).

# 3 Methods

All measurements in this study were carried out at the Danish military station, Station Nord in north-east Greenland. BC was measured in the air and EC was measured both in air and snow. In order to measure EC in air filters from a high volume sampler (HVS) were analysed using an OC-EC analyser at Aarhus University, Department of Environmental Science (AU-ENVS). This instrument was also use to determine the EC concentrations in snow samples collected at Station Nord. A PSAP continuously measured the absorption of particles collected on a filter from where BC concentration in air was estimated. The measured air concentrations of BC and EC were compared to modelled BC concentrations, which were modelled by J.H. Christensen using the DEHM. A PMF model was run in order to determine the source apportionment for BC. The measurement site, the applied instruments and methods is fully described in this section.

## 3.1 Measurement Site - Station Nord

Station Nord was established in 1952 in collaboration between the United States and Denmark. The U.S. needed an alternative runway in order to carry out their flight patrols over the Arctic Ocean and the Soviet Union. Today Station Nord's main function is to maintain Danish sovereignty over the area (Mikkelsen, 2006). The station is located approximately 30 meters above sea level on Prinsesse Ingeborg Peninsula in the northern part of Kronprins Christian Land, at 81°36'North, 16°40'West (Nguyen et al., 2013) in a distance of 933 kilometres from the North Pole (Figure 3.1). At this latitude the polar night exists from mid-October to the end of February when the sun rises. The polar day lasts from the middle of April to the beginning of September. The dominating local wind direction is from south-west, and the highest wind velocities come from south-western and north-western directions (Nguyen et al., 2013).

The majority of the measurements were carried out 2.5 km south-east from the station at Flyger's Hut (Figure 3.2). This monitoring site is the main Danish contribution to the atmospheric part of the Arctic Monitoring and Assessment Programme (AMAP). Since 1990 measurements have been carried out at Station Nord and from 1994 as part of AMAP (Nguyen et al., 2013). At Flyger's Hut, $O_3$, $NO_x$, CO, Hg and BC are routinely measured and filter samples for analysis of elements (from Al and higher), $Cl^-$, $Na^+$, $NO_3^-$, $SO_4^{2-}$ and $NH_4^+$ are collected. Furthermore, snow samples are collected on regular basis and measurements of temperature, wind direction, wind speed and height of clouds are carried out (B. Jensen, Laboratory Technician, AU ENVS, pers. comm., April 2013). The remote location of Flyger's Hut has been chosen because it is assumed that the local air pollution from Station Nord is minimal (Heidam et al., 2004). Another measurement site

located at the station is the DMI Hut, where a HVS is used to measure particles and gaseous components (B. Jensen, Laboratory Technician, AU ENVS, pers. comm., April 2013).

**Figure 3.1** Map of Greenland (Walkowiak, 2013), where Station Nord is located on Prinsesse Ingeborg Peninsula on Kronprins Christians Land (Heidam et al., 2004).

**Figure 3.2** Left: The monitoring station, Flyger's Hut, located 2.5 km south-east of Station Nord. Right: The DMI Hut located at the station.

## 3.2 Sampling Overview

An overview of the different samples taken at Station Nord in the period from August 2008 to April 2013 is provided in Table 3.1. The table includes the applied measurement instrument and analysis method together with the sampling frequency, sampling period, total sample quantity and location of the measuring instrument for each compound. Figure 3.3 shows the average wind direction on Station Nord and provides an overview of the location of the station and the runway, Flyger's Hut (2.5 km S.E. of the station), Knuths Fjeld (7 km S.E. of the station) and the icebergs (2 km N.W. of the station).

**Table 3.1** Measurement instrument, analysis method, sampling frequency, sampling period, total sample quantity and location for each compound measured at Station Nord in the period from August 2008 to April 2013.

| Compound | Measuring instrument | Analysis method | Sampling frequency | Sampling period | Total sample quantity | Location of measuring instrument |
|---|---|---|---|---|---|---|
| **BC – air** | PSAP | - | 15 min. | August 2008 – April 2013 | 159,055 | Flyger's Hut |
| **EC – air** | HVS | OC-EC analyser | 7 days | August 2008 – April 2013 | 178 | Station Nord (DMI Hut) |
| **EC – snow** | Manual sampling | OC-EC analyser | 1 day | April 2013 | 30 | Station Nord, Flyger's Hut, Knuths Fjeld, and Icebergs |
| **Al, Si, S, K, Ca, Ti, V, Cr, Mn, Fe, Ni, Cu, Zn, Ga, As, Se, Br, Rb, Sr, Zr, Pb, $SO_2$, $SO_4^{2-}$, $Na^+$, $NH_4^+$, $NH_3$, $NO_3^-$ $HNO_3$, $Br^-$, $Cl^-$** | FPS | PIXE, IC PMS, Anion IC, Ion Chromato-graphy, Autoana-lyser | 7 days | January 2008 – December 2012 | 193 | Flyger's Hut |

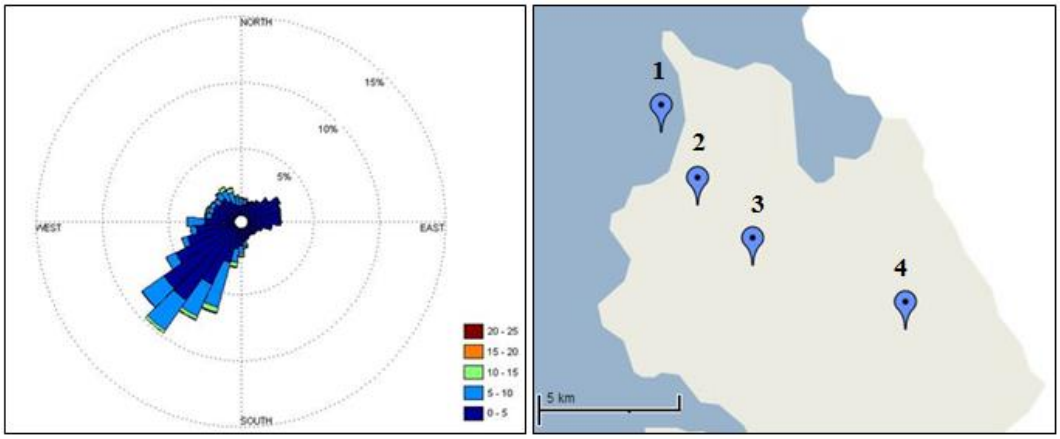


**Figure 3.3** Left: Windrose showing local wind directions at Station Nord from April 2011 to April 2013. Right: 1. The icebergs, 2: Station Nord and the runway, 3: Flyger's Hut, 4: Knuths Fjeld.

**Figure 3.4** The HVS in the DMI Hut at Station Nord. From left: The HVS inlet (1), The pump (3), The HVS with particle separator (2), The HVS filter (4), PUF/XAD (5), Flow meter (6).

## 3.3 Sampling of EC and OC in Air

Air sampling was carried out using a DIGITEL High Volume Sampler of the type DHA-80 installed in the DMI monitoring Hut. The HVS is used to sample airborne particles for further analysis including OC, EC and persistent organic pollutants. Figure 3.4 presents the HVS. Inside the DMI Hut there is a pump (3), which draws air through an inlet on the rooftop (1) with a flow of 500 L/min. The air flow is conducted into a particle separator chamber ($PM_{10}$ head) (2), where all particles larger than 10 µm in diameter (> $PM_{10}$) are separated from the airstream and held back. The air then flows through a pre-cleaned quartz filter, which has been heated to 250 ºC. The filter has a diameter of 150 mm where the exposed part has a diameter of 140 mm (4). Downstream of the filter the air flows through a sequence of polyurethane foam (PUF), a layer of polymeric absorbent (XAD) and another PUF, where gases are collected (5). The filter and the PUF sequence is changed manually once a week and the filters are packed in tinfoil. The total air mass flown through the filter and the PUF is 5040 $m^3$ after one week. After the PUF sequence, the airflow is measured with a calibrated flow meter (6) and the capacity of the pump is adapted so the flow stays constant (Aufschnaiter, 2007; B. Jensen, Laboratory Technician, AU ENVS, pers. comm., April 2013). Weekly filter samples from the HVS were analysed for EC and OC in the period from August 2008 to April 2013, comprising 178 samples in total.

## 3.4 Sampling of EC in Snow

Snow samples were taken ten times at Station Nord in triplicates from the 8$^{th}$ to 21$^{st}$ of April 2013. The plan was to take samples of fresh snow every day there had been a snow fall. Due to very little precipitation during this period the snow samples were not fresh, however, triplicates were taken seven days near Flyger's Hut in order to have as many

samples as possible. Samples were also taken once near the runway to examine the EC contamination from the airplane, which was landing and taking off twice a day at Station Nord during the sampling period. Additionally, samples were collected once approximately 7 km south-east of the station at Knuth's Fjeld and once 2 km north-west of the station near the icebergs (Figure 3.3). This was done in order to test the assumption that local pollution from the station is minimal around Flyger's Hut and also to check if the contamination from the airplane was higher near Flyger's than at Knuth's Fjeld or near the icebergs. Student's t-test was used to test whether the measurements at the runway, near the icebergs, and at Knuth's Fjeld were significantly different from the measurements near Flyger's Hut at a significance level of 0.01. In Appendix 1 extended information on sampling dates, sample sizes and locations of the collected snow samples can be found.

Three replicates were made during each sampling within a radius of 3 meters. The shovel and three 20 L milk cans were cleaned with acetone before the first samples were taken. Each milk can was filled with snow corresponding to 3 to7 L melt water. The collected snow was taken from the upper 5 cm in order to analyse the most recently fallen snow. The samples were taken in headwind to minimise the contamination from the person collecting the snow. The milk cans were subsequently mounted on the walls inside Flyger's Hut, so the snow would melt and run through the outlets in the bottom of the milk cans. To each milk can a tube was connected to the outlet to lead the melt water through a 47 mm pre-cleaned quartz filter where downstream of the filter the water was collected in a 5 L plastic bottle. In order to determine the concentration of EC in the snow, the amount of melt water in the bottles was measured. The filters were put on pins to dry, before they were packed in tinfoil and brought back to the laboratory at AU-ENVS to be analysed for EC. Figure 3.5 shows the experimental setup.

The snow samples were taken in April, where an aircraft flew to and from Station Nord with fuel from Thule twice a day. Pollution from this airplane and from local traffic such as snowmobiles may have contributed to the EC contamination. During snow collection and filter drying minor EC contamination may also have occurred.

At AU-ENVS a control experiment was set up in order to correct for EC background contamination in the experimental setup and instrumental analysis potentially affecting the measurements. The experiment included three replicates where a 20 L milk can, identical to the ones used at Station Nord, was cleaned with acetone, before it was filled with Milli-Q water. The milk can was placed on a table, so the water could run through the outlet in the bottom of the can. As on Station Nord a tube was connected to the outlet of the milk can to lead the melt water through a 47 mm pre-cleaned quarts filter where after the water was collected in a plastic bottle. The exact amount of water in the bottle was measured whereupon the filters were put on pins to dry and afterwards packed in tinfoil.

**Figure 3.5** From top left: Taking surface snow samples at Station Nord; experimental setup inside Flyger's Hut; filters drying on pins; filter container used in experimental setup.

## 3.5 OC-EC analyser

The snow samples, including control samples, and the weekly air filter samples from the HVS were analysed for OC and EC using an OC-EC analyser from Sunset Laboratory. The OC-EC analyser is a thermal-optical technique in the sense that the OC-EC speciation is obtained through temperature control and pyrolytically generated EC is corrected for by use of an optical feature (Birch & Cary). The instrument consists of a sample oven, an oxidizer oven, a methanator and a laser diode continuously shooting light through a filter sample (Figure 3.6). The analysis is divided into two parts; in the first part the concentration of OC is determined whereas the second part determines the concentration of EC (Sunset Laboratory, 2009). Quartz filters are used in the OC-EC analyser in order to withstand the high temperatures occurring during the analysis (Sunset Laboratory, 2009). The instrument output is a thermogram showing the temperature, the light transmission through the filter and the flame ionization detector (FID) response (Figure 3.7).

The lower detection limit of mass concentration on the filter is 0.2 µg/cm$^2$. For this reason filters must be pre-cleaned by heating at 700 ˚C for approximately one hour to remove any background contamination since new quartz filters otherwise hold an OC concentration of 2 to 5 µg/cm$^2$. The best concentration range for the analysis is 5-400 µg/cm$^2$ for OC and 1 to 15 µg/cm$^2$ for EC. The relative standard deviation of the instrument is typically 4 to 6 % when the concentrations fall into those ranges. The presence of non-absorbing inorganics and coloured organic and inorganic compounds are not assumed to cause any considerable effect on the OC-EC analysis (Birch & Cary, 1996; Sunset Laboratory, 2009).

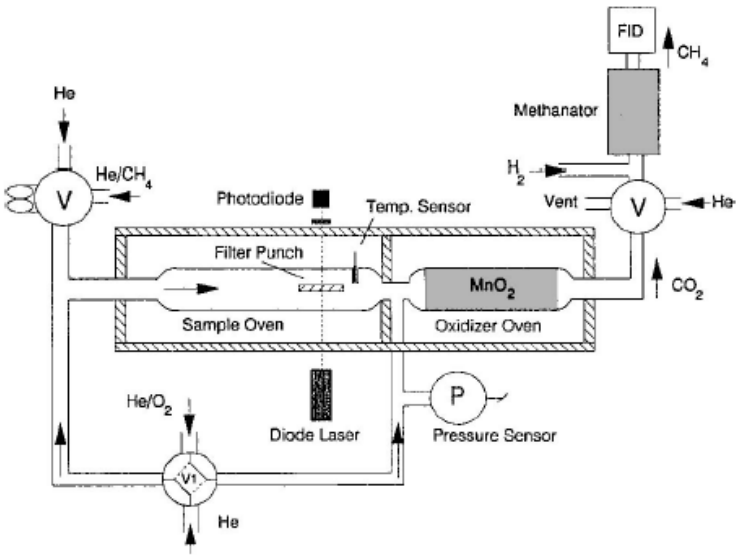


**Figure 3.6** Conceptual drawing of the OC-EC analyser showing the sample oven, the oxidizer oven, the methanator and the diode laser (Birch & Cary, 1996).

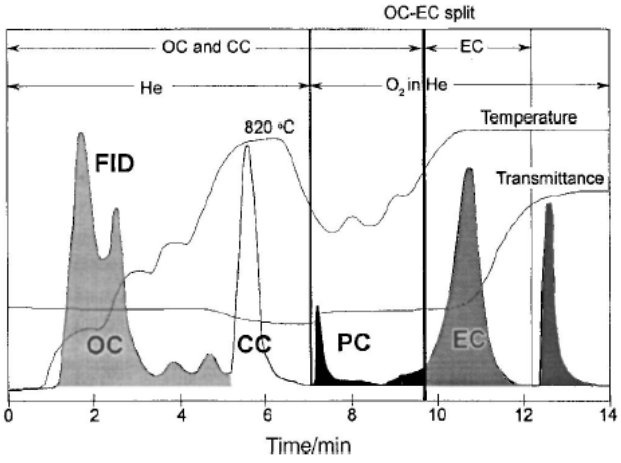


**Figure 3.7** Thermogram showing temperature, transmittance, detector (FID) response and the OC-EC split. The peaks (from left to right) in the detector response curve correspond to OC (organic carbon), CC (carbonate carbon), PC (pyrolytic carbon), EC (elemental carbon) and methane calibration (Birch & Cary, 1996).

### 3.5.1 Procedure

Every time the OC-EC analyser is started the different airflows should be set according to Table 3.2. Hydrogen is initially set to100 cc/min in order to ignite the flame in FID and is subsequently adjusted to 52-55 cc/min. When the airflows have been adjusted a blank sample is inserted into the instrument, which is hermetically sealed. Thereafter a sample with a known mass of sucrose is analysed in order to check the calibration of the

instrument. If the sucrose analysis results in an OC mass of 42.5 ± 2 µg, the instrument is ready for use.

From the samples a small filter punch is placed in the sample oven and the sample is heated in a pure helium atmosphere during the first part of the analysis. All OC and carbonate carbon (CC) (if present) is volatilized from the sample, as the temperature increases in four steps to about 820˚C. The detection of OC and CC is shown in the thermogram as the two first peaks (Figure 3.7) (Birch & Cary, 1996). Up to 30% of the OC may be converted into EC through pyrolysis. The laser diode transmits light through the filter which is measured continuously. The formation of pyrolytically generated EC (pyrolytic carbon, PC) causes a decrease in the light transmission and PC is in this way monitored (Sunset Laboratory, 2009). The volatilized carbon is oxidized to $CO_2$ in the oxidizer oven, which is held at about 900˚C, and subsequently reduced to $CH_4$ in the 450˚C methanator (Birch & Cary, 1996). The $CH_4$ enters the FID where it is burned in a hydrogen flame within an electric field. This gives rise to an ion current, which is proportional to the number of carbon atoms and thus the mass of the detected methane (Bruner, 1993).

In the second part the sample oven is cooled to 525˚C and an oxygen-helium mix is introduced. The temperature is then increased to 850˚C and due to the presence of oxygen both the originally EC and the PC is oxidized to $CO_2$. As in the first part the evolved $CO_2$ is reduced to $CH_4$, which is measured by the FID (Sunset Laboratory, 2009). The light transmittance through the filter increases as the EC and PC is oxidized. The point where the filter reaches its initial transmittance value is called the OC-EC split and is illustrated as the vertical line on the thermogram. The carbon volatalized before this point is considered OC and the carbon evolved after the peak is considered EC. This way the instrument corrects for the PC generated from the OC during the first part of the analysis (Birch & Cary, 1996). The OC-EC measurements are calibrated by injection of a known concentration and volume of methane into the sample oven. The detector response is then displayed as shown in Figure 3.7 with time [min] on the x-axis and concentration [µg-C/cm$^2$] on the y-axis (Birch & Cary, 1996).

**Table 3.2** Airflow ranges in the OC-EC analyser.

| **Gasses** | **Airflow range [cc/min]** |
|---|---|
| Air | 280-300 |
| Hydrogen | 52-55 |
| $He_1$ | 52-56 |
| $He_2$ | 12-15 |
| $He_3$ | 67-70 |
| He/Oxygen | 12-15 |
| Cal. Gas | 10-15 |

### 3.5.2 Data Processing

When the filter punches from the air samples were analysed, the area sizes being either 1.5 $cm^2$ or 2.5 $cm^2$ had to be typed into the program, and the output from the OC-EC analyser was given as µg EC or OC per $cm^2$ filter. The radius of the filter area, which is flown through with air is 7 cm. The total concentration on the filter $Conc_{Filter}$ is calculated using the area:

$$A_{Filter} = \pi \cdot 7cm = 154\ cm^2 \tag{3.1}$$

$$Conc_{Filter}[ug] = EC\ or\ OC_{Conc}\left[\frac{ug}{cm^2}\right] \cdot 154\ cm^2 \tag{3.2}$$

During one week 5040 $m^3$ air is flown through the filter, and the EC and OC air concentrations are then calculated by:

$$Air_EC\ or\ OC_{Conc}\left[\frac{ng}{m^3}\right] = \frac{Conc_{Filter}[ug]}{5040m^3} \cdot 10^3\left[\frac{ng}{ug}\right] \tag{3.3}$$

When the snow samples were examined the whole filter was used. Independently of the filter punch area, 1 $cm^2$ was typed into the program to get the absolute EC concentration. The absolute concentrations of each punch area were added up $Conc_{Filter}$ and divided by the volume of melt water $V_{melt\ water}$, which had run through the filter.

$$Snow_EC\ _{Conc}\left[\frac{ng}{L}\right] = \frac{Conc_{Filter}[ug]}{V_{Melt\ water}\ [L]} \cdot 10^3\left[\frac{ng}{ug}\right] \tag{3.4}$$

### 3.5.3 Uncertainty

The uncertainties of the OC-EC measurements are given in the output file calculated from following formula:

$$Uncertainty = 0.05 * EC\ or\ OC_{conc}\left[\frac{ug}{cm^2}\right] + 0.2 \tag{3.5}$$

The 0.05 is the standard deviation of the sucrose samples with known sugar concentrations and the 0.2 is the estimated uncertainty due to unavoidable contamination when handling a blank filter (RTI, 2009).

### 3.5.4 Quality Control

After the analysis of the samples in the OC-EC instrument a quality control of the split points was made. The quality control was conducted both for the samples analysed in this study and also for the samples analysed by Grube (2011). Due to hysteresis on the laser graph, the determination of the point where the filter reaches its initial transmittance value may not always be correct. Especially when analysing the samples with very low

EC concentrations it can be hard to differentiate between the small decrease followed by a subsequent increase on the laser graph and the general hysteresis – also for the instrument. Wrong placement of the splitpoint will result in either too low or too high concentrations of EC and vice versa for OC. Therefore a deeper look on the thermograms with low EC concentrations were necessary in order to determine whether the OC-EC analyser had placed the split point correct.

### 3.5.5 Air Samples

The filter samples to be analysed for OC-EC from the HVS were taken in the period from March 2011 to April 2013. The filters were folded, packed in tinfoil and stored in Rilsan bags by the crew working at Station Nord, from where they were sent to AU ENVS. At AU ENVS the filters were stored at -18 ˚C until the analysis was made. Typically a filter punch of 1.5 $cm^2$ is analysed (Sunset Laboratory, 2009), but filter punches of 2.5 $cm^2$ were made to ensure sufficient sample mass, due to the lower concentrations at a high Arctic location (Figure 3.8, left side). The filter deposit was assumed to be homogenously distributed, which was confirmed by inspection.

Filter samples from August 2008 to February 2011 were already analysed for OC-EC in a study conducted by Grube (2011) and those results were also used in the further data analysis of this project. Quality control of the analysis results was conducted in this study for the entire period from August 2008 to April 2013.

### 3.5.6 Snow Samples

The filters from the snow sampling were dried, packed in tinfoil and stored in Rilsan bags at -18 $^oC$ before the EC analysis. From the snow samples the whole filter was used for analysis due to uneven distribution of contaminant and because of the expected low EC concentrations for samples taken so far north. The filters were cut in pieces of similar colour depending on the distribution of the sample (Figure 3.8, right side). This was done to minimize the error from the correction of pyrolytically converted EC.

**Figure 3.8** Left: Air sample filter punch is inserted into the OC-EC analyser. Right: Filter punch from the snow samples.

## 3.6 Sampling of BC in Air by PSAP

Air sampling of BC was carried out using a PSAP. The PSAP is an instrument, which measures the light intensity that passes through a filter, where a given volume of air has been sucked through. The instrument derives the absorption of particles from the change in transmission of light through the filter, on which the particles are collected (Bond et al., 1999). The PSAP applied in this study is custom-built by Stockholm University and located at Flyger's Hut at Station Nord. A schematic drawing and a picture of the PSAP are presented in Figure 3.9.

The PSAP consists of five different sections, as indicated in Figure 3.9; a light source (1), a filter (2), two light detectors (3), an amplifier (4) and a pump (5). The light source is a light emitting laser diode that operates at a wavelength of 550 nm. Two mirrors split the light beam into two different directions, after which they hit a filter. On one path (left side of the schematic drawing in Figure 3.9) the light beam hits a filter where particles from the ambient air are collected on a filter spot area with a diameter of 2.86 mm. On the other path (right side of the schematic drawing in Figure 3.9) the light beam hits a particle-free part of the filter, in order to correct for possible variations in incident light intensity together with potential drift in electronics (Weingartner et al., 2003).

The light transmissions through the filter are monitored by two separate light detectors, which subsequently convert the transmission to voltage. The signal from the particle-loaded filter spot and the particle-free part of the filter is referred to as *the signal* and *the reference signal*, respectively. An amplifier enhances the voltage signals, after which an analogue digital converter changes the voltage signal to a digital signal that can hence be read by a computer (Grube, 2011). The light absorption by the particles can be determined from the voltage signals and is referred to as the absorption coefficient.

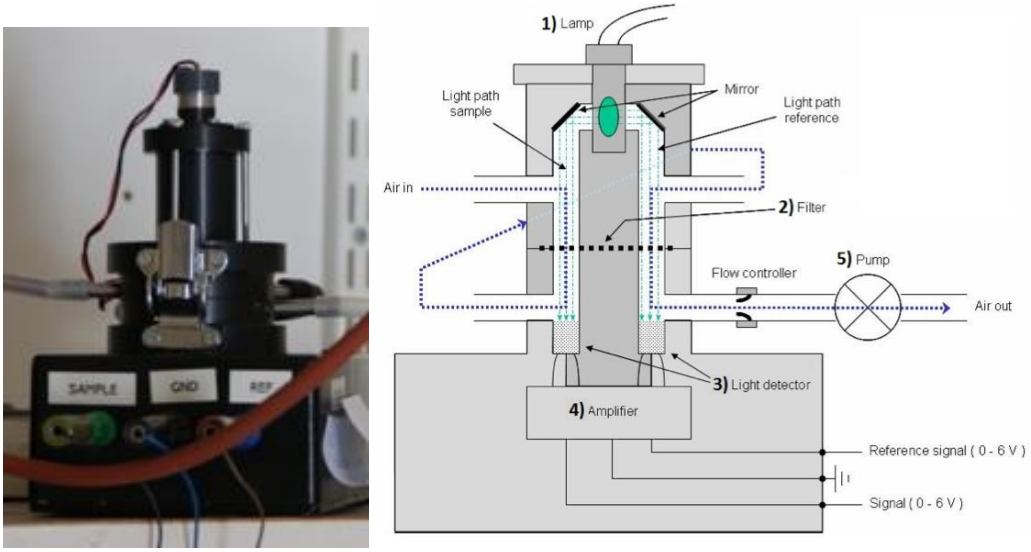


**Figure 3.9** Left: The PSAP in Flyger's Hut. Right: Schematic drawing of the cross-section of a PSAP, consisting of a light source and two mirrors (1), a filter (2), two light detectors (3), an amplifier (4) and a pump (5) (Drawing: Bjarne Jensen, AU-ENVS).

A pump and a critical orifice in the system measure the airflow with less than 1 % uncertainty (Sensidyne, 2005). The flow rate is kept relatively low to prevent top layering of particles on the filter, which potentially could result in a misleading absorption. Despite the low flow rate the filter will at some point be too loaded with particles and it is hence occasionally necessary to manually turn the filter so that a clean filter spot area with a diameter of 2.86 mm is used (referred to as a filter change). Every second, the PSAP generates a signal, which is averaged over a time interval of fifteen minutes and the data is sent via satellite connection to AU-ENVS (Grube, 2011). The flow is measured a few times per year.

### 3.6.1 Quality Control of PSAP data

Quality control of the output from the PSAP, which consists of a voltage signal and a reference signal with a time resolution of 15 minutes, was performed in order to exclude measurements influenced by instrumental errors and possible local pollution. The signal should theoretically only decrease over time due to accumulation of particulate matter on the filter. The reference signal on the other hand should remain constant since no light absorption of particles occurs on this part of the filter. This is not the case in reality where small fluctuations in the reference signal are observed due to instrumental noise. Both signals should not fall below a certain threshold limit of 3.5 V, since this is a reasonable value from which noise can be distinguished. The flow is typically measured in parallel with a filter change, which is done manually a couple of times a year. However, the flow is not necessarily measured every time and can hence remain constant through multiple filter changes. In between two filter changes (referred to as a filter period) a decrease in the signal is generally observed together with a relatively constant reference signal. In the beginning of a new filter period the signal and reference signal should start at nearly the same voltage signal. When this is not the case, it may be due to differences in thickness of the filter, which can influence the measurement. Additionally, the difference between the starting voltages after filter change may be influenced by the efficiencies of the light detectors (B. Jensen, Laboratory Technician, AU ENVS, pers. comm., April 2013).

Periods with a lot of negative noise may cause negative absorption coefficients. There is however also positive noise occurring on the instrument leading to positive absorption coefficients not caused by BC. The negative noise measurements and thereby the negative absorption coefficients have therefore not been excluded, since this would result in misleading high BC concentrations. Only measurements assumed to be caused by instrumental error and local pollution was excluded.

### 3.6.2 Calculation of BC concentration

Beer-Lambert's law describes the light intensity decrease as a function of the absorption coefficient $\sigma_{abs}$ of a medium the light has to pass through as illustrated in Figure 3.10 (Weingartner et al., 2003):

$$I = I_0 \cdot e^{-\sigma_{abs} \cdot x} \tag{3.6}$$

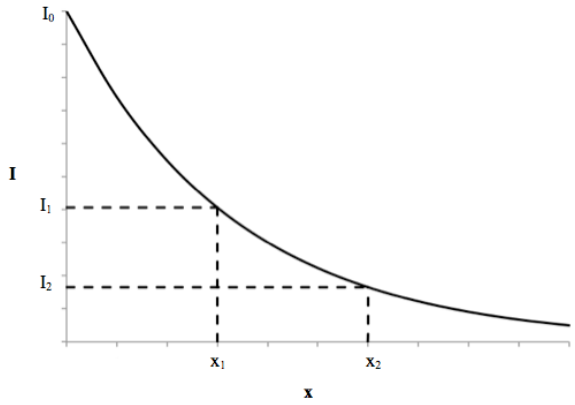


**Figure 3.10** Illustration of Beer Lambert's Law showing an exponential decrease in light intensity ($I_1$ to $I_2$) caused by an increase in thickness of the medium ($x_1$ to $x_2$). $I_0$ is incoming light intensity with no medium present.

Where $I_0$ is the intensity of the incoming light, I is the light intensity after passing through a medium with thickness x. The intensities after passing through a medium with thickness $x_1$ and $x_2$ are hence given by:

$$I_1 = I_0 \cdot e^{-\sigma_{abs} \cdot x_1} \text{ and } I_2 = I_0 \cdot e^{-\sigma_{abs} \cdot x_2}$$

$I_0$ is isolated and the equations are set equal:

$$\frac{I_1}{e^{-\sigma_{abs} \cdot x_1}} = \frac{I_2}{e^{-\sigma_{abs} \cdot x_2}} \tag{3.7}$$

The expression is simplified to:

$$I_2 = I_1 \cdot \frac{e^{-\sigma_{abs} \cdot x_2}}{e^{-\sigma_{abs} \cdot x_1}} \leftrightarrow \tag{3.8}$$

$$I_2 = I_1 \cdot e^{-\sigma_{abs} \cdot \Delta x} \leftrightarrow \tag{3.9}$$

$$I_2 = I_1 \cdot \frac{1}{e^{\sigma_{abs} \cdot \Delta x}} \leftrightarrow \tag{3.10}$$

$$\ln\left(\frac{I_1}{I_2}\right) = \sigma_{abs} \cdot \Delta x \leftrightarrow \tag{3.11}$$

$$\sigma_{abs} = \frac{1}{\Delta x} \cdot \ln\left(\frac{I_1}{I_2}\right) \tag{3.12}$$

Since it is not possible to measure the thickness of the medium in the case of the PSAP, Δx is expressed by the ratio of the volume of air (drawn through the filter area) and the filter area during a given time period:

$$\Delta x = \frac{V}{A} = \frac{Q \cdot \Delta t}{A} \tag{3.13}$$

Where V is the volume of air [ml], A is the filter spot area [$mm^2$], Q the flow rate [ml/min], and Δt the time period [min]. The intensities are expressed as the detected signal S [V] divided by the detected reference signal $S_r$ [V] in order to correct for variations of light intensity and drift in electronics (Weingartner et al., 2003). This equation does not account for any absorption by the filter medium, thus Bond et al. (1999) found a filter calibration constant ($C_{filter}$) of 2, which is also applied in this study. The absorption coefficient [$m^{-1}$] can then be determined as:

$$\sigma_{abs} = \frac{A}{C_{filter} \cdot Q \cdot \Delta t} \cdot \ln\left(\frac{\left(\frac{S_1}{S_{1r}}\right)}{\left(\frac{S_2}{S_{2r}}\right)}\right) \tag{3.14}$$

It is assumed that the absorption is only caused by BC. The BC concentration can thus be found since there is a linear relation between the absorption coefficient and the BC concentration (Petzold and Niessner, 1995):

$$C_{BC} = \frac{\sigma_{abs}}{\sigma_{specific}} \tag{3.15}$$

Where $C_{BC}$ is the BC concentration [$\mu g/m^3$] and $\sigma_{specific}$ the specific absorption coefficient of BC [$m^2/g$]. In order to investigate whether there can be shown any seasonal variations in the concentrations of BC at Station Nord the average monthly concentrations and standard deviations over the entire period are calculated. Variations in the average annual concentrations are also investigated.

As given in equation 3.15 the specific absorption coefficient is a conversion factor, which is used to convert the light absorption from the PSAP to an actual BC mass concentration. The specific absorption coefficient is found as the slope of the linear regression between the monthly absorption coefficients and the average monthly EC concentrations (Petzold and Niessner, 1995). In this study the specific absorption coefficient for BC on Station Nord is determined based on measurements for the entire period. It is also investigated whether there is a linear correlation between the measured absorption coefficients and the EC concentrations for each year, the winter months (December to February), and the summer months (June to August). This is done in order to examine possible seasonal or inter annual variations in the specific absorption coefficient. For each regression it was tested whether there was a statistical significant linear relation between the EC concentrations and the absorption coefficients at a significance level of 0.01.

## 3.7 DEHM – A Transport Model

The DEHM is a transport model developed by J. H. Christensen (Christensen, 1997) at the National Environmental Research Institute of Denmark, now part of Aarhus University. The DEHM is one of the few existing long range transport models used to study the atmospheric transport of air pollution to the Arctic. The DEHM is a 3D model

system that covers most of the Northern hemisphere and consists of a meteorological part and an air pollution part. The meteorological input is produced by the Mesoscale Model Version 5, which is based on data obtained from the European Centre for Medium Range Weather Forecasts. The air pollution input is based on national emission inventories. The DEHM is based on a set of coupled advection-diffusion equations. The horizontal mother domain contains 96×96 grid points with grid spacing of 150×150 km at 60˚N (Heidam et al., 2004). Vertically, the model covers the lower 15 km of the atmosphere, which is divided into 20 layers. The layers closest to the Earth are relatively thin (app. 60 m) in order to estimate a realistic vertical mixing and deposition of pollutants to land- and water surfaces. The upper layers, however, are relatively thick (app. 2000 m) due to more homogenous air masses in the higher part of the atmosphere (Aarhus University, 2013). DEHM includes 67 different species, which comprise several classes of particulate matter. One of those classes is related to BC. The model takes both freshly emitted BC and aged BC into account, which are treated as hydrophobic and hygroscopic respectively (J.H. Christensen, Senior Researcher, AU ENVS, pers. comm., July 2013). In this study modelled BC concentrations at Station Nord from August 2008 to April 2013 using DEHM has been provided by J. H. Christensen.

## 3.8 PMF Source Apportionment

The receptor model PMF is a statistical factor analysis tool, which can be used to determine the types of emissions sources of e.g. ambient PM, including black carbon (Reff et al., 2012; Rose, 2006). The model version used in this study is PMF 3.0 provided by the U.S. EPA (2008). The PMF analysis is based on atmospheric BC and EC measurements in addition to PM measurements using a filter pack sampler (FPS) as described in section 3.8.1. PMF is used to identify the sources contributing to PM at Station Nord from January 2011 to December 2012, focusing on BC. The results will be compared to the model solution obtained by Nguyen et al. (2013), who used PMF to analyse the origins of several different compounds including BC from March 2008 to February 2010 at the same location.

The PMF model derives a solution based on a given number of factors (also referred to as sources) and two input matrices; a data matrix with the measured sample concentrations and a matrix with the analytical uncertainty of all the elements (Paatero, 1997; Nguyen et al., 2013). The mathematical PMF model is:

$$x_{ij} = \sum_{k=1}^{p} g_{ik} f_{kj} + e_{ij} \tag{3.16}$$

Where $x_{ij}$ is the measured concentration of compound $j$ in sample $i$, $p$ is the number of factors contributing to $x_{ij}$, $g_{ik}$ is the relative source contribution of factor $k$ to sample $i$, $f_{kj}$ is the concentration of compound $j$ in factor/source profile $k$, and $e_{ij}$ is the difference between measurement $x_{ij}$ and the modelled result, i.e. the residual error of compound $j$ in sample $i$ (Reff et al., 2012; Paatero, 1997). The PMF model is constrained to positive results making the solutions physical possible (Nguyen et al., 2013). Zeroes or negative values are not permitted in the input matrices, so whenever a concentration was missing

or negative due to high uncertainty, "999" was written in the data matrix. The species concentration was then replaced by the species specific median and the associated uncertainty was calculated as four times the median concentration (U.S. EPA, 2008).

The objectives of the model is to solve equation 3.16 by determining values of $g_{ik}$, $f_{kj}$ and $p$ that minimises $e_{ij}$. The values of the matrices $g_{ik}$ and $f_{kj}$ are iterated for a given $p$ until the least possible $Q$ is found, and thereby the solution, which best fit the input data. $Q$ is defined as:

$$Q = \sum_{i=1}^{n}\sum_{j=1}^{m}\left(\frac{e_{ij}}{\sigma_{ij}}\right)^2 \tag{3.17}$$

Where $Q$ is the goodness of fit (U.S. EPA, 2008), $\sigma_{ij}$ is the analytical uncertainty of compound $j$ in sample $i$, $n$ is the number of samples and $m$ is the number of different compounds. The solution of the PMF model is hence the solution, which minimizes the sum of the residuals, weighted by the known uncertainties of each sample (Reff et al., 2012; Rose, 2006). The PMF model is said not to converge if the limited number of iterations is exceeded and no minimum value of Q is found (U.S. EPA, 2008).

When the concentration and uncertainty matrices have been put into the program a base run is performed with 20 runs and a given number of factors $p$. The optimal number of factors should be chosen based on a good understanding of the sources impacting the air masses and by examining the $Q$ values. The closer the $Q$ value is to the number of data points in the concentration matrix ($i \cdot j$), the better $p$ approximates the number of underlying factors in the data and the better is the goodness of the model fit (Reff et al., 2012). The base run summary states whether or not the runs have converged and states two types of $Qs$ for each run; $Q_{Robust}$, which exclude outliers and $Q_{True}$, which include all points. The closer the values of $Q_{Robust}$ and $Q_{True}$ are, the less is the impact from outliers (U.S. EPA, 2008) and solutions where $Q_{True}$ is up to 50 % larger than $Q_{Robust}$ is interpreted as a stable solution (Gupta et al., 2012). In PMF 3.0 a set of Base runs use the same data matrices, but different (random) starting points. Different Base runs may converge to different local minima, i.e. mathematical solutions. After having selected a base run with the lowest possible Q value, i.e. the lowest residual error between fitted and observed concentrations, a Bootstrap run serves to test the stability of the solution, i.e. the uncertainty in the source profile and the source strength (U.S. EPA, 2008). Finally, by running the Fpeak procedure, physically realistic solutions are produced from matrices, which are transformed from the base run. These solutions should have similar properties as the base run, i.e. similar source profiles etc. The Fpeak value typically ranges between -1 and 1 (Reff et al., 2012).

The model output files contain information on the concentration and the fractional distribution of each compound in the different factors together with a time profile of the factor strengths. From this information the different factors will be interpreted as possible sources contributing to BC on Station Nord.

### 3.8.1 Filter Pack Sampler

The FPS located at the roof of Flyger's Hut has been designed and constructed by H. Ahleson from AU-ENVS and is used to measure a range of different chemical compounds (Figure 3.11). The sampler consists of eight channels, which are connected to a pump that ensures a continuous volume flow of approximately 40 L/min determined with an accuracy of ± 5 % (H. Ahleson, Laboratory Mechanic, AU ENVS, pers. comm. August 2013). The flow is adjusted and checked minimum three times a year. Besides the eight channels one extra channel, with no flow, is used as a field blank. Every channel operates for one week at a time and the FPS hence runs for seven weeks without changing the filters (B. Jensen, Laboratory Technician, AU ENVS, pers. comm., April 2013).

Below each channel a 6 watts light bulb is installed in order to avoid accumulation of brine and ice on the particle filter by simple heating. The light bulb has an angel of 6 degrees that ensures a focussed light. In each channel a filter pack is installed, which consists of a sequence of three filers (B. Jensen, Laboratory Technician, AU ENVS, pers. comm., April 2013). The first filter collects particulate matter, whereas the second and third filter is impregnated in order to collect $SO_2$, $HNO_3$ and $NH_3$. The filters are analysed for a substantial number of elements (Table 3.1), $SO_4^{2-}$, $NH_4^+$ and $NO_3^-$ (Heidam et al., 2004). The compounds are subsequently analysed in laboratory using ICP-MS (Inductively Coupled Plasma Mass Spectrometry), Anion-IC (Ion Chromatography) and Autoanalysator. The results from the analyses, which are applied in this study, are provided by AU-ENVS.

**Figure 3.11** A FPS that consist of eight channels and a reference channel.

# 4 Results

In this chapter the EC and OC concentrations in air and the EC concentrations in snow are presented. The specific absorption coefficient is determined based on a calibration between the EC concentrations and the absorption coefficients from the PSAP. On the basis of the specific absorption coefficient the BC concentrations in air from the PSAP are determined. Furthermore the BC concentrations modelled by DEHM are illustrated and finally the results from the PMF analyses for the periods from 2008 to 2010 and from 2011 to 2013 are shown.

## 4.1 Measured EC and OC Concentrations

In the following the quality control of the EC and OC measurements is described and the measured concentrations of EC and OC in air and EC in snow are presented. In Appendix 6 extended information on the results of the OC-EC analysis can be found.

### 4.1.1 EC and OC Concentrations in Air

The weekly air concentrations of EC and OC on Station Nord were measured from August 2008 to April 2013 as described in section 3.3. From August 2008 to February 2010 EC samples were approximately taken every second week, whereas from March 2010 to April 2013 samples have been taken every week. Periods with missing data of three weeks or longer are shown as empty space in the concentration graphs. A detailed overview of the missing data is presented in Appendix 2. The weekly measurements were used to calculate monthly averages, which were then used to calculate annual averages. In this way weeks with missing data were accounted for.

The EC concentrations vary between the lowest concentration of 1 ng/m$^3$ measured in November 2009 and the highest concentration of 145 ng/m$^3$, which occurred in January 2011 (Figure 4.1). The highest EC concentrations occur every year in the winter months or early spring and are generally lower in the summer and autumn months even though relatively high peaking events are occasionally observed during summer, e.g. in August 2011 where a concentration of 79 ng/m$^3$ was measured. Figure 4.2 suggests a seasonal variation in the EC concentrations, although the measurements have large standard deviations. The large standard deviations indicate inter annual variations in the monthly concentrations. The highest average concentrations of 49 ng/m$^3$ to 55 ng/m$^3$ are observed in January, March and April, while the lowest concentrations of 14 ng/m$^3$ and 16 ng/m$^3$ occur in June and September. From September onwards, the concentrations start to increase and peak in winter and early spring, although with lower concentrations in February. After April the concentrations decrease again. The annual average EC

concentrations from 2008 to 2013 are illustrated in Figure 4.3, where 2008 and 2013 only consist of data from August to December and January to April, respectively. Leaving out 2008 and 2013, the figure indicates that the highest annual average EC concentrations of 36 ng/m$^3$ and 37 ng/m$^3$ are observed in 2009 and 2011, respectively and the lowest concentration of 26 ng/m$^3$ occur in 2012.

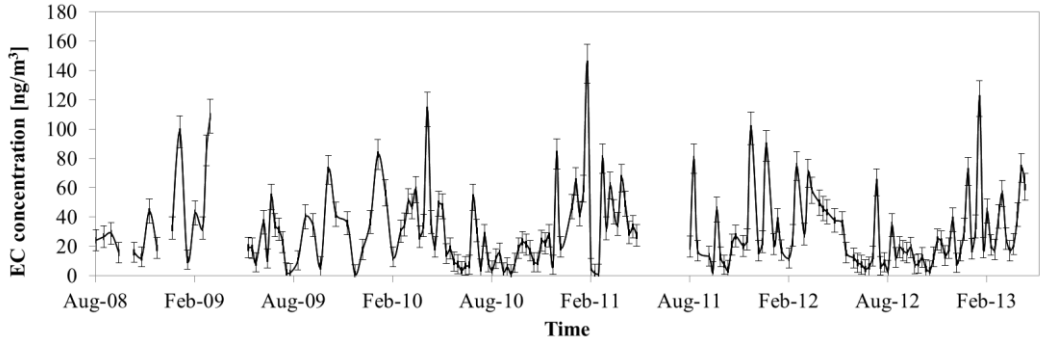


**Figure 4.1** EC concentrations [ng/m$^3$] with instrumental uncertainty at Station Nord from August 2008 to April 2013. The empty space indicates missing data periods.

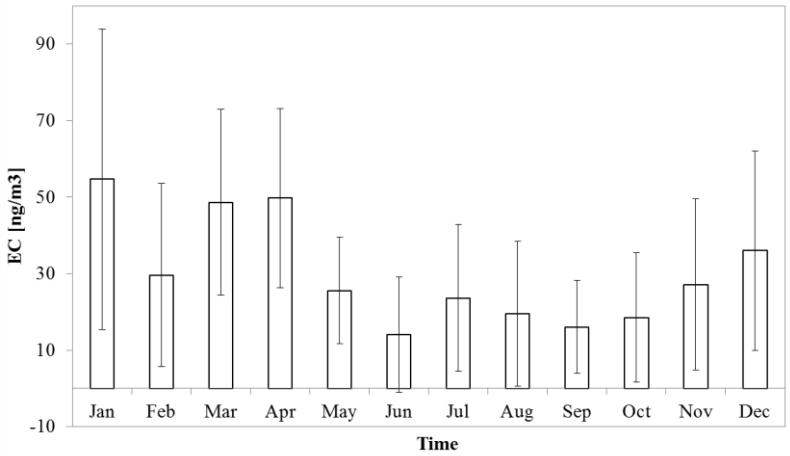


**Figure 4.2** Monthly average EC concentrations [ng/m$^3$] with standard deviations at Station Nord from 2008 to 2013.

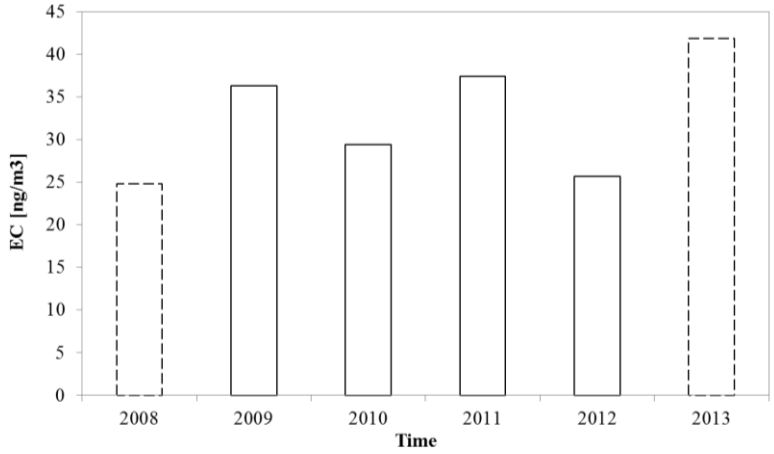


**Figure 4.3** Annual average EC concentrations [ng/m$^3$] at Station Nord from 2008 to 2013. The years 2008 and 2013 (dashed line) only contain data from August to December and January to April, respectively.

The OC concentrations are generally much higher than the EC concentrations and vary between the lowest concentration of 39 ng/m$^3$ measured in February 2011 and the highest concentration of 811 ng/m$^3$ in January 2011 (Figure 4.4). High peaks are observed in the winter of 2011 and 2013 but also in summer 2009 and the seasonal pattern is thus not as clear for the OC measurements as for the EC measurements. Figure 4.5 also suggests that there is no clear seasonal pattern. The large standard deviations indicate inter annual variations in the monthly concentrations. The highest average concentrations (279 ng/m$^3$ to 337 ng/m$^3$) occur in January, March and July, while the lowest concentrations are observed in August, September and October (134 ng/m$^3$ to 161 ng/m$^3$). Apart from July the concentrations decrease from March to October. The annual average OC concentrations from 2008 to 2013 are illustrated in Figure 4.6, where 2008 and 2013 only consist of data from August to December and January to April, respectively. Leaving out 2008 and 2013, the figure indicates that the highest that the highest concentration of 289 ng/m$^3$ is observed in 2009 and decreases to 162 ng/m$^3$ in 2012.

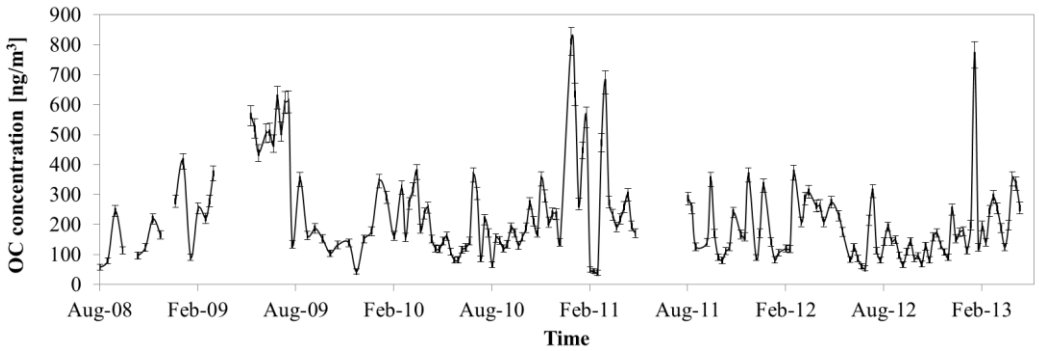


**Figure 4.4** OC concentrations [ng/m$^3$] with instrumental uncertainty at Station Nord from August 2008 to April 2013. The empty space indicates missing data periods.

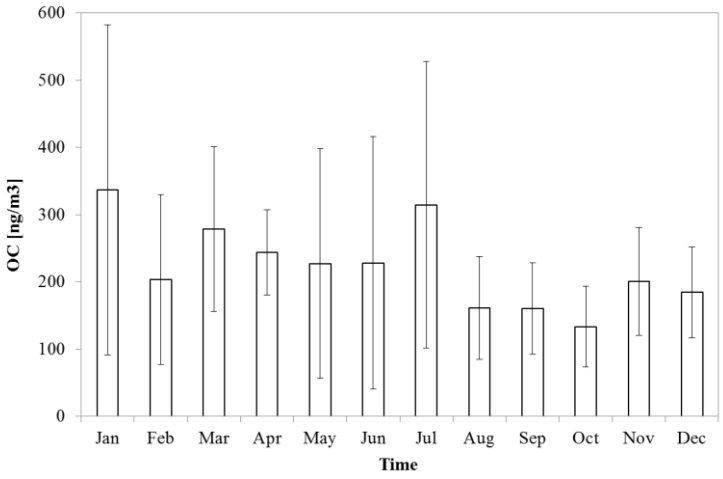


**Figure 4.5** Monthly average OC concentrations [ng/m$^3$] with standard deviations at Station Nord from 2008 to 2013.

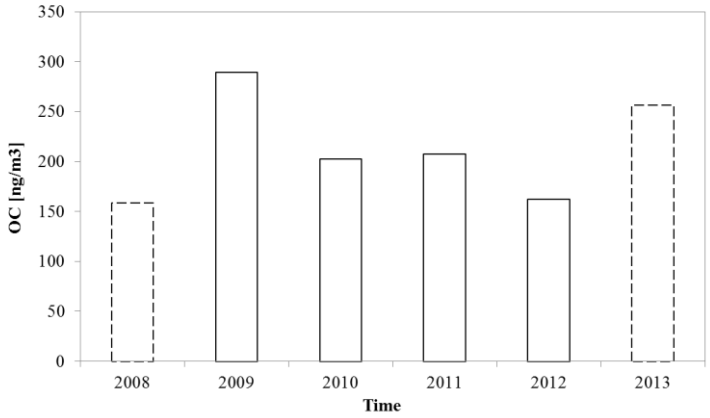


**Figure 4.6** Annual average OC concentrations [ng/m$^3$] at Station Nord from 2008 to 2013. The years 2008 and 2013 (dashed line) only contain data from August to December and January to April, respectively.

The EC/OC ratio may tell something about the combustion source as explained in section 2.1. Due to the higher OC concentrations the EC/OC ratio is always below one and varies between 0.0 in July 2009 and 0.7 in November 2009 (Figure 4.7). Peaking EC/OC ratios are observed in winter and spring months, e.g. 0.5 in January 2012. During summer months a high ratio of 0.4 was measured one week in August 2008 and other smaller peaks are also observed. Figure 4.8 suggests that there may be a very weak seasonal pattern, although with high standard deviations. The large standard deviations indicate inter annual variations in the monthly ratios. The EC/OC ratios appear to be higher in winter and spring than in summer, where the highest monthly ratios of 0.20 and 0.21 seem to occur in December and April, respectively, while it is indicated that the lowest monthly average ratio of 0.07 occur in June. The annual average EC/OC ratios from 2008 to 2013 are illustrated in Figure 4.9, where 2008 and 2013 only consist of data from August to December and January to April, respectively. Leaving out 2008 and 2013, the figure indicates that there are no major differences between the years 2009 to 2012, which range between 0.14 and 0.16.

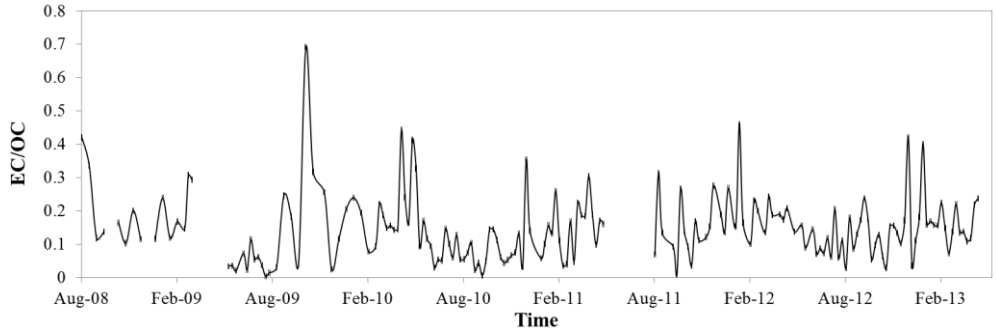


**Figure 4.7** The ratio between measured EC and OC concentrations at Station Nord from August 2008 to April 2013. The empty space indicates missing data periods.

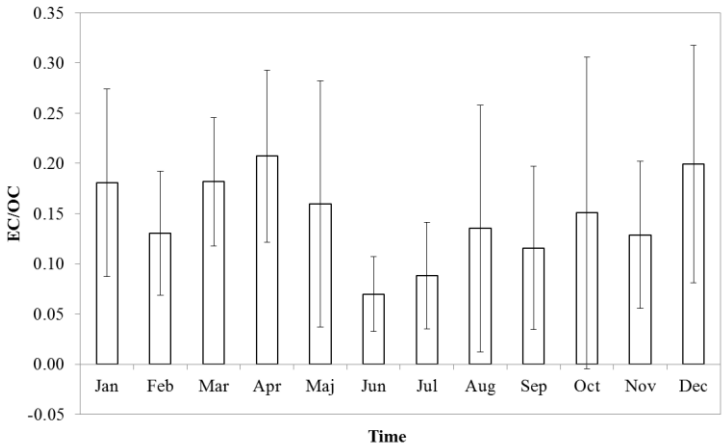


**Figure 4.8** Monthly average EC/OC ratio with standard deviations at Station Nord from 2008 to 2013.

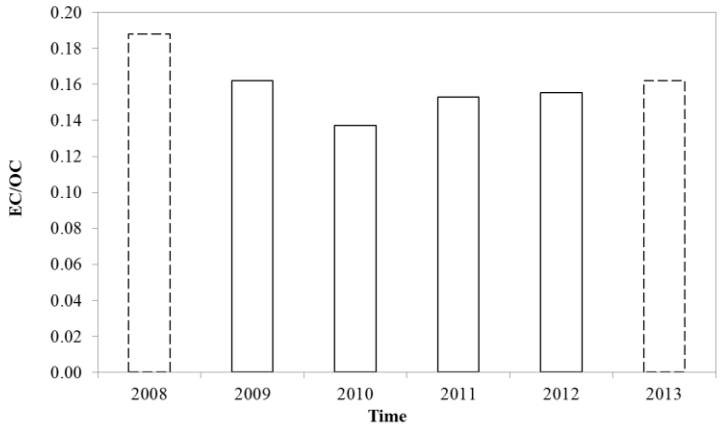


**Figure 4.9** Annual average EC/OC ratios at Station Nord from 2008 to 2013. The years 2008 and 2013 (dashed line) only contain data from August to December and January to April, respectively.

### 4.1.2 EC Concentrations in Snow

Snow samples were taken at Station Nord in April 2013 as explained in section 3.4 and analysed in the laboratory using the OC-EC analyser. At AU-ENVS a control experiment was setup in order to estimate the blind value, which was subtracted from the measured concentrations in the snow samples. Three replicates were made and an average blind concentration of 3 ng/l was found, ranging from 1 to 7 ng/l. The results of the EC concentrations in the snow samples after subtracting the blind value are given in Table 4.1. Seven samples (three replicates of each) were taken around Flyger's Hut where an average EC concentration of 521 ng/l was obtained, ranging from 1 to 1754 ng/l (Table 4.2). One sample (three replicates) was taken close to the icebergs 2 km north-west of the station, where an average concentration of 483 ng/l was found, ranging from 9 to 837 ng/l. At Knuths Fjeld, 7 km south-east of the station, an average EC concentration of 1159 ng/l was obtained, ranging from 0 to 3082 ng/l based on three replicates. The highest average concentration of 1449 ng/l, ranging from 274 to 2283 ng/l, was found on the runway where three replicates were taken. It was indicated by using Student's T-test that there is no significant difference between the measured concentrations at Knuths Fjeld, the icebergs and Flyger's Hut. The average concentration measured at the runway is on the other hand suggested to be higher than the mean concentration at Flyger's Hut when applying Student's T-test. In Appendix 7 extended information on the collected snow samples and the results of the OC-EC analysis can be found.

**Table 4.1** The EC concentrations in snow at Flyger's Hut, the icebergs, Knuths Fjeld and the runway. The concentrations are given in ng EC/ l melt water.

| Date | Location | Replicate 1 [ng/l] | Replicate 2 [ng/l] | Replicate 3 [ng/l] |
|---|---|---|---|---|
| **08-04-2013** | Flyger's Hut | 1 | 700 | 463 |
| **09-04-2013** | Flyger's Hut | 285 | - | - |
| **10-04-2013** | Flyger's Hut | 13 | 712 | 505 |
| **11-04-2013** | Flyger's Hut | 473 | 800 | 1754 |
| **14-04-2013** | Flyger's Hut | 375 | - | 933 |
| **15-04-2013** | Flyger's Hut | 42 | 950 | - |
| **16-04-2013** | Flyger's Hut | 32 | 536 | 648 |
| **18-04-2013** | Icebergs | 9 | 837 | 603 |
| **20-04-2013** | Knuths Fjeld | 0 | 3082 | 397 |
| **21-04-2013** | The runway | 274 | 2283 | 1791 |
| **03-07-2013** | Blind ENVS | 6 | 1 | 1 |

**Table 4.2** Average EC concentrations [ng/l] and standard deviations for snow samples taken at Flyger's Hut, the icebergs, Knuths Fjeld, and the Runway. The average EC blind concentration [ng/l] and standard deviation is also stated. For each sample location and the blind, the concentration range [ng/l], the number of samples and the sample depth [cm] are given.

| Location | EC [ng/l] | Range [ng/l] | Number of samples | Depth [cm] |
|---|---|---|---|---|
| **Flyger's Hut** | 521 ± 441 | 1-1754 | 7 (3 replicates) | 5 |
| **Icebergs** | 483 ± 427 | 9-837 | 1 (3 replicates) | 5 |
| **Knuths Fjeld** | 1159 ± 1677 | 0-3082 | 1 (3 replicates) | 5 |
| **The runway** | 1449 ± 1047 | 274-2283 | 1 (3 replicates) | 5 |
| **Blind** | 3 ± 3 | 1-7 | 1 (3 replicates) | - |

## 4.2 Measured BC Concentrations in Air

In this section the results of the quality control of the PSAP measurements from August 2008 to April 2013 are described, followed by the resulting absorption coefficient. The year 2009 is explained thoroughly as an example. Thereafter the specific absorption coefficient is determined for the whole time period, annually and seasonally. Finally the BC concentrations are calculated. Extended information on the PSAP data for 2008 to 2013 can be found in Appendix 8.

### 4.2.1 Quality Control

From 2008 to 2013 the signal and the reference signal vary between 3.7 and 7.2 V, and 6.1 and 7.8 V respectively (Table 4.3). None of the signals fall below the threshold limit of 3.5 V. During most of the period from 2008 to 2013 a decrease in the signal is observed together with a relatively constant reference signal in between two filter periods (in between two filter changes). The filter changes are illustrated by arrows (Figure 4.11). In general the signal and the reference signal start at nearly the same voltage in the beginning of a new filter period, although few exemptions occur. For all years the maximum variation in the reference signal is 0.2 V, meeting the assumption of nearly constant behaviour. The signal, reference signal and flow in 2009, before the quality control, are presented in Figure 4.10, while Figure 4.11 presents the data after the quality control.

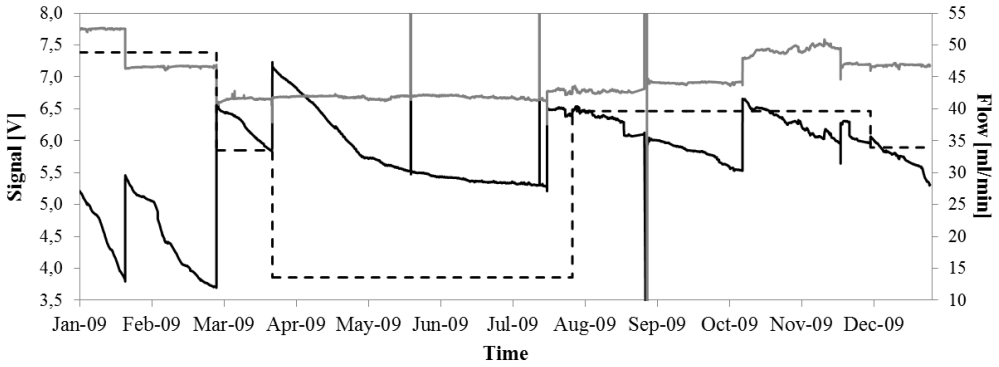


**Figure 4.10** The signal [V] (black line), the reference signal [V] (grey line) and the flow [ml/min] (dashed line) with a time interval of 15 min. at Station Nord from January to December 2009 before the quality control.

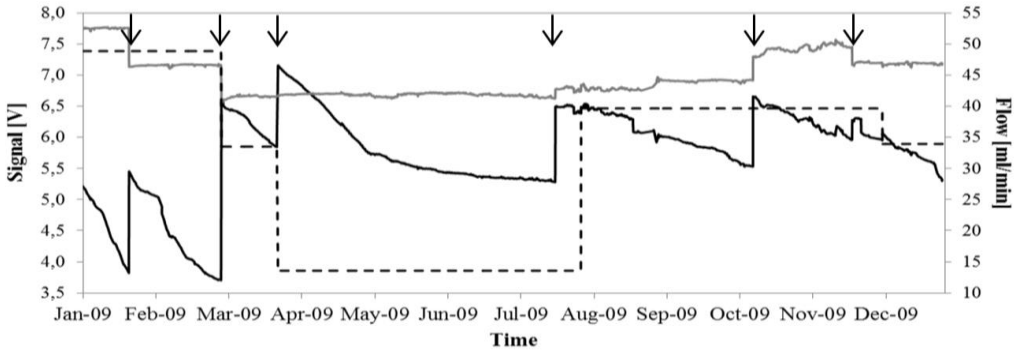


**Figure 4.11** The signal [V] (black line), the reference signal [V] (grey line) and the flow [ml/min] (dashed line) with a time interval of 15 min at Station Nord from January to December 2009 after the quality control. The arrows indicate filter changes.

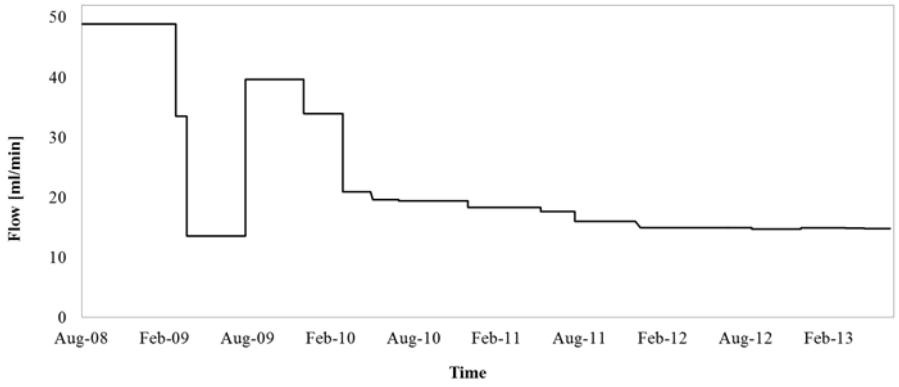


**Figure 4.12** The flow [ml/min] used by the PSAP instrument from August 2008 to April 2013.

The quality controlled data from 2009 includes five filter periods, where the signal in each period decreases over time. There are however few occurrences of relatively small increases in the signal, which does not happen simultaneously with a filter change (e.g. July and August 2009, Figure 4.11). During these periods the reference signal shows the same degree of increase as the signal, and the given periods are thus not excluded. The reference signal only varies within a range of 0.2 V, which can be considered as nearly constant behaviour. The signal and the reference signal start at nearly the same voltage in the beginning of a new filter period for three of the five filter periods in 2009. In January 2009 the signal is relatively lower than the reference signal after a filter change and in April 2009 the signal is relatively higher than the reference signal. The signals and flows before and after quality control for the remaining years, 2008 and 2010 to 2013, can be found in Appendix 3.

Over the entire time period the flow varies from 14 ml/min in 2009 to 49 ml/min in 2008 (Figure 4.12). In general the highest flow is observed during the period from August 2008 to February 2010, where it fluctuates between 34 and 49 ml/min. There is however a period from April to July in 2009 where the flow is only 14 ml/min. From March 2010 to April 2013 the flow is notably lower ranging from 15 to 21 ml/min.

### 4.2.2 Absorption Coefficient

Based on the quality controlled data, the absorption coefficients were calculated for each time interval of 15 minutes from the signals, the reference signals, the flow and the filter spot area (equation 3.14). An area of 6.42 $mm^2$ was used based on the loaded filter spot diameter of 2.86 mm. During the period from 2008 to 2013 the absorption coefficients (after the quality control) vary between -28 $\mu m^{-1}$ measured in 2012 and 130 $\mu m^{-1}$ 2008 (Table 4.3). The negative absorption is a result of noise on the instrument. The absorption coefficients from January to December 2009 before and after the quality control are presented in Figure 4.13 and Figure 4.14, respectively. After the quality control of 2009 the absorption coefficient ranges from -17 in March to 80 $\mu m^{-1}$ in February. The absorption coefficients after the quality control for the remaining years can be found in Appendix 4.

**Table 4.3** The minimum and maximum signal [V], reference signal [V] and absorption [$\mu m^{-1}$] at Station Nord for 2008 to 2013.

| Year | Signal [V] | | Reference Signal [V] | | Absorption coefficient [$\mu m^{-1}$] | |
|---|---|---|---|---|---|---|
| | *Min* | *Max* | *Min* | *Max* | *Min* | *Max* |
| **2008** | 3.7 | 7.0 | 7.5 | 7.8 | -6 | 130 |
| **2009** | 3.7 | 7.2 | 6.6 | 7.8 | -34 | 125 |
| **2010** | 4.1 | 6.6 | 6.1 | 7.3 | -22 | 119 |
| **2011** | 4.5 | 6.9 | 6.4 | 7.6 | -18 | 66 |
| **2012** | 5.5 | 7.2 | 7.0 | 7.7 | -28 | 87 |
| **2013** | 3.8 | 5.5 | 7.3 | 7.6 | -20 | 79 |

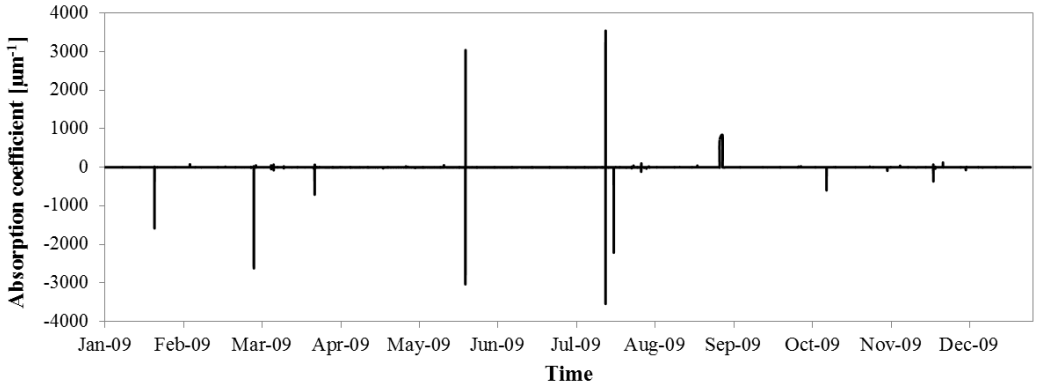


**Figure 4.13** The absorption coefficients [$\mu m^{-1}$] with a time interval of 15 minutes at Station Nord from January to December 2009 before the quality control.

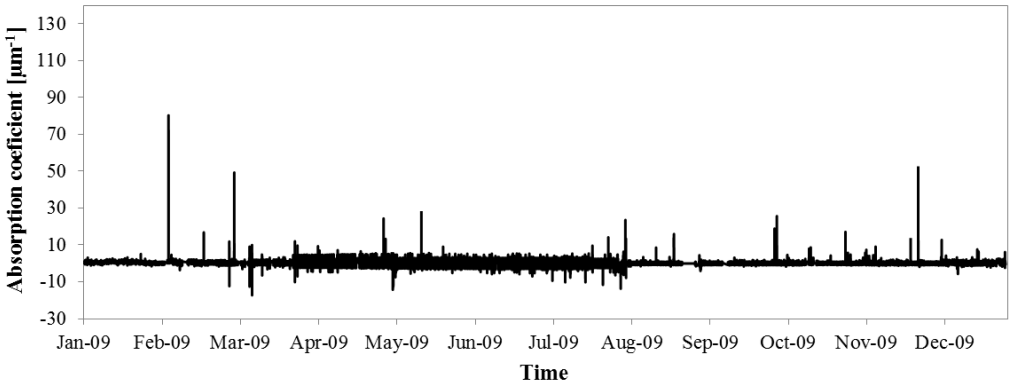


**Figure 4.14** The absorption coefficients [$\mu m^{-1}$] with a time interval of 15 minutes at Station Nord from January to December 2009 after the quality control.

### 4.2.3 Specific Absorption Coefficient

In order to convert the measurements of the absorption coefficient from the PSAP into BC mass concentrations it is necessary to determine the specific absorption coefficient as explained in section 3.6.2. The specific absorption coefficient is found as the slope of the linear regression between EC concentrations and the absorption coefficients from August 2008 to April 2013. In this section monthly average EC concentrations and absorption coefficients from the PSAP are applied. The monthly average absorption coefficients are based on weighted averages of the 15 minutes intervals. Investigating both the average daily and weekly absorption coefficients, it was found that the noise on the instrument

affected the absorption coefficients too much, leading to repeating negative absorption coefficients. The problem was however not observed to the same extent for the average monthly absorption coefficients, which is why these are presented here, assuming that the observed noise leading to negative values is random hence the average noise is reduced with increasing number of measurements.

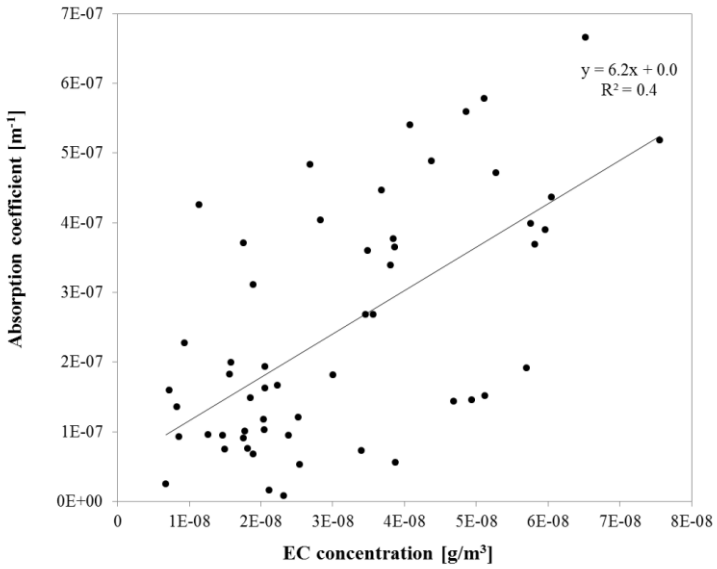


**Figure 4.15** The monthly absorption coefficients [$m^{-1}$] as a function of the monthly EC concentrations [$g/m^3$] at Station Nord from 2008 to 2013. The resulting specific absorption coefficient is 6.2 $m^2/g$ with a coefficient of determination ($R^2$) of 0.4.

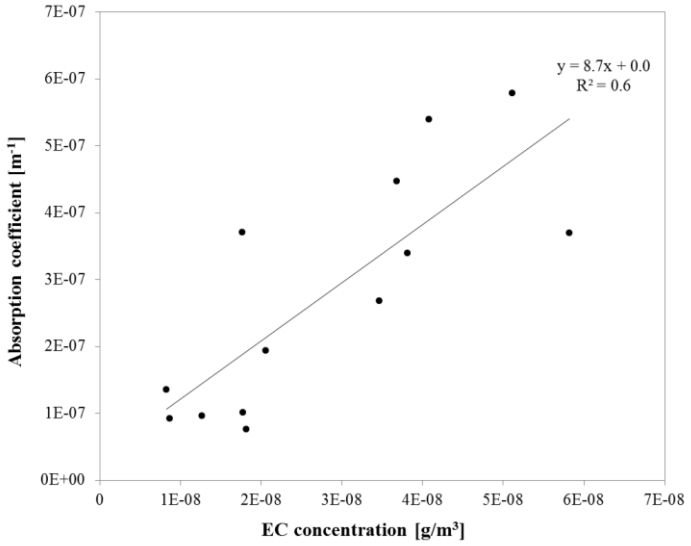


**Figure 4.16** The monthly absorption coefficients [$m^{-1}$] as a function of the monthly EC concentrations [$g/m^3$] at Station Nord for 2010. The resulting specific absorption coefficient is 8.7 $m^2/g$ with a coefficient of determination ($R^2$) of 0.6.

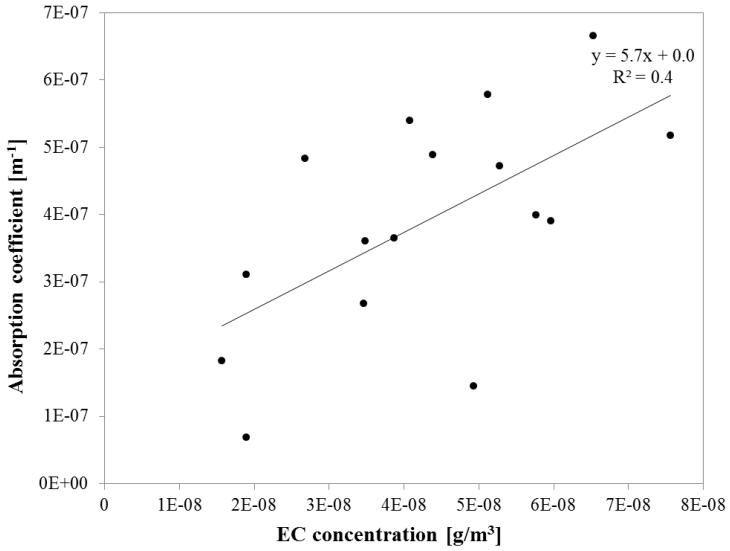


**Figure 4.17** The monthly absorption coefficients [$m^{-1}$] as a function of the monthly EC concentrations [$g/m^3$] at Station Nord for the winter months, December to February, from 2008 to 2013. The resulting specific absorption coefficient is 5.7 $m^2/g$ with a coefficient of determination ($R^2$) of 0.4.

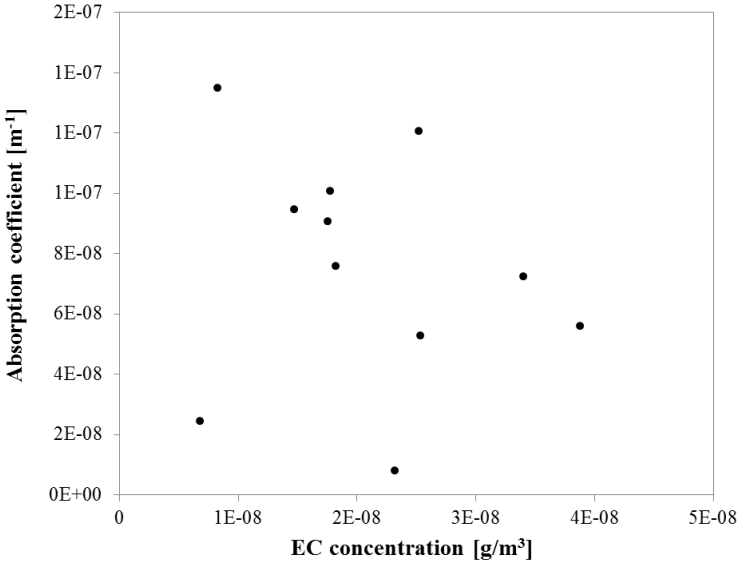


**Figure 4.18** The monthly absorption coefficient [$m^{-1}$] as a function of the monthly EC concentration [$g/m^3$] at Station Nord for the summer months, June to August, from 2008 to 2012.

It was found that there is a significant linear correlation between monthly EC concentrations and monthly absorption coefficients from 2008 to 2013. A linear regression on data from 2008 to 2013 hence reveals a specific absorption coefficient of 6.2 $m^2/g$ with a coefficient of determination ($R^2$) of 0.4 (Figure 4.15). The closer the $R^2$ is to 1, the better the correlation is (Johnson, 2005); thus a value of 0.4 indicates a weak linear relationship between the absorption coefficients and the EC concentrations. Annual calibrations have also been made, where a significant linear correlation is found between monthly EC concentrations and monthly absorption coefficients in 2009, 2010 and 2012.

The best yearly correlation is observed in 2010 with a determination coefficient of 0.6 and a specific absorption coefficient of 8.7 $m^2/g$ (Figure 4.16). The annual specific absorption coefficients are found to be 5.8 $m^2/g$ in 2009 ($R^2 = 0.4$) and 5.5 $m^2/g$ in 2012 ($R^2 = 0.5$). No significant linear correlation is found between monthly EC concentrations and monthly absorption coefficients from 2008 and 2011 and hence no specific absorption coefficient is determined. Furthermore no specific absorption coefficient is identified in 2013 due to limited data points. The graphs showing the annual correlations for 2008, 2009, 2011, 2012 and 2013 can be found in Appendix 5.

Figure 4.17 and Figure 4.18 present the analysis for the winter months from December to February and the summer months from June to August for 2008 to 2013, respectively. It was found that there is a significant linear correlation between monthly EC concentrations and monthly absorption coefficients during winter months from 2008 to 2013. The linear regression hence results in a specific absorption coefficient of 5.7 $m^2/g$, however with a poor correlation ($R^2 = 0.4$). No significant linear correlation is found for the summer period and no specific absorption coefficient is thus determined.

### 4.2.4 BC Concentrations

The BC concentrations are calculated by dividing the absorption coefficient by the specific absorption coefficient (equation 3.15). The linear regression is found too weak to describe the correlation between EC and the absorption coefficient from the PSAP thus the specific absorption coefficient found in this study will not be used to determine the BC concentration. Instead a specific absorption coefficient of 5.5 $m^2/g$ is used, which is based on observations on Svalbard and found with a very good correlation between absorption coefficients and EC measurements (Hegg et al., 2011; J. Ström, Professor, Stockholm University, pers. comm., June 2013). Since Hegg et al. (2011) also determined the specific absorption coefficient at a wavelength of 550 nm, and because Svalbard is a remote Arctic location, although with more local sources than Station Nord, it is considered reasonable to apply the same specific absorption coefficient for Station Nord.

As previously explained investigating both the average daily and weekly BC concentrations, it was found that the noise on the instrument affected the concentration too much, leading to repeating negative concentrations. The fraction of weekly negative concentrations increases from 2008 to 2013 with 0 % in 2008, 5.7 % in 2009, 7.8 % in 2010, 7.7 % in 2011, 13.5 % in 2012 and 11.1 % in 2013. For this reason the average monthly concentrations are used since the negative noise on the instrument was counterbalanced to a greater extent by the positive noise, resulting in only one negative concentration in May 2012 (Figure 4.19). The average monthly concentrations are applied under the assumption that the observed noise leading to negative values is random; hence the average noise is reduced with increasing number of measurements. The monthly average absorption coefficients are based on weighted averages of the 15 minutes intervals. Periods with missing data are evident for all years where 7 days are missing in 2008, 19 days in 2009, 30 in 2010, 53 days in 2011, 6 days in 2012 and 60 days in 2013. It must be emphasised that 2008 only consists of measurements from August to December and 2013 only covers January to April. A detailed overview of the missing

data is presented in Appendix 2. Periods with missing data are shown as empty spaces in the concentration graphs.

The BC concentrations vary between the lowest concentration of -1 ng/m$^3$ in May 2012 and the highest concentration of 161 ng/m$^3$ in March 2009 (Figure 4.19). In general, the BC concentrations are found to vary both seasonally and annually. Peaking BC concentrations occur every year during winter months and early spring, from December to April, whereas lower concentrations appear during summer and autumn months, from June to September. The monthly average BC concentrations from 2008 to 2013 are presented in Figure 4.20, which indicates that a seasonal variation can be observed despite the relatively large standard deviations. The large standard deviations indicate inter annual variations in the monthly concentrations. The figure suggests that monthly concentrations are higher during winter and early spring from January to April (between 64 and 94 ng/m$^3$) compared to concentrations during summer, from June to August (between 9 and 14 ng/m$^3$). From June onwards, the concentrations are increasing until January.

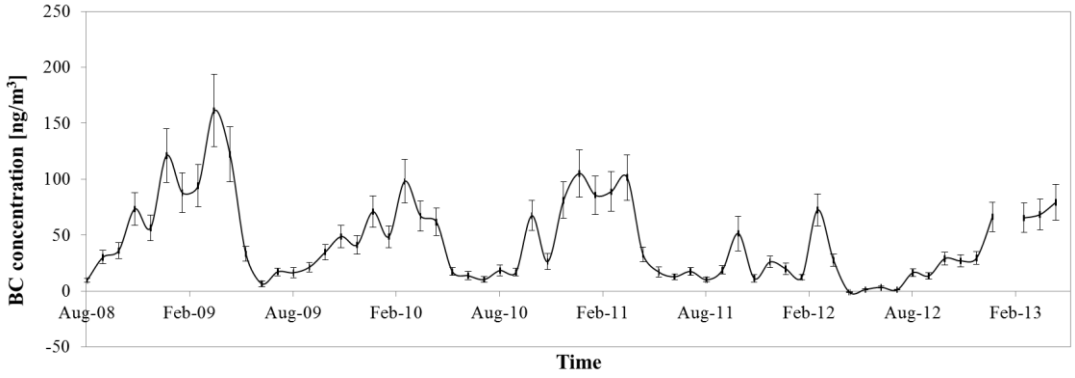


**Figure 4.19** The BC concentrations [ng/m$^3$] with instrumental uncertainties at Station Nord from August 2008 to April 2013 derived from the PSAP instrument applying a specific absorption coefficient of 5.5 m$^2$/g. The empty space indicates missing data periods.

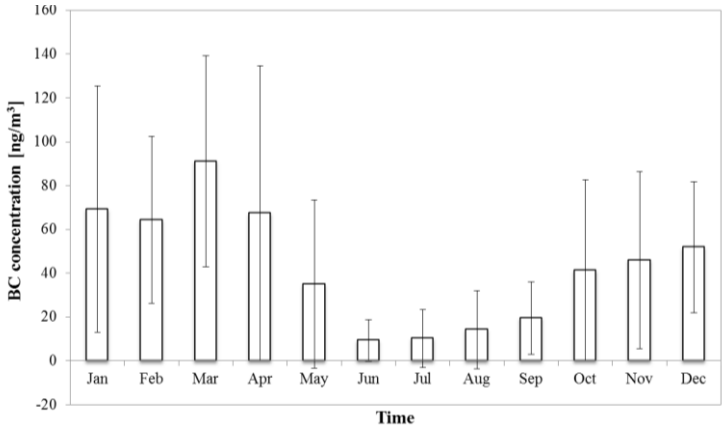


**Figure 4.20** Monthly average BC concentrations [ng/m$^3$] with standard deviations at Station Nord from 2008 to 2013.

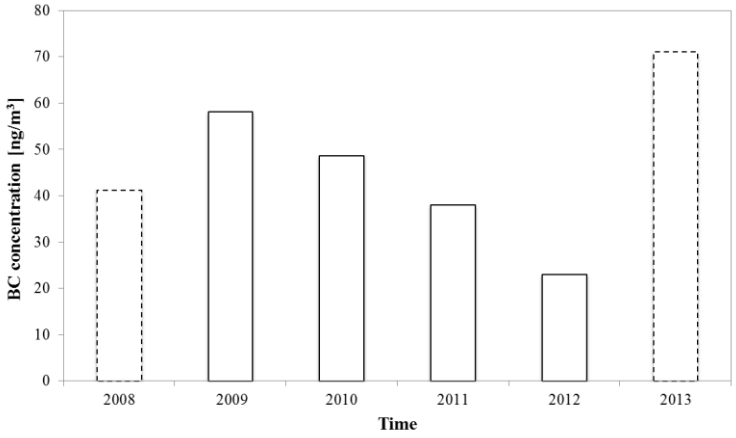


**Figure 4.21** Annual average BC concentrations [ng/m$^3$] at Station Nord from 2008 to 2013. 2008 and 2013 (dashed line) only contain data from August to December and January to April, respectively.

The annual average BC concentrations from 2008 to 2013 are illustrated in Figure 4.21, where 2008 and 2013 only consist of data from August to December and January to April, respectively. Leaving out 2008 and 2013, the annual average BC concentration is decreasing over time with 58 ng/m$^3$ in 2009, 49 ng/m$^3$ in 2010, 38 ng/m$^3$ in 2011 and 23 ng/m$^3$ in 2012.

## 4.3 Modelled BC Concentrations at Station Nord

Daily BC concentrations at Station Nord have been modelled by J.H. Christensen using DEHM from August 2008 to April 2013. The BC input concentrations are *based* on national emission inventories. The modelled BC concentrations vary between the lowest concentration of 1 ng/m$^3$ in August 2011 and the highest concentration of 234 ng/m$^3$ in February 2012 (Figure 4.22). This high peak is a single day event, which is seen again in January 2013 with a concentration of 230 ng/m$^3$. Peaking BC concentrations occur every year in the winter months or early spring and are generally lower in the summer and autumn months even though relatively high peaking events are occasionally observed during summer, e.g. in August 2011 where a concentration of 108 ng/m$^3$ was modelled. Figure 4.23 suggests that there is a seasonal variation in the BC concentrations, although the measurements have large standard deviations. The large standard deviations indicate inter annual variations in the monthly concentrations. It seems like the concentrations are highest in winter and early spring. The highest monthly average concentrations (39 ng/m$^3$ to 41 ng/m$^3$) are observed in January, February and March, while the lowest concentrations (7 ng/m$^3$ to 9 ng/m$^3$) occur in May, September, and October. The modelled annual average BC concentrations from 2008 to 2013 are illustrated in Figure 4.24, where 2008 and 2013 only consist of data from August to December and January to April, respectively. Leaving out 2008 and 2013, the figure suggests that the concentrations from 2009 to 2012 are very similar, ranging from 19 ng/m$^3$ to 23 ng/m$^3$. The daily concentrations modelled by DEHM are presented in Appendix 9.

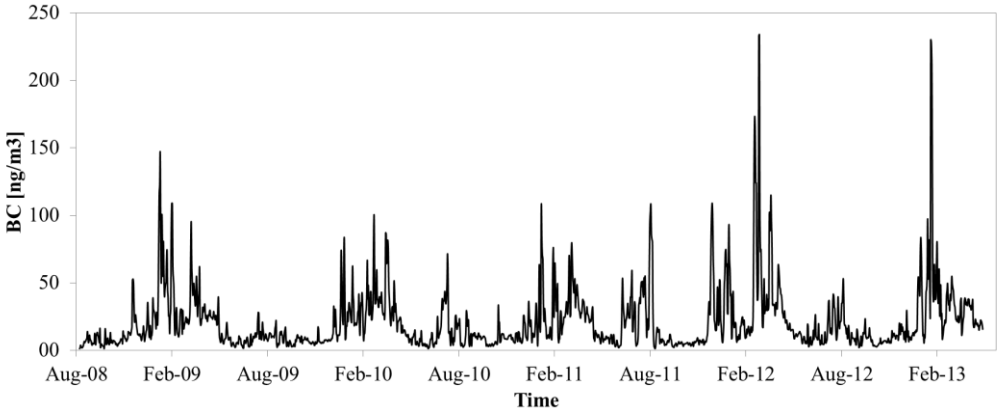


**Figure 4.22** Modelled BC concentrations [ng/m$^3$] in air at Station Nord from August 2008 to April 2013. The empty space indicates missing data periods.

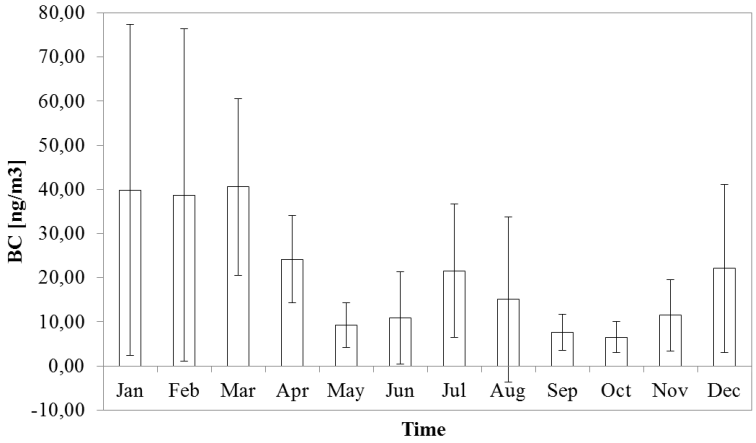


**Figure 4.23** Monthly average modelled BC concentrations [ng/m$^3$] with standard deviations at Station Nord from 2008 to 2013.

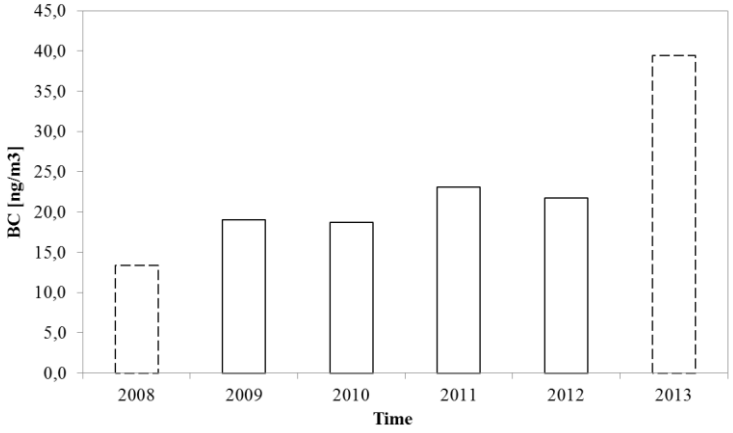


**Figure 4.24** Annual average modelled BC concentrations [ng/m$^3$] at Station Nord from 2008 to 2013. The years 2008 and 2013 (dashed line) only contain data from August to December and January to April, respectively.

## 4.4 PMF Analysis

In this study, the PMF analysis is initially run with the inputs used by Nguyen et al., (2013) in order to reproduce the results at Station Nord from March 2008 to February 2010. Thereafter the concentration input from January 2011 to December 2012 is used and a comparison of the source apportionment from the two periods is made in section 5. First, the input matrices to the PMF analysis are described followed by a presentation of the results from the two analyses.

### 4.4.1 Input Matrices

The PMF analysis conducted by Nguyen et al. (2013) was based on measurements of BC, elements and inorganic ions collected from March 2008 to February 2010 and analysed by the different methods given in Table 4.4. In this study, an improved specific absorption coefficient has been derived instead of the one used by Nguyen et al. (2013). Therefore, the analysis was run again in order to reproduce the source apportionment profiles from 2008-2010 with updated BC concentrations found in this study. The analytical uncertainties are stated for all methods in Table 4.4. No good data exist from February 2010 to December 2010 due to problems with the analytical methods, when changing from PIXE (Proton Induced X-ray Emission) to ICP-MS; hence these data are excluded from PMF analysis. Due to the change of method a few species were replaced, which caused small changes in the input matrix for the PMF analysis in this study, compared to the study by Nguyen et al. (2013). In the PMF model, which analyse data from January 2011 to December 2012, EC measurements from the HVS have been used instead of BC measurements, due to the high noise level on the PSAP causing many average weekly negative BC values in this period. Table 4.5 shows the different compounds, the analytical methods and the uncertainties used in the PMF model. In the following analyses $SO_x$ is the sum of $SO_2$ + $SO_4^{2-}$, $NO_3^-$ the sum of $NO_3^-$ + $HNO_3$ and $NH_4^+$ the sum of $NH_4^+$ + $NH_3$. Some compounds are given in $\mu g/m^3$ instead of $ng/m^3$ in order to avoid their magnitude dominating the PMF analysis. The complete concentration and uncertainty matrices for both time periods can be found in Appendix 10.

**Table 4.4** Compounds, analytical methods, time resolutions and uncertainties used in the PMF analysis based on measurements at Station Nord from January 2008 to February 2010 (Nguyen et al., 2013).

| Compound | Analytical method | Time resolution | Uncertainty |
|---|---|---|---|
| Al, Si, S, K, Ca, Ti, V, Cr, Mn, Fe, Ni, Cu, Zn, Ga, As, Se, Br, Rb, Sr, Zr, Pb | PIXE | 7-days | 18 % |
| $SO_2$, $SO_4^{2-}$, $Na^+$, $NH_4^+$, $NH_3$, $NO_3^-$, $HNO_3$, $Br^-$, $Cl^-$ | IC | 7-days | 20 % |
| BC | PSAP | 7 days | 20 % |

**Table 4.5** Compounds, analytical methods, time resolutions and uncertainties used in the PMF analysis based on measurements at Station Nord from January 2011 to December 2012.

| Compound | Analytical method | Time resolution | Uncertainty |
|---|---|---|---|
| Al, Si, S, K, Ca, Ti, V, Cr, Mn, Fe, Ni, Cu, Zn, Ga, As, Se, Br, Rb, Sr, Zr, Pb, $Na^+$ | ICP-MS | 7 days | 18 % |
| $Cl^-$ | Anion-IC | 7 days | 15 % |
| $NO_3^-$, $HNO_3$, $SO_2$, $SO_4^{2-}$ | Anion-IC | 7 days | 10 % |
| $NH_4^+$, $NH_3$ | Autoanalysator | 7 days | 15 % |
| EC, OC | OC-EC analyser | 7 days | C [ug/cm$^2$] * 0.05 +0.2 |

### 4.4.2 PMF from 2008 to 2010

The PMF analysis based on measurements from January 2008 to February 2010 includes the following species: $Na^+$, Al, K, Ca, Ti, V, Si, S, Zr, Cr, Mn, Fe, Ni, Cu, Zn, Ga, As, Se, Br, Rb, Sr, Pb, $Cl^-$, $NH_4^+$, $NO_3^-$, $SO_x$ and BC. The compounds $Na^+$, $Cl^-$, $NH_4^+$, $NO_3^-$, $SO_x$, and BC are given in µg/m$^3$ whereas the remaining species are given in ng/m$^3$. The analysis was conducted with both four and five emission sources based on Heidam et al. (2004) and Nguyen et al. (2013). It was found that five different sources were necessary in order to describe the measurements of the species composition during this time period. In the base run all 20 runs converged and the best solution showed a $Q_{robust}$ and $Q_{true}$ value of 6794 and 9902 respectively. To check the stability of the solution 100 bootstrap runs were successfully conducted and all converged. Furthermore, Fpeak runs with strength of 0.1 to 0.5 showed $Q_{robust}$ and $Q_{true}$ values of 6799 to 6906 and 9902 to 9904, respectively. The Q values were only to a small extent influenced by the Fpeak runs ($Q_{true}/Q_{robust} < 1.5$), which imply that local minimum has been found and that a stable solution is obtained. The five different source profiles are presented in Figure 4.25 to Figure 4.29.

Al, K, Ca, Ti, V, Si, Zr, Mn, Fe and Rb dominate source 1 where no BC is present. As seen from the time profile this source has peaking concentrations during spring and summer months (Figure 4.25). The peaks are however much more evident in 2008 compared to 2009. In source 2 there are only two dominating species; $Cl^-$ and $Na^+$. This source also includes species such as K, Ca, V and Sr together with small amounts of $SO_x$ and BC (17 %). An annual trend where the concentrations during summer are low contrary to higher concentrations during autumn and winter periods is observed (Figure 4.26). The highest abundance of Pb, Br, As and BC (57 %) are found in source 3. Almost all of the remaining species are also evident in source 3 except for $Cl^-$ and $NO_3^-$. For this source a seasonal pattern is observed with peaking concentrations during winter periods and decreasing concentrations during summer periods (Figure 4.27). A high abundance of Cu, Ni, S, $NH_4^+$, $NO_3^-$ and $SO_x$ are evident in source 4, where 9 % of BC is present. A seasonal pattern is observed with peaking concentrations in the spring months (Figure 4.28). Finally, the highest abundance of Zn and Cr are found in source 5. It also includes high concentrations of Al, K, Si, S and Fe and approximately 17 % BC is evident in the source. It is not to the same extent possible to find a seasonal pattern for this source compared to the other sources. The highest concentrations occur in January 2009 and in general the concentrations are higher in 2009 compared to 2008 (Figure 4.29).

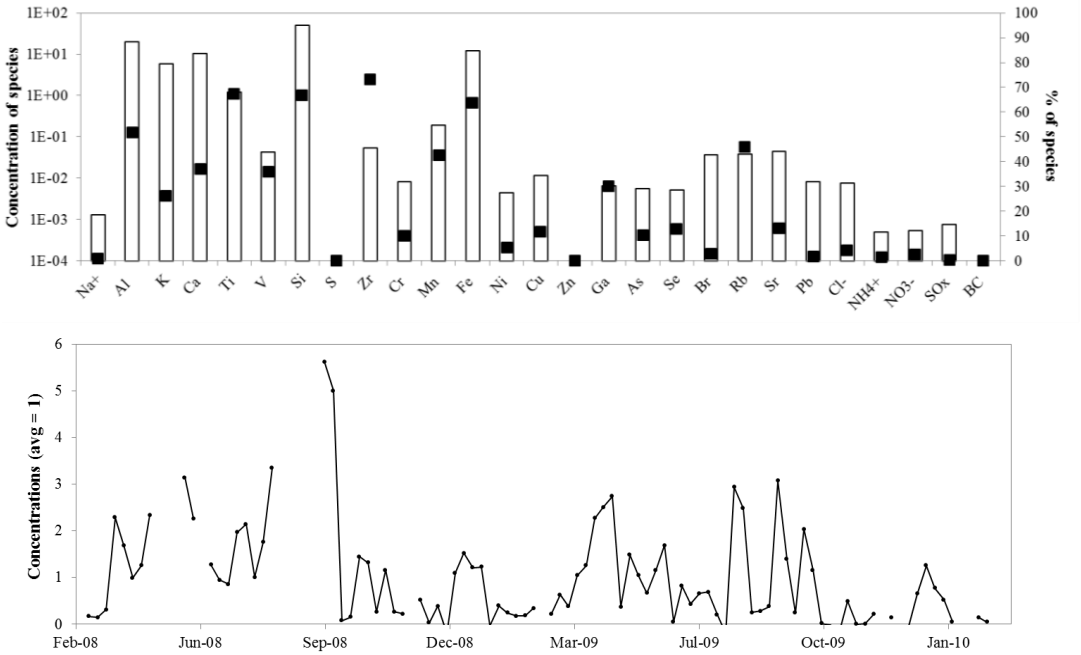


**Figure 4.25** Source 1 from the PMF analysis based on measurements taken at Station Nord from March 2008 to February 2010. Upper: The columns represent the concentration of the species, where the magnitude is read on the primary y-axis and the squares indicate the percentage of the species that is apportioned to this source which is read on the secondary y-axis. Lower: Time profile showing the source strength, where the average concentration is normalised to 1.

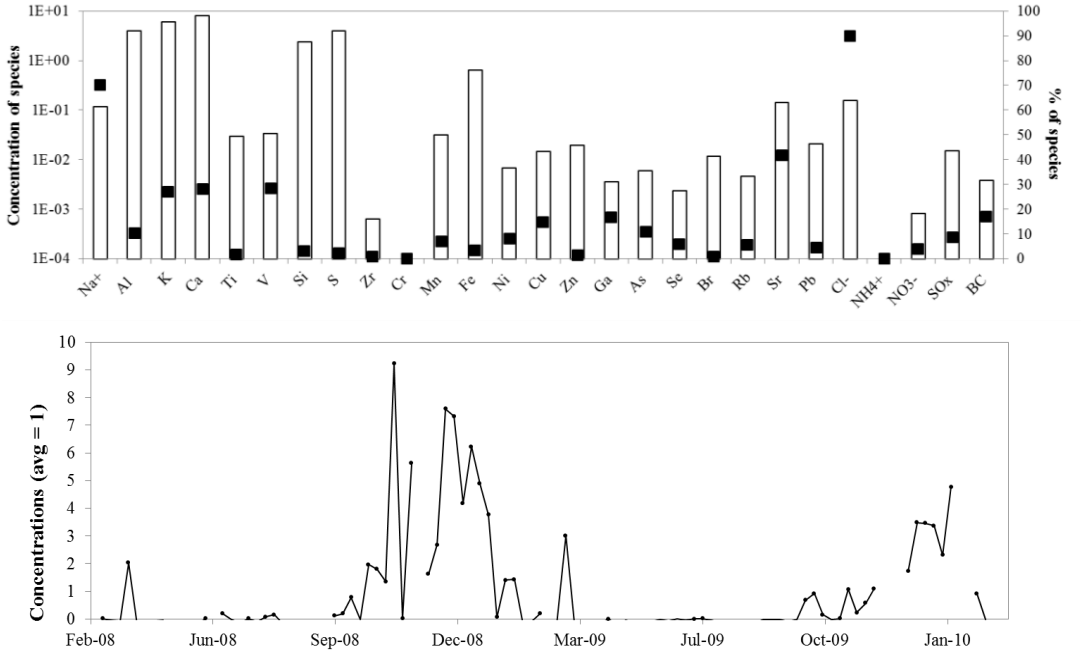


**Figure 4.26** Source 2 from the PMF analysis based on measurements taken at Station Nord from March 2008 to February 2010. Upper: The columns represent the concentration of the species, where the magnitude is read on the primary y-axis, and the squares indicate the percentage of the species that is apportioned to this source, which is read on the secondary y-axis. Lower: Time profile showing the source strength, where the average concentration is normalised to 1.

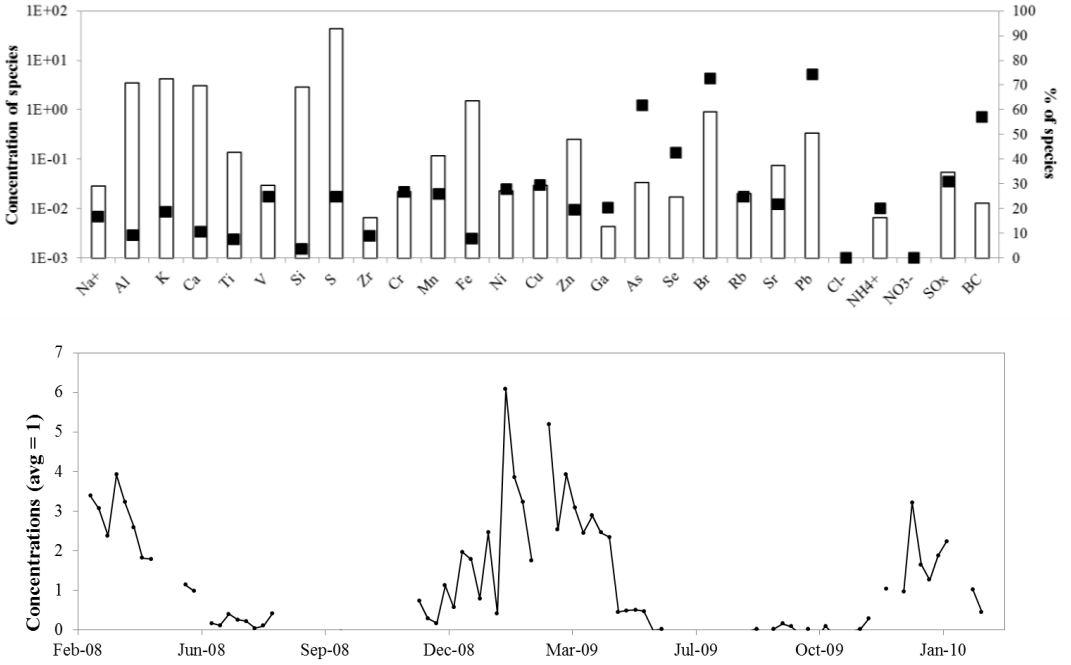


**Figure 4.27** Source 3 from the PMF analysis based on measurements taken at Station Nord from March 2008 to February 2010. Upper: The columns represent the concentration of the species, where the magnitude is read on the primary y-axis, and the squares indicate the percentage of the species that is apportioned to this source, which is read on the secondary y-axis. Lower: Time profile showing the source strength, where the average concentration is normalised to 1.

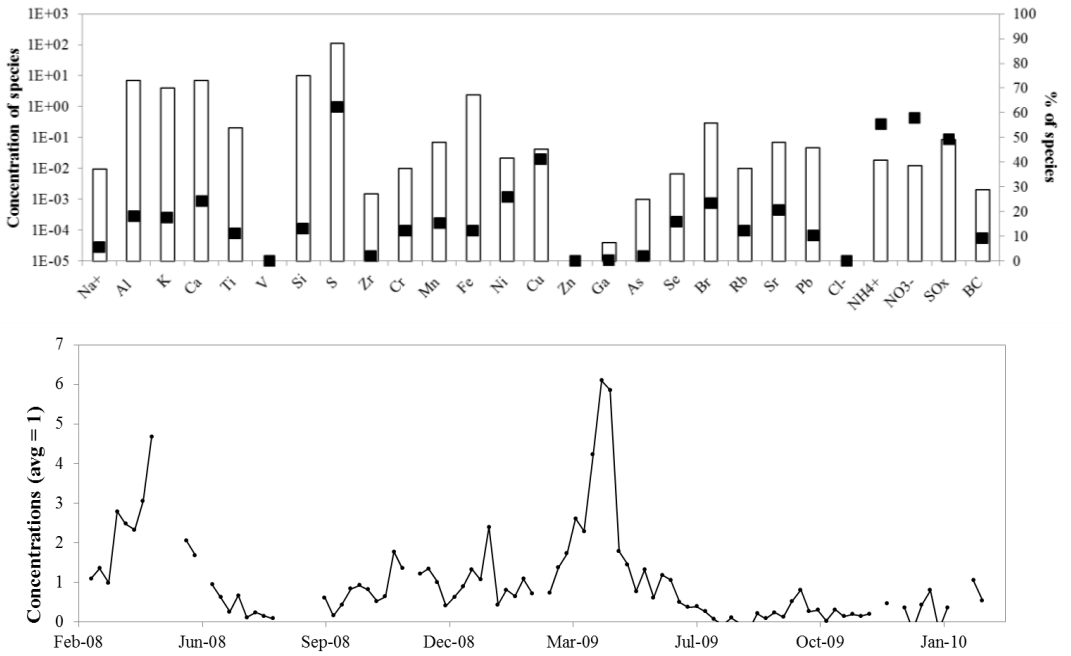


**Figure 4.28** Source 4 from the PMF analysis based on measurements taken at Station Nord from March 2008 to February 2010. Upper: The columns represent the concentration of the species, where the magnitude is read on the primary y-axis, and the squares indicate the percentage of the species that is apportioned to this source, which is read on the secondary y-axis. Lower: Time profile showing the source strength, where the average concentration is normalised to 1.

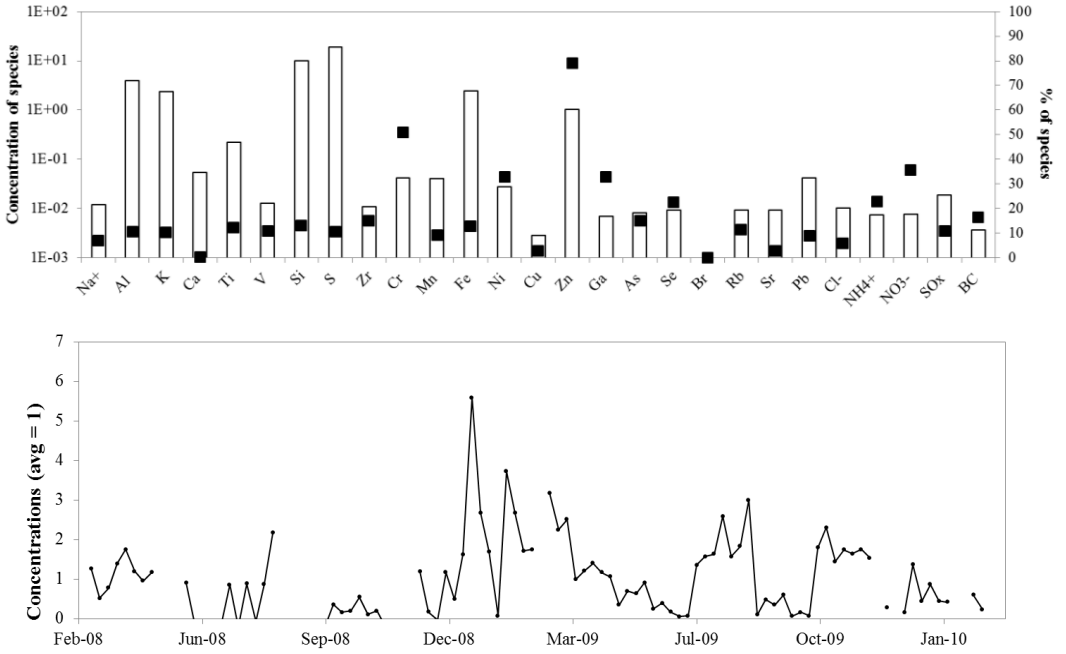


**Figure 4.29** Source 5 from the PMF analysis based on measurements taken at Station Nord from March 2008 to February 2010. Upper: The columns represent the concentration of the species, where the magnitude is read on the primary y-axis, and the squares indicate the percentage of the species that is apportioned to this source, which is read on the secondary y-axis. Lower: Time profile showing the source strength, where the average concentration is normalised to 1.

### 4.4.3 PMF from 2011 to 2012

The PMF analysis based on measurements from January 2011 to December 2012 includes the same species as PMF (2008-2010) except from Si, S, Zr and BC, which are not included in 2011-2012. Instead EC and OC are added to the analysis. The compounds $Na^+$, $Cl^-$, $NH_4^+$, $NO_3^-$, $SO_x$, EC and OC are given in µg/m$^3$, whereas the remaining species are given in ng/m$^3$. Based on Heidam et al. (2004) and Nguyen et al. (2013) the analysis was conducted with four and five sources. As for the previous time period five different sources were necessary in order to describe the measurements of the species composition at Station Nord during this time period. In the base run, 19 out of 20 runs converged and the best solution resulted in a $Q_{robust}$ and $Q_{true}$ value of 3575 and 3887 respectively. The stability of the solution was checked by running 100 bootstraps for which all converged. Furthermore, Fpeak runs with strengths of 0.1 to 0.5 gave $Q_{robust}$ and $Q_{true}$ values of 3580 to 3662 and 3887 to 3892 respectively. The Q values were only to a small extent influenced by the Fpeak runs ($Q_{true}/Q_{robust} < 1.5$), which imply that local minimum has been found and that a stable solution is obtained. The five different sources are presented in Figure 4.30, Figure 4.31, Figure 4.32, Figure 4.33 and Figure 4.34.

In source 1, Al, K, Ca, Ti, V, Mn Fe, Ga, and Rb are the dominating species. EC and OC are not present in this source. The time profile of the source does not indicate any seasonal variation. In autumn 2011 there is a very high peak, which is not seen in the autumn of 2012 (Figure 4.30). $Na^+$ and $Cl^-$ are the two dominating species in source 2, which also includes smaller amount of K, Ca, Se, Sr, $SO_x$, EC (21 %) and OC (20 %).

The abundance of EC and OC is 21 % and 20 % respectively. Figure 4.31 indicates a seasonal trend where the concentrations during summer are low contrary to higher concentrations during autumn and winter periods. The peaks are however much more profound in 2011 than in 2012. The highest abundance of Zn, As and Pb are found in source 3, where less than 10 % of BC is present. Figure 4.32 suggests a seasonal pattern for this source, where concentrations are peaking during winter and spring months and are lower during summer months. In source 4 the highest abundance of Cu, $NH_4^+$, $NO_3^-$ and $SO_x$ is found. Both EC and OC are present in this source with 8 % and 14 % respectively. No seasonal pattern is indicated to the same extent compared to the previous sources. The highest concentrations are generally found in 2011 compared to 2012 (Figure 4.33). Finally source 5 holds the highest abundance of Ni, Cr, Br, EC and OC, where 64 % EC and 66 % OC is apportioned to this source. No seasonal pattern is indicated and the concentrations are more evenly distributed over the two-year period although with higher peaks occurring in winter 2012 (Figure 4.34).

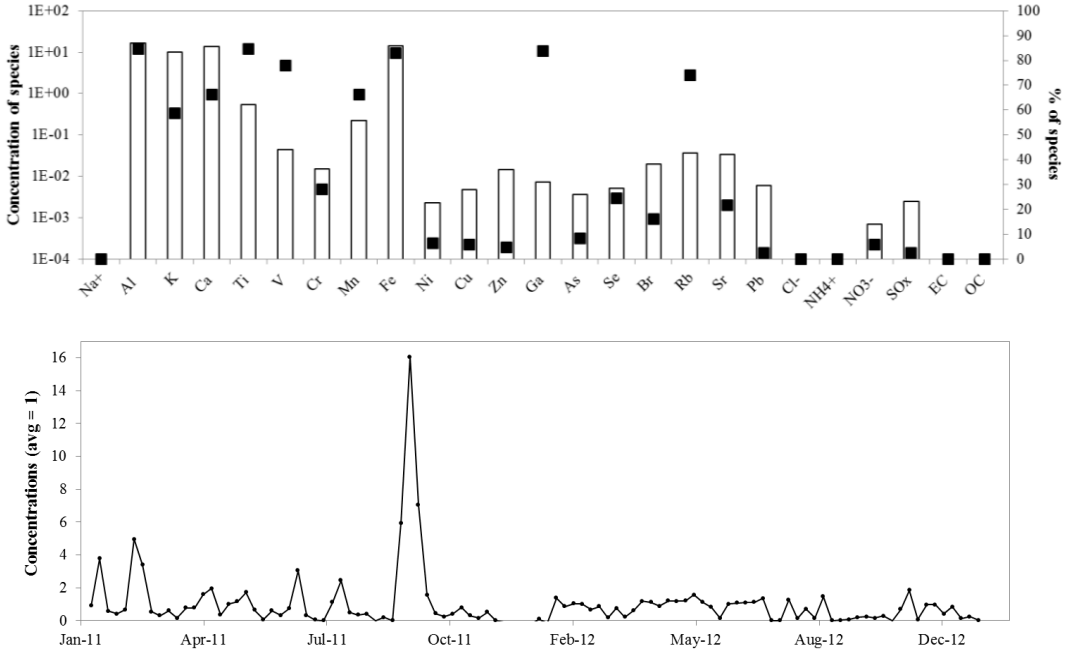


**Figure 4.30** Source 1 from the PMF analysis based on measurements taken at Station Nord from January 2011 to December 2012. Upper: The columns represent the concentration of the species, where the magnitude is read on the primary y-axis, and the squares indicate the percentage of the species that is apportioned to this source, which is read on the secondary y-axis. Lower: Time profile showing the source strength, where the average concentration is normalised to 1.

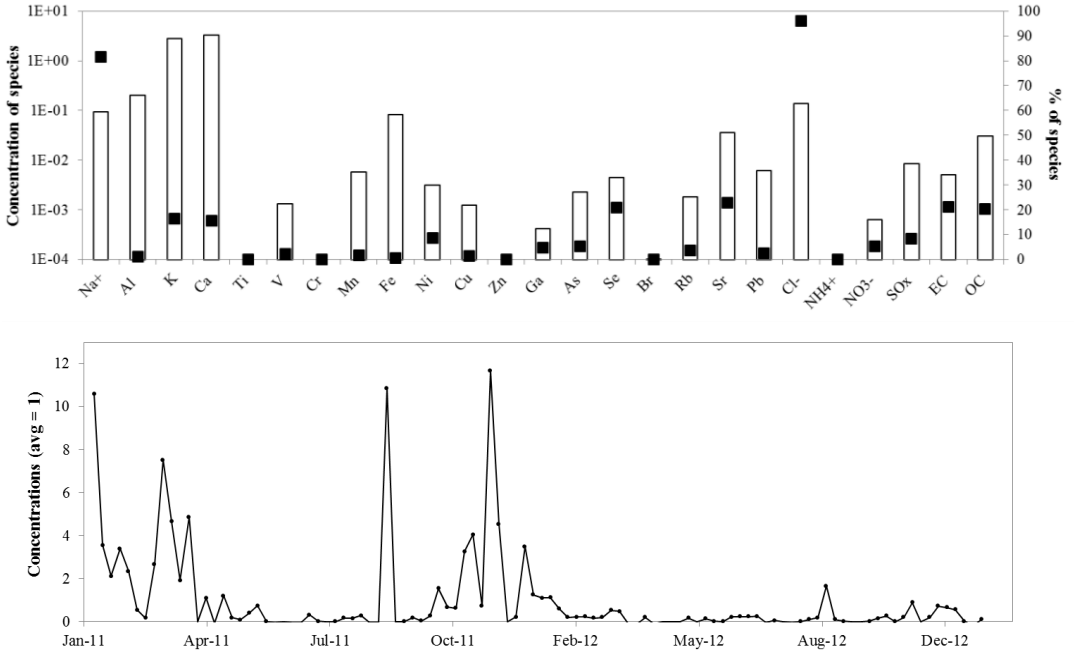


**Figure 4.31** Source 2 from the PMF analysis based on measurements taken at Station Nord from January 2011 to December 2012. Upper: The columns represent the concentration of the species, where the magnitude is read on the primary y-axis, and the squares indicate the percentage of the species that is apportioned to this source, which is read on the secondary y-axis. Lower: Time profile showing the source strength, where the average concentration is normalised to 1.

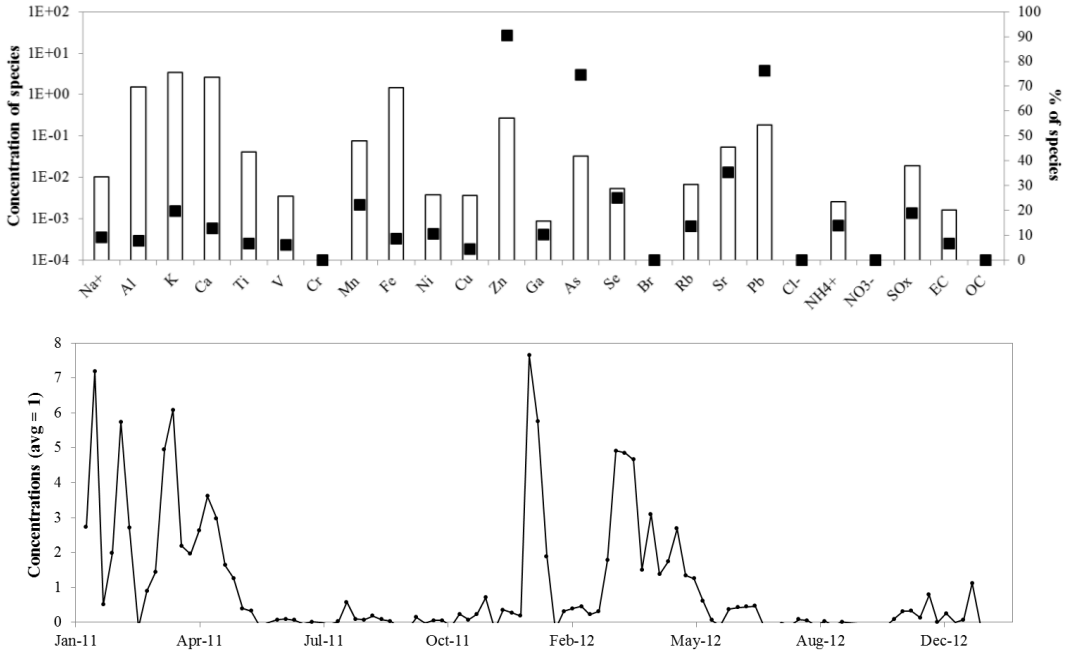


**Figure 4.32** Source 3 from the PMF analysis based on measurements taken at Station Nord from January 2011 to December 2012. Upper: The columns represent the concentration of the species, where the magnitude is read on the primary y-axis, and the squares indicate the percentage of the species that is apportioned to this source, which is read on the secondary y-axis. Lower: Time profile showing the source strength, where the average concentration is normalised to 1.

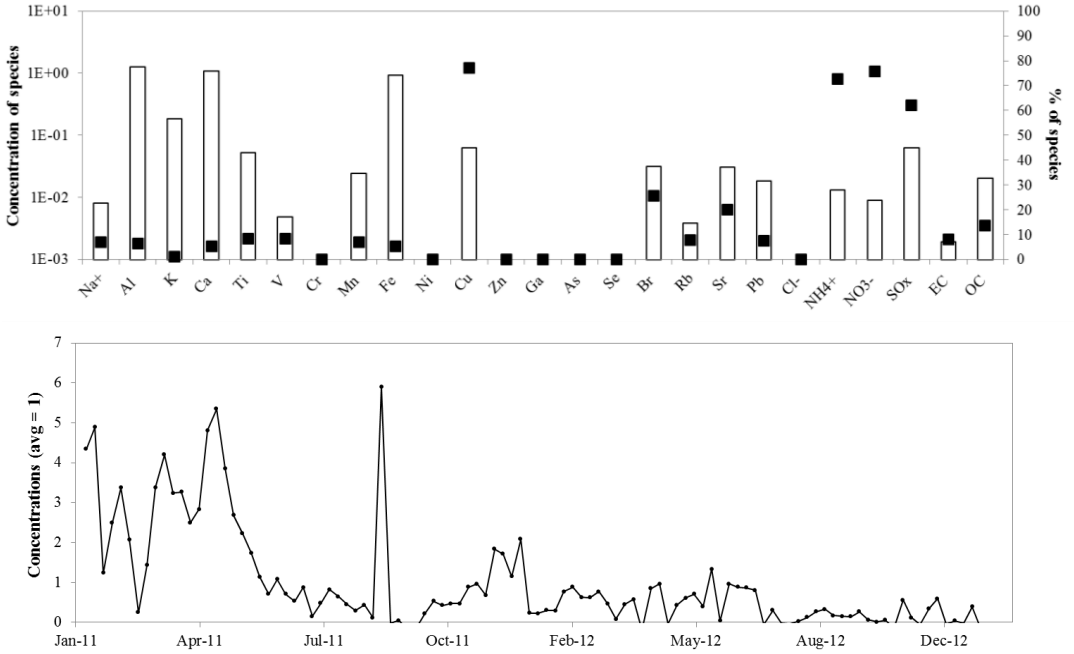


**Figure 4.33** Source 4 from the PMF analysis based on measurements taken at Station Nord from January 2011 to December 2012. Upper: The columns represent the concentration of the species, where the magnitude is read on the primary y-axis, and the squares indicate the percentage of the species that is apportioned to this source, which is read on the secondary y-axis. Lower: Time profile showing the source strength, where the average concentration is normalised to 1.

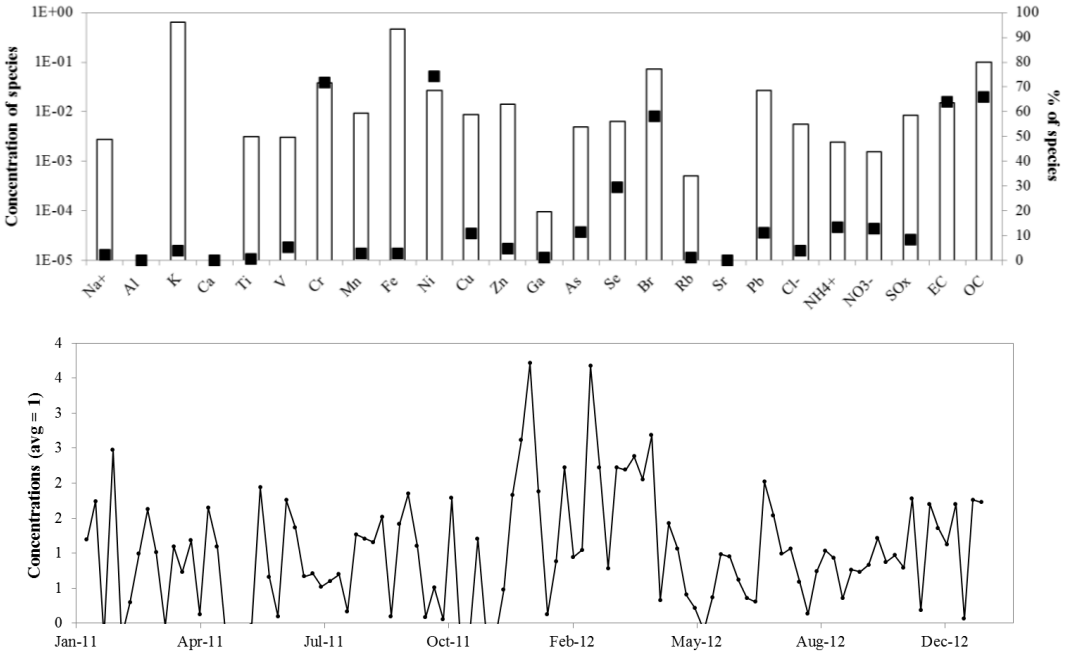


**Figure 4.34** Source 5 from the PMF analysis based on measurements taken at Station Nord from January 2011 to December 2012. Upper: The columns represent the concentration of the species, where the magnitude is read on the primary y-axis, and the squares indicate the percentage of the species that is apportioned to this source, which is read on the secondary y-axis. Lower: Time profile showing the source strength, where the average concentration is normalised to 1.

# 5 Discussion

In the following section the measured and modelled BC concentrations in air and snow will be described together with the source apportionment of BC obtained from the PMF analyses.

## 5.1 Measured and Modelled Concentrations of BC

Monthly averages of BC, EC and modelled BC concentrations are shown in Figure 5.1. Due to the low flow very small amounts of particles hit the filter every 15 minutes resulting in high noise levels on the PSAP. The high noise level caused several negative weekly concentrations and the measured BC concentrations were therefore treated as monthly averages. The measured weekly EC concentrations and the daily BC concentrations modelled by DEHM have therefore also been treated as monthly averages, resulting in more smooth concentration curves, in order to obtain a better comparison (Figure 5.1). The concentrations of BC (black line), EC (grey line) and the concentrations modelled by DEHM (dashed line) are in the same order of magnitude, indicating that the DEHM model is good. There are some exceptions, especially in winter 2009 and 2011, where the measured BC concentrations are considerably higher. If BC this year came from sources closer to Station Nord, it would be fresher thus having a higher specific absorption coefficient than 5.5 $m^2/g$ (Bond & Bergström, 2006; Petzold, 1995). If a higher specific absorption coefficient was used for those years it would have resulted in lower BC concentrations. For 2011 it was not possible to find the specific absorption coefficient due to no significant linear correlation and for 2009 it was found to be 5.8 $m^2/g$, which is not that different from the one used.

The measurements of EC and BC concentrations have been conducted by two different methods located 2.5 km apart, which may explain why the concentrations are different. The HVS is placed at Station Nord in the DMI hut, which is approximately 2.5 km north-west of Flyger's hut, where the PSAP is installed. If local air pollution, to some extent, has an impact on the concentrations, the EC measurements will be affected the most, since the activity including traffic is much higher on the station. This would result in higher EC concentrations compared to BC, which is observed occasionally. Another issue, which may explain differences in BC and EC concentrations, is possible differences in the analysed air masses. The main wind direction is approximately perpendicular to the bee-line between the two measurements sites, hence the air masses, which are transported to Station Nord and analysed by the two machines may not be identical (Figure 3.3). The assumption that all absorption measured by the PSAP is due to BC may also impact the measured concentrations. Absorption caused by BrC, which is

actually a type of OC, as explained in section 2.1, is also measured as BC, because of its absorptive properties. In the OC-EC analysis the BrC is accounted for as OC and is therefore not included in the EC concentration.

Figure 5.1 indicates that the measured and modelled BC and EC concentrations approximately follow the same seasonal pattern, with low concentrations during summer and peaking concentrations during winter and spring. This is consistent with the typical seasonal cycle of Arctic haze promoted by the expansion of the polar dome during winter and spring. Towards the southern boundaries of the polar dome, the Arctic front acts as a transport barrier as explained in section 2.4.1. During winter the Arctic front can extend as far south as 40˚N in Eurasia, hence opening up for long range transport of air pollution into the Arctic from various kinds of sources. During summer, on the other hand, the Arctic front approximately follows the Northern coastline of Eurasia meaning that low-level transport is almost eliminated at this time of year. However, small concentration peaks are observed both for the modelled and measured BC and EC concentrations. Air masses originating from forest fires during summer in source regions outside the Arctic may be lifted into the free troposphere and subsequently penetrate the polar dome. However, the chance of measuring those particles close to sea level at Station Nord would be small, due to the high stratification inside the polar dome. The peaks could more likely be ascribed to oil flaring and the increased Arctic shipping in summer due to the reduced sea ice extent (Corbett et al., 2010) Those two emission sources are north enough to be inside the polar dome during summer. Finally, it is assumed that local pollution from Station Nord is minimal, but there could be a chance that waste burning during summer also may contribute to BC contamination.

The specific absorption coefficient for BC of 6.2 $m^2/g$ found in this study had a poor coefficient of determination ($R^2$) of 0.4. Nevertheless, the value is close to other determinations of BC specific absorption coefficients, e.g. 5.5 $m^2/g$ found by Hegg et al. (2011) and 7.5 $m^2/g$ found by Bond and Bergström (2006). Due to the poor determination, the specific absorption coefficient of 5.5 $m^2/g$ obtained by Hegg et al. (2011) on Svalbard was used. An explanation of the poor determination obtained in this study may be the low flow, which increases the noise to signal ratio. On Svalbard a much higher flow was used and a very good correlation was obtained (J. Ström, Professor, Stockholm University, pers. comm., June 2013). If the specific absorption coefficient of 6.2 $m^2/g$ found in this study on Station Nord would have been used instead, the BC and EC concentrations would differ less (Figure 5.2). The specific absorption coefficient is not only assumed to be site-dependant but also seasonal dependant (e.g. AMAP, 2012) due to different emission sources and aging of the BC. In this study the summer and winter correlations were too bad to make reasonable conclusions, but it should be kept in mind that this would also change the BC concentrations a little on a seasonal basis. A higher specific absorption coefficient would lead to smaller concentrations and vice versa.

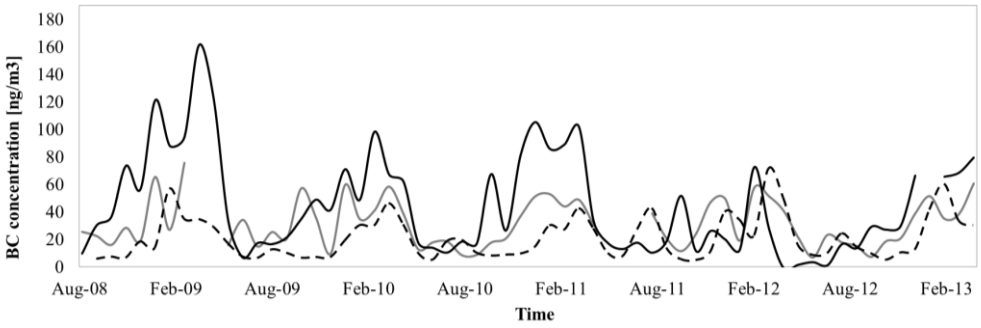


**Figure 5.1** Measured EC (grey line) and BC (black line) concentrations in air using a specific absorption coefficient of 5.5 $m^2/g$ at Station Nord from August 2008 to April 2013 compared to BC concentrations modelled by DEHM (dashed line). Empty space indicates missing data periods.

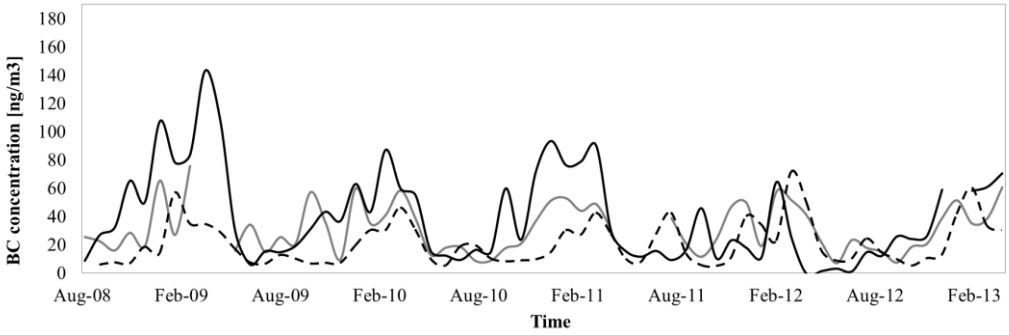


**Figure 5.2** Measured EC (grey line) and BC (black line) concentrations using a specific absorption coefficient of 6.2 $m^2/g$ at Station Nord from August 2008 to April 2013 compared to BC concentrations modelled by DEHM (dashed line). Empty space indicates missing data periods.

On top of being too low, the flow was also quite unstable, especially in the first two years and it was not measured very often. The flow and the concentrations are inversely proportional, so the size of the flow has a great impact on the size of the concentrations; a halving of the flow would result in a doubling of the concentrations and vice versa. In between August 2008 and March 2009, where the flow has not been measured, a big decrease occurs (Figure 4.12). If the flow in part of this period was actually lower than 48.85 ml/min the BC concentrations would be higher. This does not explain why the measured BC concentrations seem higher than the measured EC concentrations and the modelled BC concentrations, but the issue adds uncertainty to the BC concentrations in periods with no flow measurements where a decrease or increase is observed. Chow et al. (2009) use a flow rate of 50 mL/min in California, where the BC concentration is assumed to be higher than at Station Nord. Hence a flow higher than 50 ml/min would be recommended for Station Nord.

As explained in section 2.1 the EC/OC ratio may tell something about what kind of combustion the particles originate from. A high EC/OC ratio indicate combustion fossil fuels (app. 1.0 for diesel), while a low ratio indicates biofuel or biomass burning (app. 0.25 and 0.11, respectively). There is a week indication of seasonal variations of the EC/OC ratios measured at Station Nord with the highest ratios occurring in winter and spring (app. 0.20) and the lowest during summer (app. 0.07). The relatively low annual

average ratios between 0.14 and 0.16 indicate that part of the OC found on Station Nord is secondary OC. The very low EC/OC ratios observed during summer may be due to higher production of secondary OC. The larger EC/OC ratios during winter and spring are consistent with the high EC concentrations at this time explained by the expansion of the polar dome. In order to determine what kinds of combustion sources the OC and EC origin from, it is recommended to look at the concentrations of trace elements as well; e.g. low EC/OC ratios together with high concentrations of $K^+$ would indicate emissions from biomass burning (Zhou et al., 2012).

When comparing the measured BC concentrations at Station Nord to the measured concentrations at other Arctic locations it should be kept in mind that even though the stations are all located in the Arctic, they all receive different air masses. It should also be emphasised that the measurement periods at the monitoring stations Alert, Zeppelin and Barrow are very short (section 2.4.2). It is noticed that the concentrations at these locations follow the same pattern as for Station Nord. The measured BC concentrations found at Station Nord are approximately twice as large compared to Alert and Zeppelin, whereas the measured EC concentrations are closer to the concentrations measured at Alert and Zeppelin. Compared to the measured concentrations at Barrow both the measured EC and BC concentrations on Station Nord seem higher. This may be due to the absorption coefficient used in the present study. Until recently a specific absorption coefficient of 10 $m^2/g$ has generally been accepted for remote areas and has often been used in previous studies. Additionally, it has to be noticed, that the different Arctic locations cannot be simply compared with regard to the level of BC concentration as the source origins for BC might differ because of varying transport routes among the stations.

Measured BC and EC concentrations at Station Nord are not very different from concentrations measured in rural areas of Denmark. Massling et al. (2011) found that rural Danish BC concentrations vary between 120 $ng/m^3$ and 130 $ng/m^3$ and urban concentrations vary between 340 $ng/m^3$ and 380 $ng/m^3$ based on a specific absorption coefficient of 10 $m^2/g$. It is quite alarming that the average concentrations found at Station Nord during winter are approximately half of the concentrations measured in Danish rural areas and within the same order magnitude as in Danish urban areas (Massling et al., 2011). Since there are almost no emission sources so far north, this indicates that long range transport of BC from source regions outside the Arctic is important. As described in section 2.5 especially emissions from the Arctic Council Nations are of great importance in the Arctic.

### 5.1.1 BC Concentrations in Snow

The average measured BC concentration of 521 ± 441 ng/l in snow at Station Nord (Flyger's Hut) is quite uncertain, which is indicated by the large standard deviation. The high variability (relative standard deviation of 85 %) indicates a high method uncertainty. Despite the high uncertainty, the results are still important, since BC has never been measured in snow at Station Nord before. It is valuable to have snow measurements from as many locations in the Arctic as possible to improve climate - and transport models.

The indication of no significant differences between the measurements near the icebergs, at Knuth's Fjeld and Flyger's Hut supports the assumption of minimal local air pollution from Station Nord around Flygers Hut. This makes good sense when looking at the prevailing wind direction in the area (coming from south-west), which is approximately perpendicular to the bee-line between the station and Flyger's Hut (Figure 3.3). The Student's t-test indicated that the BC concentration measured at the runway was significantly higher than at Flyger's Hut. Airplanes were flying in from north-west and therefore it is assumed that Knuth's Fjeld, which is located approximately 7 km south-east of Station Nord (and the runway) was not influenced by pollution from the air craft, when taking the wind direction into consideration. The Student's T-test indicated that there was no significant difference between the concentrations measured at Flyger's Hut and Knuth's Fjeld; hence it was assumed that the impact from aircrafts on BC concentrations of samples taken around Flyger's Hut was insignificant.

When comparing the BC concentrations in snow found at Station Nord to the other Arctic concentrations found by Doherty et al. (2010) the average BC concentration at Station Nord seems significant lower. It should be stated that there are also high uncertainties related to the concentrations found by Doherty et al. (2010). The BC concentration found at Station Nord during April is most similar to the concentrations of 1000 ng/l (± 1000 ng/l) and 4000 ng/l (± 2000 ng/l) found by Doherty et al. (2010) in Greenland (measured on the GIS) during summer and spring, respectively. Equal concentrations at Station Nord and the GIS are however, not expected since the areas are influenced by different air masses. The study by Doherty et al. (2010) indicates that BC concentrations in snow, especially in Russia and Norway, are much higher than at Station Nord. This could be explained by the closer proximity to emission sources.

## 5.2 Source Apportionment

The results from the PMF analysis covering data from March 2008 to February 2010 with new BC concentrations shows great comparability with the results obtained by Nguyen et al. (2013). This was expected since only minor changes in the BC concentrations were introduced compared to the run by Nguyen et al. (2013). Consequently, the main difference is observed in the apportionment of BC.

The PMF analyses for March 2008 to February 2010 and January 2011 to December 2012 showed the best data-fit with a five-source solution. Three sources recurred in both analyses: *Soil*, *Marine* and *Combustion*. PMF (2008-2010) also included a *Cu/Ni* and a *Zn* source, while in PMF (2011-2012) a *Cu* and *Ni/Cr* source were identified. It should be clarified, that a source consists of several point sources, which have approximately the same seasonal pattern, indicating that the species have been transported to Station Nord with the same air masses. When a source is referred to as, e.g. "the *Cu* source", this simply implies that Cu is one of the dominating compounds contributing to the source. It does not mean that all the different compounds necessarily origin from the Cu industry or the same geographical location, but it indicates that the compounds are transported to Station Nord with the same air masses as the Cu in this source.

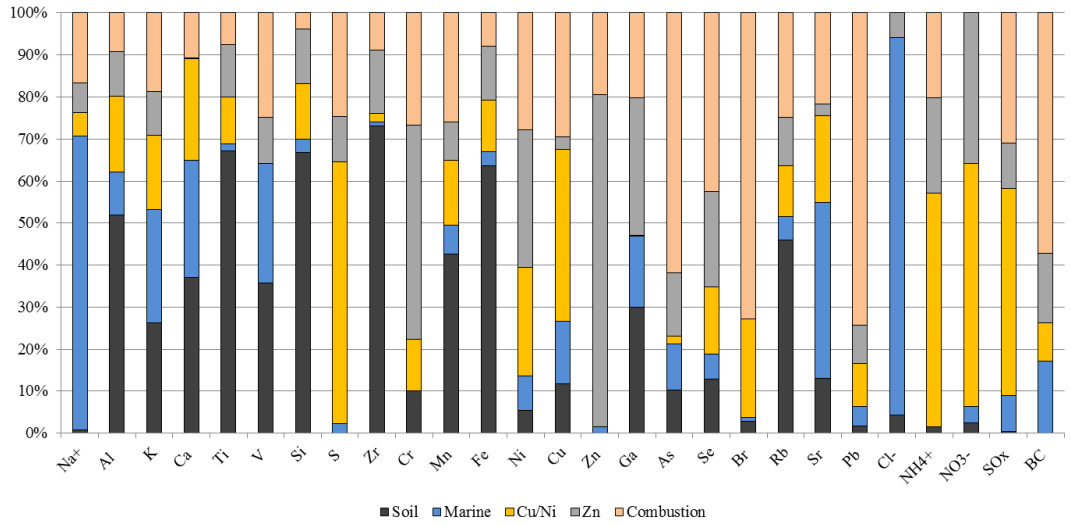


**Figure 5.3** Source origins of chemical species apportioned by PMF analysis conducted with data from Station Nord in the period from March 2008 to February 2010. The columns indicate the percentage of the species that is apportioned to the five different sources: *Soil, Marine, Cu/Ni, Zn* and *Combustion.*

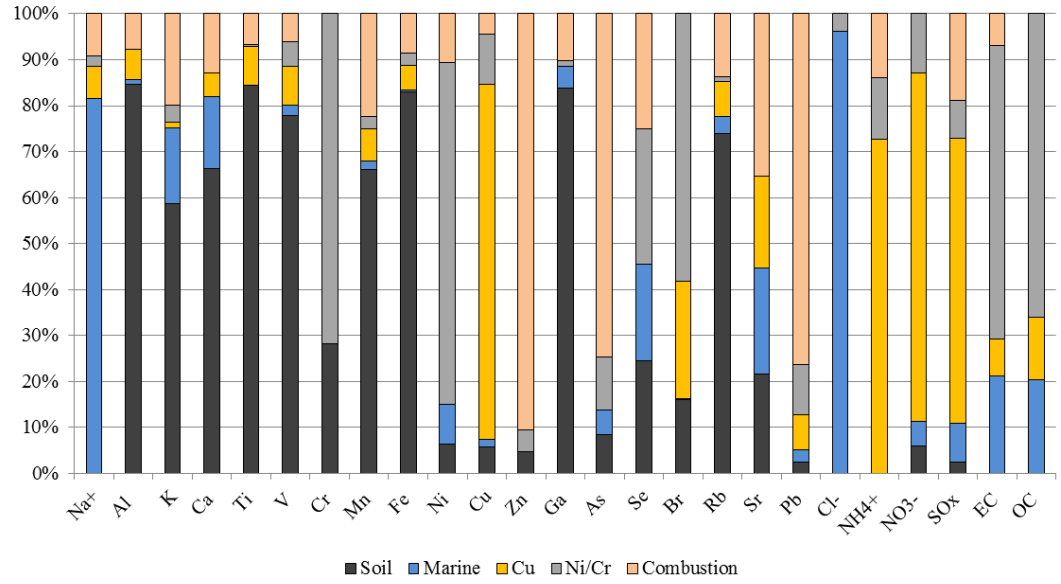


**Figure 5.4** Source origins of chemical species apportioned by PMF analysis conducted with data from Station Nord in the period from January 2011 to December 2012. The columns indicate the percentage of the species that is apportioned to the five different sources: *Soil, Marine, Cu, Ni/Cr* and *Combustion.*

The source origins of the chemical species for the PMF analyses for 2008 to 2010 and 2011 to 2012 are presented in Figure 5.3 and Figure 5.4, respectively. Source 1 for both analyses is interpreted as a *Soil* source since it mainly contains Al, Si, Ti, Zr and Fe. These compounds are often associated with crustal elements, which are emitted to the atmosphere as windblown dust and soil (Heidam et al., 1999; Heidam et al., 2004). Also V has been associated with the crustal source in other Arctic studies and is especially seen in the PMF (2011-2012). The source has previously been described as peaking during spring and late summer (Heidam et al., 1999; Heidam et al., 2004), which is also observed in PMF (2008-2010) but not to the same extent in PMF (2011-2012). In the

latter a high peak during autumn 2011 is observed, which may indicate terrestrial storms. BC is not related to soil and is hence not found in this source in any of the analyses.

Source 2 is interpreted as a *Marine* source for both data-sets due to its high amount of $Na^+$ and $Cl^-$. The *Marine* source also includes Ca, K and Sr, which are abundant in sea water and hence in sea spray aerosols (Heidam et al., 1999; Nguyen et al., 2013). In PMF (2008-2010) Al, Si, Ti and Fe are also abundant in the *Marine* Source, which could imply that the source may be mixed with the *Soil* source. This is however not the case in PMF (2011-2012). The increased concentrations in this source during autumn could be a result of ocean storms, which can lead to a higher production of sea spray aerosols favoured by the decreasing extent of sea ice, as described in section 1. Since the oceans around Station Nord are frozen during winter the increased concentrations at this time of year cannot originate from open waters. Another possibility is that the increased concentrations during winter can be caused by frost flowers torn at high wind speeds (Fenger et al. 2013). BC (17 %), EC (21 %) and OC (20%) are evident in the *Marine* source for both analyses and could be a result of the increased Arctic shipping (Corbett et al., 2010) or long range transport.

Source 3 is for both analyses interpreted as a *Combustion* source due to high abundance of Pb, As and Mn. The fraction of the species is more or less the same in the two analyses. A major difference is the abundance of BC and EC, where 57 % BC is ascribed to the *Combustion* source in PMF (2008-2010) compared to only 7 % EC in PMF (2011-2012). High OC and BC or EC concentrations would be anticipated in the *Combustion* source, but no OC and only low EC concentrations are observed in PMF (2011-2012). This would indicate very clean combustion, which is not assumed to be the case. The poor data set for 2011-2012 may be the reason for the low concentrations. EC and OC seem to be linked to especially Ni and Cr, which were poorly determined in the laboratory due to the change of analysis method.

As previously described, the polar dome formed over the lower Artic troposphere affect the transport of emissions into the Arctic. The boundary of the dome, the Arctic front, may extend as far south as 40º N in January in the northern Eurasia, thus opening up for long range transport of air pollution into the Arctic (Law & Stohl, 2007; Stohl, 2006). The high concentrations during winter and spring followed by lower concentrations during summer and autumn, observed in the *Combustion* source, are hence consistent with the cycle of Arctic haze due to expansion of the polar dome during winter and spring. In the Arctic Council Nations, BC emissions from domestic heating is higher during winter than in summer, which also supports the indication of such seasonal pattern. It should be clarified though, that it is not possible to distinguish between fossil fuel and biomass combustion in the analysis.

Source 4 in PMF (2008-2010) is identified as a *Cu/Ni* source obviously due to the high abundance of Cu and Ni. According to Nguyen et al. (2013) the *Cu/Ni* source could originate from Eurasia, where especially the Siberian Cu and Ni industry contributes to pollution in the Arctic. Furthermore, the abundance of $NO_3^-$, $SO_x$ and BC (9 %) indicate emissions from combustion sources transported with the same air masses. A similar type

of source is not found in PMF (2011-2012). Source 4 has a high abundance of Cu but not Ni and is hence referred to as the *Cu* source, which could come from the Siberian Cu industry that contributes to pollution in the Arctic. The abundance of $NO_3^-$, $SO_x$, OC and EC (8 %) in the source could originate from combustion processes in connection to the metal industry. Both the *Cu/Ni* and *Cu* source has a high abundance of $NH_4^+$, which may be a result of air masses from agricultural areas.

Source 5 in PMF (2008-2010) is interpreted as a *Zn* source due to its high fraction of Zn. Based on air mass back trajectories Nguyen et al. (2013) discussed that the *Zn* source could originate from a major Zn mine in Canada – the Canadian Arctic Archipelago mine. A *Zn* source is not found in PMF (2011-2012) since the main fraction of Zn is apportioned to the *Combustion* source. Heidam et al. (2004) also investigated source apportionment at Station Nord using the Constrained Physical Receptor Model (COPREM). This study looked at a time horizon of 11 years and also found that the majority of Zn was contributed to a *Combustion* source. The reason for not finding the same extent of Zn in the *Combustion* source in 2008-2009 could be due to different meteorological conditions varying those years. This implies the necessity of looking at longer time periods. The abundance of BC is 17 % in the *Zn* source, which indicates that emissions from combustion sources have been transported with the same air masses.

Source 5 in PMF (2011-2012) is interpreted as a *Ni/Cr* source due to the high abundance of Cr and Ni, which could origin from the mining industry. Russia is one of the dominating source regions, which impact the site (Heidam et al., 2004); hence the emissions from the mining industry could originate from Russia. The source does not have a clear annual trend, which may be reasonable if considering a constant yearly mining production. However, this is only true if the source is located within the polar dome, which is confined to about 70° N during summertime (AMAP, 2011). If not, the seasonal pattern would be expected to show high concentrations during winter and lower concentrations during summer. In the *Ni/Cr* source the largest abundance of EC (64 %) and OC (66 %) is found, which implies some sort of combustion process originating from Russia. This agrees with the fact that large-scale industries are located in Siberia. Through back trajectories Nguyen et al. (2013) also found that the *Combustion* source, which included the largest proportion of BC in 2008-2010, most likely originated from Siberia. Thus both PMF analyses suggest that BC mainly originates from Russia. The *Ni/Cr* source indicates that EC and OC are mainly connected to Ni and Cr, which were found to be some of the problematic species when shifting from the PIXE to the ICP-MS method. When implementing the IC-PMS analysis, blank values were too high resulting in negative concentrations due to start-up problems. Since the PMF is constrained to positive values, a lot of median values were used, increasing the uncertainty for Ni and Cr. The BC apportionment could hence be misinterpreted, explaining the low abundance of BC in the *Combustion* source.

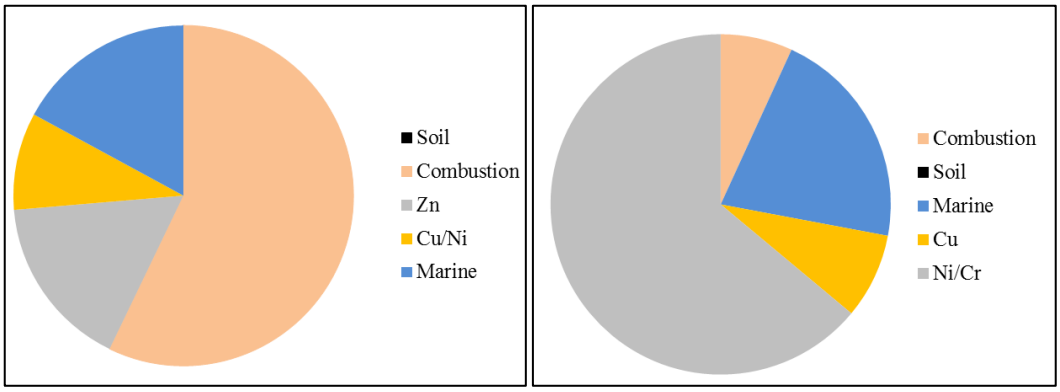


**Figure 5.5** The apportionment of BC on the five sources obtained from the PMF analysis of the period from 2008 to 2010 (left side) and from 2011 to 2012 (right side).

Figure 5.5 shows a detailed overview of BC's distribution in the five sources identified in PMF (2008-2010) and PMF (2011-2012). Overall, it is difficult to compare the five sources for BC found in this study with the emission inventories estimating the sectorial distribution of BC in the Arctic council nations (section 2.5.1). It has not been possible to subdivide the five sources in order to identify exactly from where BC is emitted, hence this apportionment analysis is not as specific as the emission inventories. As an example, it is not possible to determine whether the BC in the *Combustion* source mainly originates from the combustion of fossil fuels or biomass.

The differences in the source apportionments between the two analyses may be due to different reasons. First of all, it must be emphasized that the data set from 2011-2012 is connected with large uncertainty. As previously mentioned, several problems were discovered in the measurements from the ICP-MS when creating the input matrices for 2011-2012. Due to start-up problems with the new analytical method the blank values were too high resulting in many negative concentrations. The PMF is constrained to positive values, and thus a lot of median values were used for Ni, Cr, Cu, Br and Zn. The concentration determinations of these species were hence problematic and a lot of extra work was required to solve the issue with negative concentrations.

The samples used for the analysis are taken once a week. Within this time period the wind patterns may change and it is therefore possible that the measured concentrations origin from different emission sources. The metrological conditions may also change in certain years, which will impact the results of that period. This, of course adds uncertainty to the source apportionment, but the uncertainty may be reduced if a longer time period is examined. The study conducted by Heidam et al. (2004) using COPREM investigated measurements from a time horizon of 11 years and the analysis was therefore based on much more data, but concentrations of BC and OC were not available until 2008. Heidam et al. (2004) found that only four sources were necessary to describe the particulate concentrations at Station Nord. Future recommendations would hence be to run a PMF analysis for a longer time period, e.g. a five years period in 2015. This could proof whether the source apportionment is actually better described by five sources compared to four sources in the 1990'ies. Meanwhile it is highly recommended to reduce the

uncertainty on the ICP-MS and the blind values used for this analysis method. In order to better localise the sources it would furthermore be recommended to run back trajectory models as done by Nguyen et al. (2013). If an improved source apportionment can be obtained and the geographical origins of the BC concentrations at Station Nord are approximated, this information may be used together with the emission inventories described in section 2.5 to develop and improve mitigation strategies.

# 6 Conclusion

The BC air concentrations at Station Nord from August 2008 to April 2013 have been measured using two different methods; the thermal-optical OC-EC analysis and the light absorption method, PSAP. The EC concentrations determined by the OC-EC analysis vary between 1 ng/m$^3$ (November 2009) and 145 ng/m$^3$ (January 2011). There is an indication of seasonal variation with the highest average monthly concentrations of 49 ng/m$^3$ to 55 ng/m$^3$ occurring in January, March and April, and the lowest average concentrations of 14 ng/m$^3$ and 16 ng/m$^3$ occurring in June and September. There is a week indication of seasonal variations of the EC/OC ratios measured at station Nord with the highest ratios occurring in winter and spring (app. 0.20) and the lowest in summer (app. 0.07). The relatively low annual average ratios between 0.14 and 0.16 indicate that part of the OC found on Station Nord is secondary OC

A specific absorption coefficient of 6.2 m$^2$/g, based on measurements from the entire period, was determined from the EC concentrations and the absorption coefficients measured by the PSAP. The coefficient of determination ($R^2$) was only 0.4 indicating a weak linear relation. Therefore it was found reasonable to use a specific absorption coefficient of 5.5 m$^2$/g, determined with a very good correlation on Svalbard in Norway - another remote location in the Arctic. For the winter months (December to January), a specific absorption coefficient of 5.7 m$^2$/g was obtained, however with a poor correlation ($R^2$ = 0.4). No significant linear correlation was found for the summer period and it is therefore not possible to conclude anything on the seasonal variation of the specific absorption coefficient at Station Nord. An annual specific absorption coefficient was determined for 2009, 2010, and 2012. No significant linear correlation was found between monthly EC concentrations and monthly absorption coefficients for the remaining years.

The BC concentrations determined by using a specific absorption coefficient of 5.5 m$^2$/g vary between -1 ng/m$^3$ (May 2012) and 161 ng/m$^3$ (March 2009). The negative concentration is due to noise on the PSAP instrument. There is an indication of a seasonal variation, with the highest average monthly concentrations of 64 ng/m$^3$ to 94 ng/m$^3$ occurring between January and April and the lowest average concentrations of 9 ng/m$^3$ to 14 ng/m$^3$ occurring from June to August. The EC and BC concentrations obtained from the two different methods are generally in the same order of magnitude and approximately follow the same seasonal pattern with higher concentrations in winter and

spring and lower concentration in summer. There are some exceptions, especially during winter 2009 and 2011, where the measured BC concentrations are much higher. In order to improve the correlation between the two methods it is recommended to increase the flow to more than 50 ml/min and to make sure it is stable. It is also suggested to place the HVS and the PSAP next to each other to make sure the two instruments measure BC from the same air masses. The BC concentrations modelled by DEHM are also in the same order of magnitude as the measured concentrations and they approximately follow the same seasonal pattern, indicating that the DEHM model is good. Both the measurements and the model show the highest BC concentrations during winter and the lowest during summer. This is consistent with the typical seasonal cycle of Arctic haze.

EC concentrations in snow were measured for the first time at Station Nord. An average concentration of 525±441 ng/l was found in the upper 5 cm snow based on 7 samples of three replicates. The concentration was found near Flyger's Hut and was not assumed to be influenced by local pollution from Station Nord or from the air craft landing and taking of twice a day during the campaign. This was supported by the concentrations found at Knuth's Fjeld and near the icebergs which did not differ significantly from the concentration measured around Flyger's Hut. The BC concentrations at Station Nord seem smaller compared to snow concentrations at other Arctic sites. However, the standard deviations are very large.

It was found that five sources best describe the concentrations of air pollution at Station Nord in both periods analysed by PMF (2008-2010 and 2011-2012). Two natural sources, *Soil* and *Marine*, were found in both analyses. As expected no BC was found in the *Soil* source, since BC has no crustal origin. BC was evident in the *Marine* source in both analyses with 17 % of total BC in 2008-2010 and 21 % of total BC in 2011-2012. This could either be explained by increased Arctic shipping or long range transport of air pollutants mixed with sea spray.

In addition to the natural sources, three anthropogenic sources were identified in both analyses. The *Combustion* source consisted of the same species for the two periods, however with a major difference in the abundance of BC, with 57 % of total BC in 2008-2010 compared to only 7 % in 2011-2012. High abundance of BC concentrations is anticipated in the *Combustion* source so the low concentrations observed in 2011-2012, were mainly assigned the poor data set for the period. The high winter and spring concentrations followed by lower concentrations in summer and autumn in the *Combustion* source are consistent with the seasonal cycle of Arctic. The two remaining anthropogenic sources were influenced by metal industries, but determined differently for the two periods. In 2008-2010 the two sources were identified as *Cu/Ni* (9 % of total BC) and *Zn* (17 % of total BC) contrary to *Cu* (9 % of total BC) and *Ni/Cr* (64% of total BC) in 2011-2012. The *Cu/Ni* and *Cu* sources are believed to originate from Eurasia, where especially the Siberian Cu and Ni industry is assumed to contribute to pollution in the Arctic. The abundance of BC in both Cu-sources indicates emissions from combustion sources transported with the same air masses. Based on air mass back trajectories made by Ngyuen et al. (2013) the *Zn* source identified in 2008-2010 is suggested to originate from a major *Zn* mine in Canada. The *Ni/Cr* source is thought to originate from the

mining industry in Russia. The biggest abundance of BC (64 %) was found in this source indicating emissions from combustion sources transported with the same air masses. The differences in the source apportionments between the two analyses could be connected to the large uncertainty of the data from 2011-2012 due to start-up problems with a new analytical method. It could also be caused by changes in metrology in the two time periods. The future recommendation is hence to run a PMF analysis for a longer time period to better determine the sources contributing to BC at station Nord.

BC is an important contributor to climate change through its absorption of solar radiation and through the albedo effect when deposited on snow and ice (AMAP, 2011). It is quite alarming that the average concentrations found on Station Nord during winter are approximately half of the concentrations measured in Danish rural areas and within the same order magnitude as in Danish urban areas (Massling et al., 2011). Since there are almost no emission sources so far north, this indicates that long range transport of BC from source regions outside the Arctic is important. Due to the short lifetime of BC, emission reductions will result in an almost immediate decrease in radiative forcing. Hence BC mitigation strategies through introduction of appropriate technologies and air pollution policies would be a fast way to start limiting the radiative forcing and thus postpone tipping points in the Arctic (Lenton, 2012). It is therefore of great importance to reduce the anthropogenic BC emissions, which would at the same time have positive effects on human health. Improved climate models, transport models and receptor models are necessary to better localise the most significant emission sources and the results obtained in this study will hopefully take us a little step further.

# 7 References


AMAP, 2011, 'The Impact of Black Carbon on Arctic Climate (2011)', By: P.K. Quinn, A. Stohl, A. Arneth, T. Berntsen, J. F. Burkhart, J. Christensen, M. Flanner, K. Kupiainen, H. Lihavainen, M. Shepherd, V. Shevchenko, H. Skov, and V. Vestreng. *Arctic Monitoring and Assessment Programme (AMAP)*, Oslo. 72 pp.

Arctic Council, 2011, 'An Assessment of Emissions and Mitigation Options for Black Carbon', Technical Report of the Arctic Council Task Force on Short-Lived Climate Forcers, accessed November 2012 from: http://www.arctic-council.org/index.php/en/environment-a-climate/climate-change/172-slcf.

Aarhus University, 2013, '*DEHM', Aarhus University*, accessed 3 July 2013 from http://envs.au.dk/videnudveksling/luft/model/dehm/.

Aquarius.NET, 2013, 'Universal Polar Stereographic', accessed August 2013 from: http://www.mgaqua.net/AquaDoc/Projections/Projections_Azimuthal.aspx.

Aufschnaiter, T., 2007, 'DIGITEL High Volume Aerosol Sampler, Manual', *DIGITEL Elektronik GmbH*

Bauer, S. E., Menon, S., Koch, D., Bond, T. C., Tsigaridis, K., 2010, 'A global modeling study on carbonaceous aerosol microphysical characteristics and radiative effects', *Atmospheric Chemistry and Physics,* Vol.10, pp.7439-7456.

Birch, M. E. & Cary, R. A., 1996, 'Elemental Carbon-based method for Occupational Monitoring of Particulate Diesel Exhaust: Methodology and Exposure Issues', *The Analyst,* Vol. 121, issue 9, pp. 1183-1190.

Bond, T.C., Anderson, T.L, Campbell, D., 1999, 'Calibration and Intercomparison of Filter-Based Measurements of Visible Light Absorption by Aerosols', *Aerosol Science and Technology*, 30:6, pp. 582-600.

Bond, T.C, Streets, D.G., Yarber, K.F., Nelson, S.M., Woo, J.H., Klimont, Z., 2004, 'A Technology-based global inventory of black and organic carbon emissions from combustion', *Journal of Geopphysical Research*, Vol. 109, doi:10.1029/2003JD003697.

Bond, T.C., Bergström, R.W., 2006, 'Light absorption by carbonaceous particles, an investigative review', *Aerosol Science and Technology,* Vol. 40, Issue 1, pp.1-41.

Bond, T.C., Doherty, S. J., Fahey, D. W., Forster, P. M., Berntsen, T., DeAngelo, B. J., Flanner, M. G., Ghan, S., Kärcher, B., Koch, D., Kinne, S., Kondo, Y., Quinn, P. K., Sarofim, M. C., Schultz, M. G., Schulz, M., Venkataraman, C.,

Zhang, H., Zhang, S., Bellouin, N., Guttikunda, S. K., Hopke, P. K., Jacobson, M. Z., Kaiser, J. W., Klimont, Z., Lohmann, U., Schwarz, J. P., Shindell, D., Storelvmo, T., Warren, S. G., Zender, C. S., 2013, 'Bounding the role of black carbon in the climate system: A scientific assessment', *Journal of Geophysical Research: Atmospheres*.

Bruner, F., 1993, 'Gas Chromatographic Environmental Analysis', *VCH Publishers*, USA.

Cakmak, S., Dales, R.E., Angelica, R.M., Blanco, V.C., 2011, 'The risk of dying on days of higher air pollution among the socially disadvantaged elderly', *Environmental Research*, Vol. 111, Issue 3, pp. 388-393.

Chakra, O.R.A., Joyeux, M., Nerriere, E., Strub, M.P., Zmirou-Navier, D., 2007, 'Genotoxicity of organic extracts of urban airborne particulate matter: an assessment within a personal exposure study', *Chemosphere*, Vol. 66, pp. 1375-1381.

Chow, J. C., Watson, J. G, Doraiswamy, P., Chen, A. L., Sodeman, D. A., Lowenthal, D. H., Park, K., Arnott, W. P., Motallebi, N., 2009, 'Aerosol light absorption, black carbon, and elemental carbon at the Fresno Supersite, California', *Atmospheric Research*, 93, pp. 874-887.

Christensen, J.H., 1997, 'The Danish Eulerian Hemispheric Model – A Three-Dimensional Model used for the Arctic', *Atmospheric Environment*, vol. 31, no. 24, pp. 4169-4191.

Chýlek, P., Videen, G., Ngo, D., Pinnick, R.G., Klett, J., D., 1995, 'Effect of black carbon on the optical properties and climate forcing of sulphate aerosols', *Journal of Geographical Research*, Vol. 100, No. D8, pp. 16,325-16,332.

Confalonieri, U., B. Menne, R. Akhtar, K.L. Ebi, M. Hauengue, R.S. Kovats, B. Revich and A. Woodward, 2007, 'Human health. Climate Change 2007: Impacts, Adaptation and Vulnerability', Contribution of Working Group II to the Fourth Assessment Report of the Intergovernmental Panel on Climate Change, M.L. Parry, O.F. Canziani, J.P. Palutikof, P.J. van der Linden and C.E. Hanson, Eds., Cambridge University Press, Cambridge, UK, 391-431.

Corbett, J., J., Lack, D.,A., Winebrake, J., J., Harder, S., Silberman, J., A. and Gold, M., 2010, 'Arctic shipping emissions inventories and future scenarios', *Atmospheric Chemistry and Physics*, 10: 9689-9704.

De Kok, T.M., Hogervorst, J.G., Briede, J.J., Van Herwijnen, M.H., Maas, L.M., Moonen, E.J., Driece, H.A., Kleinjans, J.C., 2005, 'Genotoxicity and physicochemical characteristics of traffic-related ambient particulate matter', *Environmental and Molecular Mutagenesis*, Vol. 46, pp. 71-80.

Doherty, S. J., Warren, S. G., Grenfell, T. C., Clarke, A. D., Brandt, R. E., 2010, 'Light-absorbing impurities in Arctic snow', *Atmospheric Chemistry and Physics*, Vol. 10, pp.11647–11680, doi:10.5194/acp-10- 11647-2010.

Fenger, M., Sørensen, L.L., Kristensen, K., Jensen, B., Nguyen, Q.T., Nøjgaard, J.K., Massling, A., Skov, H., Becker, T., Glasius, M., 2013, 'Sources of anions in aerosols in northeast Greenland during late winter', *Atmospheric Chemistry and Physics*, Vol.13, Issue 3, pp.1569-1578.

Forster, P., V. Ramaswamy, P. Artaxo, T. Berntsen, R. Betts, D.W. Fahey, J. Haywood, J. Lean, D.C. Lowe, G. Myhre, J. Nganga, R. Prinn, G. Raga, M. Schulz and R. Van Dorland, 2007, 'Changes in Atmospheric Constituents and in Radiative Forcing'. In: Climate Change 2007: The Physical Science Basis. Contribution of Working Group I to the Fourth Assessment Report of the Intergovernmental Panel on Climate Change [Solomon, S., D. Qin, M. Manning, Z. Chen, M. Marquis, K.B. Averyt, M.Tignor and H.L. Miller (eds.)]. Cambridge University Press, Cambridge, United Kingdom and New York, NY, USA.

Fuglestvedt, J.S., Shine, K.P., Berntsen, T., Cook, J., Lee, D.S., Stenke, A., Skeie, R.B., Velders, G.J.M., Waitz, I.A., 2010, 'Transport impacts on atmosphere and climate: Metrics', *Atmospheric Environment*, Vol. 44, pp. 4648-4677.

Grube, A.G., 2011, 'Particulate air pollution and its characteristic sources in the high Arctic at Station Nord, N.E. Greenland', Master thesis, *University of Copenhagen*, Denmark.

Gupta, I., Slunkhe, A., Kumar, R., 2012, 'Source Apportionment of $PM_{10}$ by Positive Matrix Factorization in Urban Area of Mumbai, India', *The Scientific World Journal*, Vol.2012.

Han, Y. M., Cao, J.J., Lee, S. C., Ho, K. F., and An, Z. S., 2010, 'Different characteristics of char and soot in the atmosphere and their ratio as an indicator for source identification in Xi'an, China', *Atmospheric Chemistry and Physics*, Vol. 10, pp. 595-607.

Halsnæs, K., P. Shukla, D. Ahuja, G. Akumu, R. Beale, J. Edmonds, C. Gollier, A. Grübler, M. Ha Duong, A. Markandya, M. McFarland, E. Nikitina, T. Sugiyama, A. Villavicencio, J. Zou, 2007, 'Framing issues'. In Climate Change 2007: Mitigation. Contribution of Working Group III to the Fourth Assessment Report of the Intergovernmental Panel on Climate Change [B. Metz, O. R. Davidson, P. R. Bosch, R. Dave, L. A. Meyer (eds)], Cambridge University Press, Cambridge, United Kingdom and New York, NY, USA.

Hegg, D.A., Clarke, A.D., Doherty, S.J., Ström, J., 2011, 'Measurements of black carbon aerosol washout ratio on Svalbard', *Tellus*, Vol. 63, Issue 5, pp.891-900.

Heidam, N.Z., Wålin, P., Christensen, J.H., 1999, 'Tropospheric Gases and Aerosols in Northeast Greenland', *Journal of the Atmospheric Sciences*, Vol.56, Issue 2, pp.261-278.

Heidam, N.Z., Christensen, J., Wåhlin, P., Skov, H., 2004, 'Arctic atmospheric contaminants in NE Greenland: levels, variations, origins, transport, transformations and trends 1990 – 2001', *Science of the Total Environment*, vol. 331, pp. 5-28.

IGSD, 2013, 'Primer on Short-Lived Climate Pollutants - Slowing the rate of global warming over the near term by cutting short-lived climate pollutants to complement carbon dioxide reductions for the long term', *Institute for Governance & Sustainable Development*, accessed May 2013 from: http://www.unep.org/ccac/Publications.aspx.

IPCC, 2007, 'Climate Change 2007: Synthesis Report', Contribution of Working Groups I, II and III to the Fourth Assessment Report of the Intergovernmental Panel

on Climate Change [Core Writing Team, Pachauri, R.K and Reisinger, A. (eds.)], IPCC, Geneva, Switzerland, 104 pp.

Ito, K., Mathes, R., Ross, Z., Nádas, A., Thurston, G., Matte, T., 2011, 'Fine particulate matter constituents associated with cardiovascular hospitalizations and mortality in New York City', *Environmental Health Perspectives*, Vol. 119, Issue 4, pp.467-473, doi: 10.1289.ehp.1002667.

Johnson, R.A., 2005, 'Miller & Freund's Probability and Statistics for Engineer', International Edition, 7th Edition, *Pearson Prentice Hall*.

Laden, F., Schwartz, J., Speizer, F.E., Dockery, D.W., 2006, 'Reduction in fine particulate air pollution and mortality: extended follow-up of the Harvard Six Cities study', *American Journal of Respiratory and Critical Care Medicine*, Vol. 173, pp. 667-672.

Law, K.S., Stohl, A., 2007, 'Arctic Air Pollution: Origins and Impacts', *Science*, Vol 315, 1537-1540.

Lenton, T., 2012, 'Arctic Climate Tipping Points', *AMBIO*, Vol. 41, pp.10-22.

Lenton, T., M., Held, H., Kriegler, E., Hall, J.W., Rahmstorf, S., and Schellnhuber, H.J., 2007, 'Tipping elements in the Earth's climate system', *PNAS*, vol. 105, no. 6, 1786-1793.

Massling, A., Nøjgaard, J. K., Ellermann, T., Ketzel, M., Nordstrøm, C., 2011: 'Particle project report 2008 – 2010', *National Environmental Research Institute*, Aarhus University. 62 pp., NERI Technical Report No. 837.

McCarty, J., L., Korontzi, S., Justice, O., C. and Loboda, T., 2009, The spatial and temporal distribution of crop residue burning in the contiguous United States, *Science of the Total Environment* 407 (2009) 5701–5712

Meehl, G.A., T.F. Stocker, W.D. Collins, P. Friedlingstein, A.T. Gaye, J.M. Gregory, A. Kitoh, R. Knutti, J.M. Murphy, A. Noda, S.C.B. Raper, I.G. Watterson, A.J. Weaver and Z.-C. Zhao, 2007, 'Global Climate Projections'. In: Climate Change 2007: The Physical Science Basis. Contribution of Working Group I to the Fourth Assessment Report of the Intergovernmental Panel on Climate Change', [Solomon, S., D. Qin, M. Manning, Z. Chen, M. Marquis, K.B. Averyt, M. Tignor and H.L. Miller (eds.)]. *Cambridge University Press*, Cambridge, United Kingdom and New York, NY, USA.

Mikkelsen, P.S., 2006, 'TWIN OTTER – flyvning og rejser i Grønland', Peter Schmidt Mikkelsen & Aschehoug Dansk Forlag A/S, 1st edn, Viborg, Denmark.

Mordukhovich, I., Wilker, E., Suh, H., Wright, R., Sparrow, D., Vokonas, P.S., Schwartz, J., 2009, 'Black carbon exposure, oxidative stress genes, and blood pressure in a repeated-measures study', *Environmental Health Perspectives*, Vol. 117, Issue 11, pp.1767–1772, doi: 10.1289/ehp.0900591.

Nguyen, Q.T., Skov, H., Sørensen, L. L., Jensen, B. J., Grube, A. G., Massling, A., Glasius, M., Nøjgaard, J. K., 2013, 'Source apportionment of particles at Station Nord, North East Greenland during 2008–2010 using COPREM and PMF analysis', *Atmospheric Chemistry and Physics Discussions*, vol. 12, pp. 24173-24204.

Paatero, P., 1997, 'Least squares formulation of robust non-negative factor analysis', *Chemometrics and Intelligent Laboratory Systems*, Vol.37, pp.23-35.

Perovich, D., Meier, W., Tschudi, M., Gerland, S., Richter-Menge, J., 2012, 'Sea Ice', Arctic Report Card, accessed 13 June 2013 from: http://www.arctic.noaa.gov/reportcard/sea_ice.html.

Petzold, A., Niessner, R., 1995, 'Method Comparison Study on Soot-Selective Techniques', Mikrochim. Acta, Vol. 117, pp. 215-237.

Petzold, A., Kopp, C., Niessner, R., 1997, 'The dependence of the specific attenuation cross-section on black carbon mass fraction and particle size', *Atmospheric Environment*, Vol.31, Issue 5, pp.661-672.

Rasmussen, E.A., Turner, J., Ninomiya, K., Carleton, A.M., 2003, 'Polar Lows Mesoscale Weather Systems in the Polar Regions', *Cambridge University Press*, UK.

Reff., A, Eberly, S.I., Bhave, P.V., 2007, 'Receptor modeling of ambient particulate matter data using positive matrix factorization: Review of existing methods', *Journal of the Air & Waste Management Association*, Vol.57, Issue 2, pp.146-154.

Rose, K.A., 2006, 'Source allocation and visibility impairment in two class I areas with positive matrix factoriztion', *U.S. Environmental Protection Agency.*

RTI, 2009, 'Standard Operating Procedure for the Determination of Carbon Fractions in Particulate Matter Using the IMPROVE_A Heating Protocol on a Sunset Laboratory Dual-Mode Analyzer', *Research Triangle Institute*, North Carolina.

Seinfield, J.H., Pandis, S.N., 2006, 'Atmospheric Chemistry and Physics – From Air Pollution to Climate Change' 2nd edition, *John Wiley & Sons, Inc*.

Sensidyne, 2005, 'Gilian Gilibrator 2 – Calibration system operation & service manual', *Sensidyne Inc.*

Sharma, S., Brook, J.R., Cachier, H., Chow, J., Gaudenzi, A., Lu, G., 2002, 'Light absorption and thermal measurements of black carbon in different regions of Canada', *Journal of Geophysical Research*, Vol. 107, Issue 24, pp.4771.

Shaw, GE, 1995, 'The Arctic Haze Phenomenon', *Bulletin of the meteorological American society*, Alaska accessed May 2013 from: http://journals.ametsoc.org/doi/pdf/10.1175/1520-0477(1995)076%3C2403%3ATAHP%3E2.0.CO%3B2.

Sodemann, H., Pommier, M., Arnold, S.R., Monks, S.A., Stebel, K., Burkhart, J.F., Hair, J.W., Diskin, G.S., Clerbaux, C., Coheur, P.-F., Hurtmans, D., Schlager, H., Blechschmidt, A.-M., Krisjánsson, J.E., and Stohl, A., 2011, 'Episodes of cross-polar transport in the Arctic troposphere during July 2008 as seen from models, satellite, and aircraft observations', *Atmos. Chem. Phys.*, 11, 3631-3651.

Spira-Cohen, A., Chen, L.C., Kendall, M., Lall, R., Thurston, G.D., 2011, 'Personal exposures to traffic-related air pollution and acute respiratory health among

Bronx schoolchildren with asthma', *Environmental Health Perspectives*, Vol. 119, Issue 4, pp. 559-565..

Stroeve, J., Holland, M.M., Meier, W., Scambos, T., Serreze, M., 2007, 'Arctic sea ice decline: Faster than forecast', *Geophysical Research Letters*, Vol. 34, L09501.

Stohl, A., 2006, 'Characteristics of atmospheric transport into the Arctic troposphere', *J. Geophys. Res., 111*, D11306.

Stohl, A., Klimont, S, Eckhardt, S. and Kupiainen, K., 2013, 'Why models struggle to capture Arctic Haze: the underestimated role of gas flaring and domestic combustion emissions', *Manuscript prepared for Atmos. Chem. Phys*.

Suglia, S.F., Gryparis, A., Schwartz, J., Wright, R.J., 2008, 'Association between traffic-related black carbon exposure and lung function among urban women', *Environmental Health Perspectives*, Vol. 116, pp.1333-1337.

Sunset Laboratory, 2009, 'Sample Analysis Method for Organic and Elemental Carbon Aerosols', *Sunset Laboratory,* accessed February 2013 from < http://www.sunlab.com/about/technology.html >

WHO, 2012, 'Health Effects of Black Carbon', By: Janssen, N.AH., Gerlofs-Nijland, M.E., Lanki, T., Salonen, R.O., Cassee, F., Hoek, G., Fischer, P., Brunekreef, B., Krzyzanowski, M., *World Health Organization Regional Office for Europe.*

Weingartner, E., Saathoff, H., Schnaiter, M., Streit, N., Bitnar, B., Baltensperger, U., 2003, 'Absorption of light by soot particles: determination of the absorption coefficient by means of aethalometers', *Aerosol Science*, vol. 34.

Wilker, E.H., Baccarelli, A., Suh, H., Vokonas, P., Wright, R.O., Schwartz, J., 2010, 'Black carbon exposures, blood pressure, and interactions with single nucleotide polymorphisms in microRNA processing genes', *Environmental Health Perspectives*, Vol. 118, Issue 7, pp. 943-948.

UNEP and WMO, 2011, 'Integrated Assessment of Black Carbon and Tropospheric Ozone', *The United Nations Environment Programme and World Meteorological Organization*.

U.S. EPA, 2008, 'EPA Positive Matrix factorization (PMF) 3.0, Fundamentals & User Guide', EPA 600/R-08/108, *U.S. Environmental Protection Agency*, Washington.

U.S. EPA, 2009, 'Integrated Science Assessment for Particulate Matter (Final Report)', *U.S. Environmental Protection Agency*, Washington, DC, EPA/600/R-08/139F.

U.S. EPA, 2012, 'Report to Congress on Black Carbon', U.S. Environmental Protection Agency, EPA-450/R-12-001.

Zhou, J., Ito, K., Lall, R., Lippmann, M., Thurston, G., 2011, 'Time-series analysis of mortality effects of fine particulate matter components in Detroit and Seattle', *Environmental Health Perspectives*, Vol. 119, Issue 4, pp.461-466.

Zhou, S., Wang, Z., Gao, R., Xue, L., Yuan, C., Wang, T., Gao, X., Wang, X., Nie, W., Xu, Z., Zhang, Q., Wang, W., 2012, 'Formation of secondary organic carbon

and long-range transport of carbonaceous aerosols at Mount Heng in South China', *Atmospheric Environment*, 63, pp. 203-212.

# Appendices

**Appendix 1** Snow samples

**Appendix 2** Missing data for OC-EC analyser and PSAP

**Appendix 3** Signals and flow before and after quality control for 2008 and 2010 to 2013

**Appendix 4** Absorptions coefficients after the quality control for 2008 and 2010 to 2013

**Appendix 5** The linear correlation between monthly absorption coefficient and EC concentration for 2008 to 2009 and 2011 to 2013

**Appendix 6** OC and EC data (attached DVD)

**Appendix 7** Snow sample data from April 2013 (attached DVD)

**Appendix 8** PSAP data for 2008 to 2013 (attached DVD)

**Appendix 9** DEHM data for 2008 to 2013 (attached DVD)

**Appendix 10** PMF concentration and uncertainty matrices for 2008 to 2010 and 2011 to 2012 (attached DVD)

# Appendix 1

Overview of the sampling dates, the sampling sizes and the locations on the collected snow samples taken at Station Nord.

| Date | EC-1 [L] | EC-2 [L] | EC-3 [L] | Coordinates N | Coordinates W |
|---|---|---|---|---|---|
| **08-04-2013** | 6+ | 6+ | 6+ | 81˚34.852 | 016˚37.129 |
| **09-04-2013** | 2.75 | 5 | 5.1 | 81˚34.866 | 016˚37.059 |
| **10-04-2013** | 3.7 | 5 | 3.25 | 81˚34.887 | 016˚36.965 |
| **11-04-2013** | 4.5 | 3.7 | 3.9 | 81˚34.904 | 016˚36.977 |
| **12-04-2013** | - | - | - | | |
| **13-04-2013** | - | - | - | | |
| **14-04-2013** | 4.2 | 4.2 | 3 | 81˚34.872 | 016˚37.316 |
| **15-04-2013** | 3.7 | 3.8 | 3.7 | 81˚34.924 | 016˚37.116 |
| **16-04-2013** | 3.5 | 4.5 | 3.6 | 81˚34.863 | 016˚37.379 |
| **17-04-2013** | - | - | - | | |
| **18-04-2013** | 3.2 | 3.4 | 3.4 | 81˚36.416 | 016˚46.776 |
| **19-04-2013** | - | - | - | | |
| **20-04-2013** | 3.9 | 3.9 | 2 | 81˚33.632 | 016˚19.034 |
| **21-04-2013** | 2.2 | 3.6 | 3.9 | 81˚35.728 | 016˚40.593 |

# Appendix 2

The table below presents the time intervals from 2008 to 2013 where no OC-EC data exists.

| Year | Missing measurements (date and hour) | Total [days] |
|---|---|---|
| **2008** | 34, 36, 38, 40, 41, 42, 44, 46, 48, 50, 51, 52 | 12 weeks |
| **2009** | 2, 4, 6, 8, 12, 13, 14, 15, 16, 17, 18, 19, 20, 24, 33, 35, 37, 39, 41, 43, 45, 46, 48, 50, 52 | 25 weeks |
| **2010** | 1, 3, 5, 7, 51, 52 | 6 weeks |
| **2011** | 19, 20, 21, 22, 23, 24, 25, 26, 27, 28, 29, 30, 31, 35, 36, 45, 49 | 17 weeks |
| **2012** | 1, 5, 9, 13, 17, 19, 22 | 7 weeks |
| **2013** | | 0 weeks |

The table below presents the time intervals from 2008 to 2013 where no PSAP data exist.

| Year | Missing measurements [date and hour] | Total [days] |
|---|---|---|
| **2008** | 27/8 at 23:45 – 29/8 at 00:00<br>12/9 at 23:45 – 14/9 at 00:00<br>18/10 at 23:45 – 22/10 at 00:00<br>22/10 at 16:00 – 23/10 at 14:45<br>29/12 at 23:45 – 31/12 at 00:00 | 7 days |
| **2009** | 1/2 at 23:45 – 3/2 at 00:01<br>8/2 at 23:45 – 11/2 at 00:00<br>26/2 at 20:00 – 27/2 at 10:30<br>2/3 at 23:45 – 4/3 at 00:00<br>15/3 at 23:45 – 17/3 at 00:00<br>18/4 at 23:45 – 20/4 at 00:00<br>14/5 at 23:15 – 15/5 at 11:45<br>12/6 at 23:45 – 14/6 at 00:00<br>31/7 at 17:00 – 1/8 at 12:15<br>25/8 at 23:45 – 31/8 at 00:00<br>31/8 at 09:45 – 1/9 at 11:30<br>10/9 at 23:45 – 13/9 at 00:00<br>13/10 at 23:45 – 15/10 at 00:00<br>16/10 at 23:45 – 18/10 at 00:00 | 18.5 days |
| **2010** | 17/3 at 23:45 – 20/3 at 00:00<br>15/4 at 23:45 – 17/4 at 00:00<br>21/4 at 23:45 – 23/4 at 00:00<br>2/5 at 23:45 – 7/5 at 00:00<br>8/5 at 23:45 – 11/5 at 00:00<br>24/5 at 23:45 – 8/6 at 00:00<br>28/11 at 23:45 – 30/11 at 00:00<br>2/12 at 23:45 – 3/12 at 12:00<br>14/12 at 23:45 – 19/12 at 00:00 | 29.5 days |
| **2011** | 7/3 at 23:45 – 9/3 at 00:00<br>10/3 at 23:45 – 13/3 at 00:00<br>28/6 at 23:45 – 30/6 at 00:00 | |

| | | |
|---|---|---|
| | 4/8 at 23:45 – 8/8 at 00:00<br>26/9 at 23:45 – 16/10 at 00:00<br>24/10 at 23:45 – 26/10 at 00:00<br>27/10 at 23:45 – 1/11 at 00:00<br>2/11 at 23:45 – 15/11 at 00:00<br>5/12 at 23:45 – 16/12 at 00:00 | 53 days |
| **2012** | 29/4 at 21.00 – 2/5 at 15.15<br>20/9 at 16.45 – 24/9 at 10.15 | 6 days |
| **2013** | 9/1 at 23:45 – 19/2 at 00:00<br>25/2 at 23:45 – 27/2 at 00:00<br>11/3 at 23:45 – 14/3 at 00:00<br>15/3 at 23:45 – 18/3 at 00:00<br>19/3 at 23:45 – 2/4 at 00:00<br>16/4 at 23:45 – 18/4 at 00:00<br>18/4 at 23:45 – 20/4 at 00:00<br>24/4 at 23:45 – 26/4 at 00:00 | 60 days |

# Appendix 3

The following figures present the signal [V] (black line), the reference signal [V] (grey line) and the flow [ml/min] (dashed line) from 2008, 2009, 2010, 2011 and 2013. For each year two figures illustrate the data before and after the quality control.

**2008 - Before quality control**

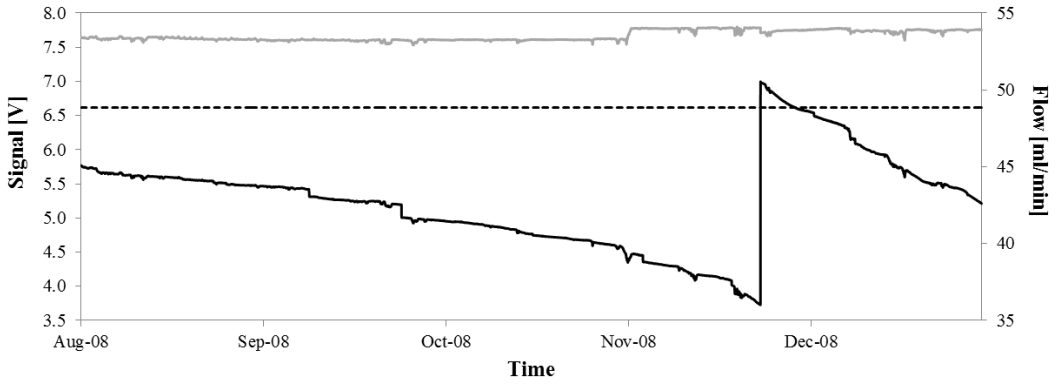


**2008 - After quality control**

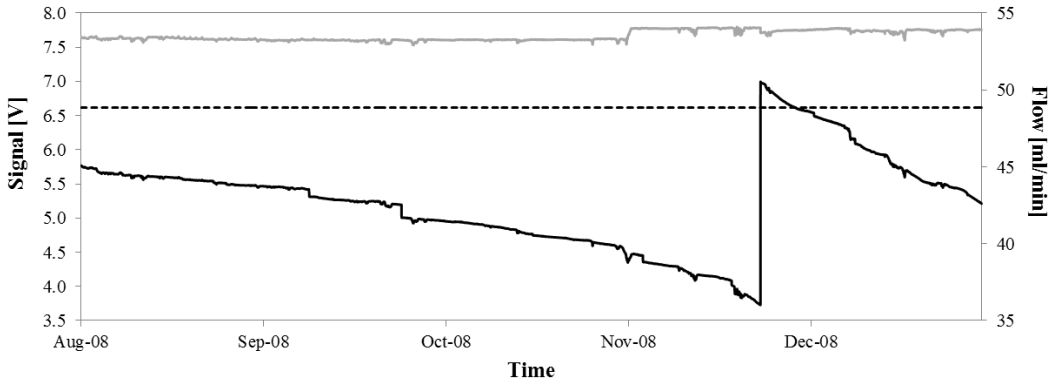

## 2010 - Before quality control

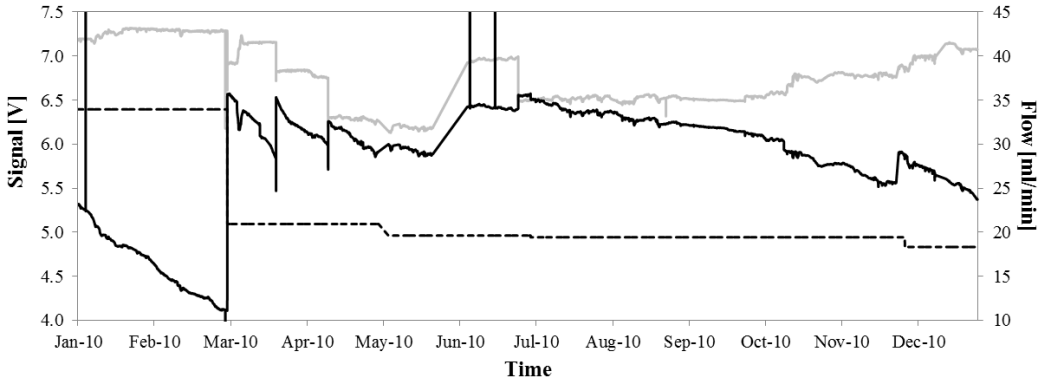


## 2010 - After quality control

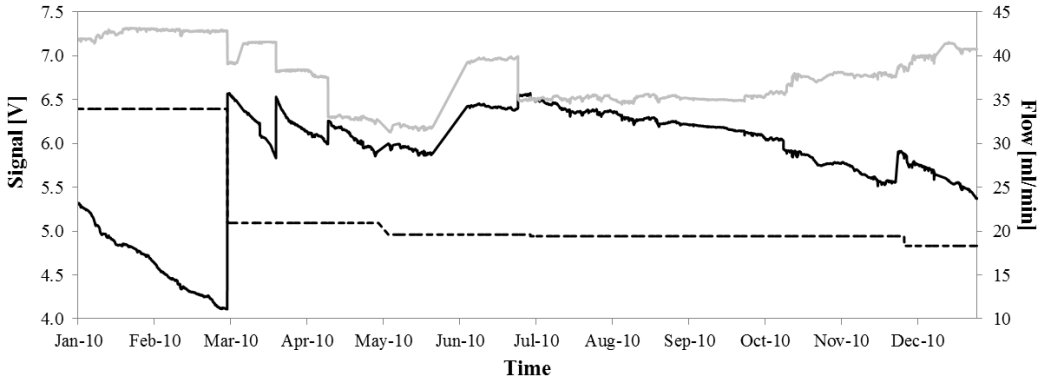


## 2011 - Before quality control

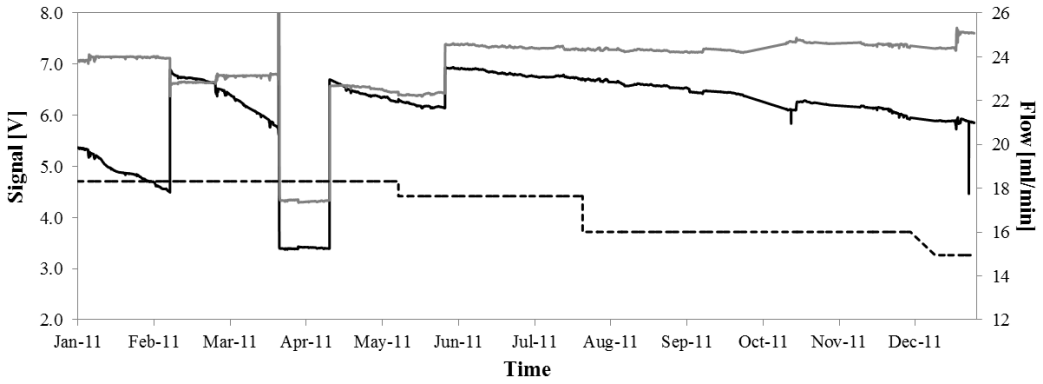

## 2011 - After quality control

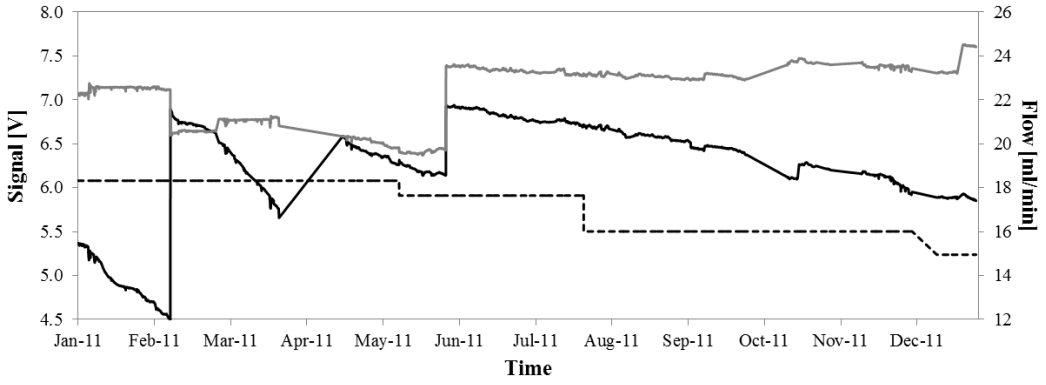


## 2012 - Before quality control

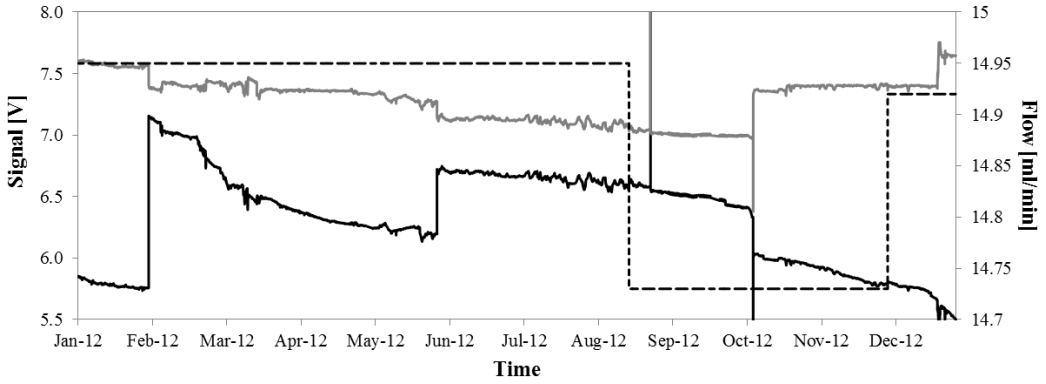


## 2012 - After quality control

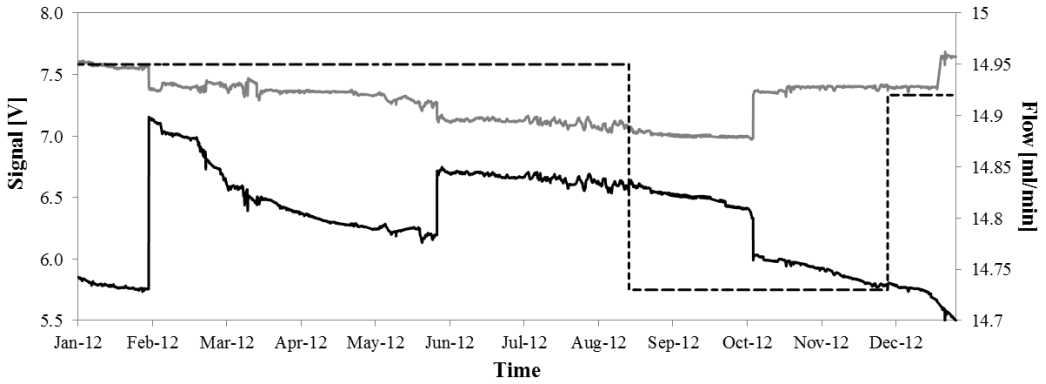

## 2013 - Before quality control

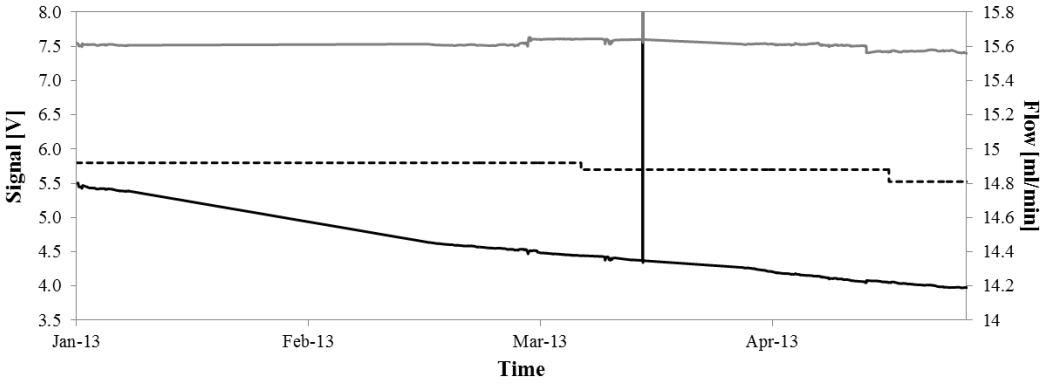


## 2013 - After quality control

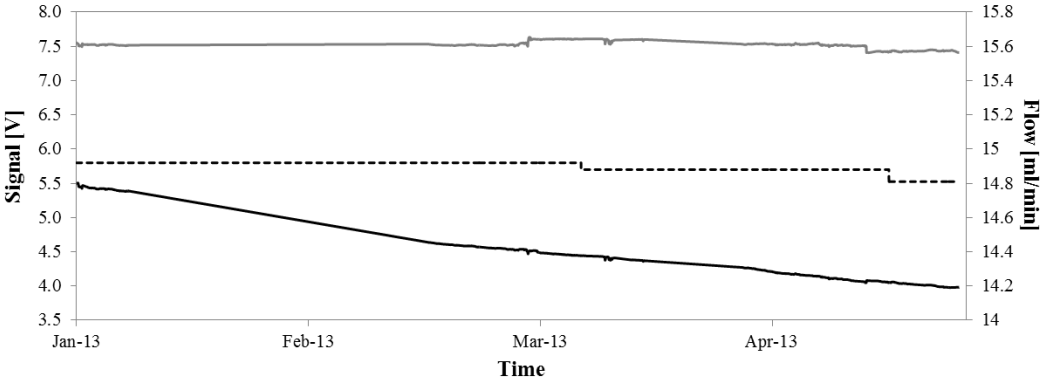

# Appendix 4

The following figures present the absorption coefficient [$\mu m^{-1}$] after the quality control for 2008, 2009, 2010, 2011 and 2013.

**2008**

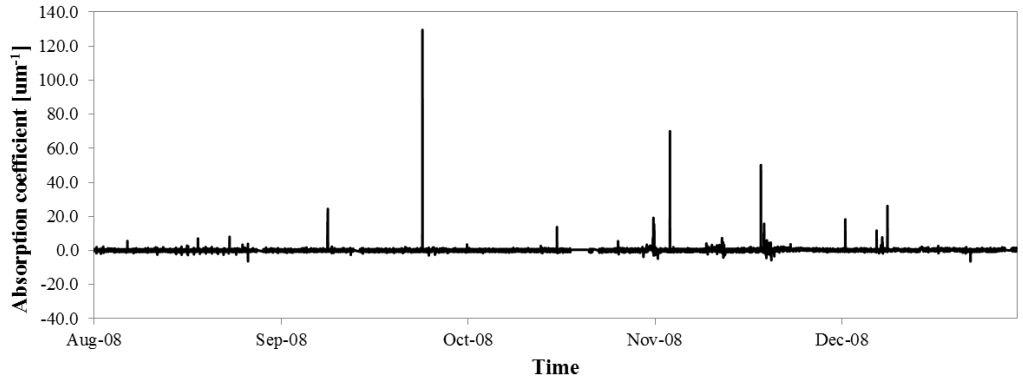


**2010**

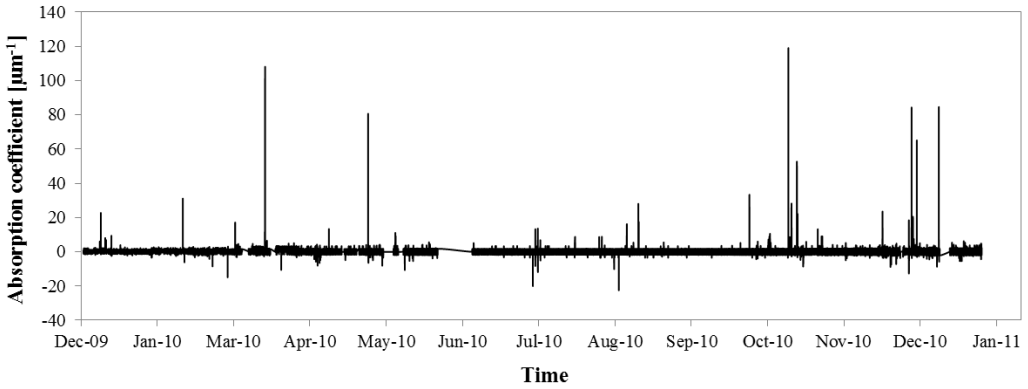

**2011**

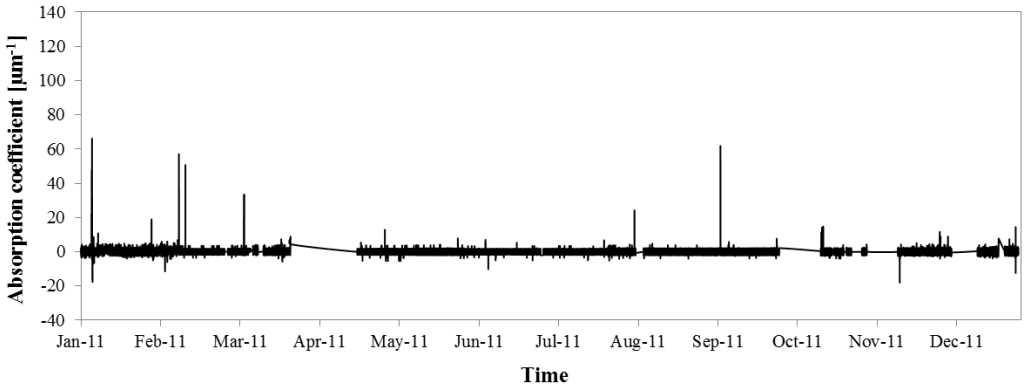


**2012**

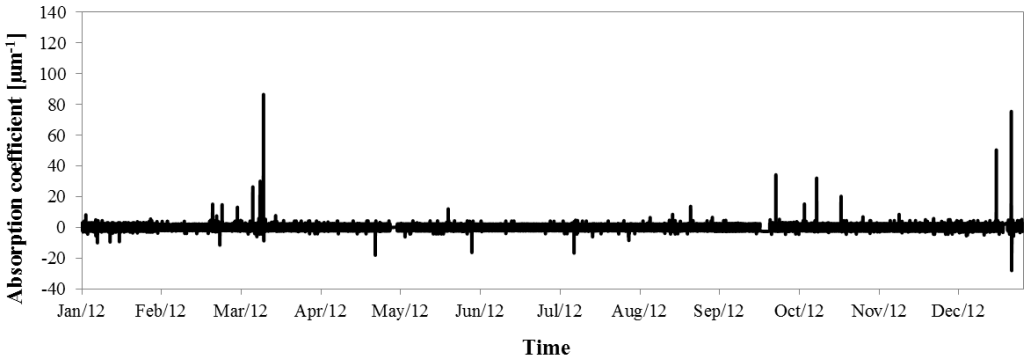


**2013**

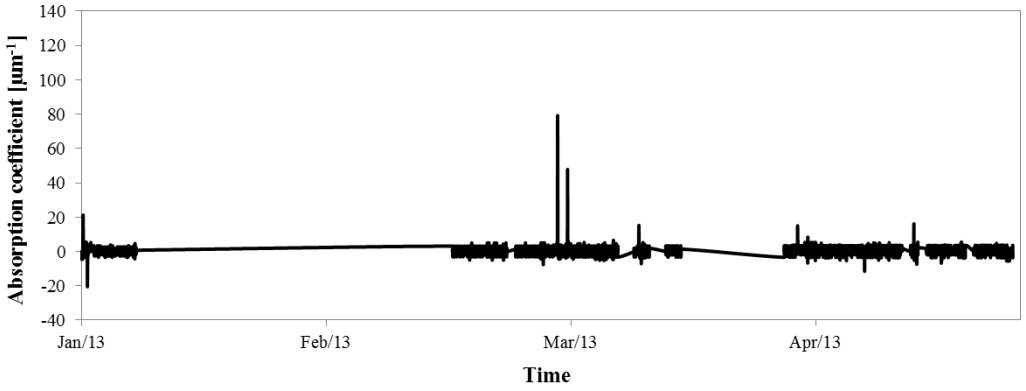

# Appendix 5

The following figures present the monthly absorption coefficient [$m^{-1}$] as a function of the monthly EC concentration [$g/m^3$] for 2009, 2011 and 2012. The correlation and the slope of the linear regression line are illustrated on the figures. No significant linear correlation is found between monthly EC concentrations and monthly absorption coefficients from 2008 and 2011 and hence no specific absorption coefficient is determined. Furthermore no specific absorption coefficient is identified in 2013 due to limited data points.

**2008**

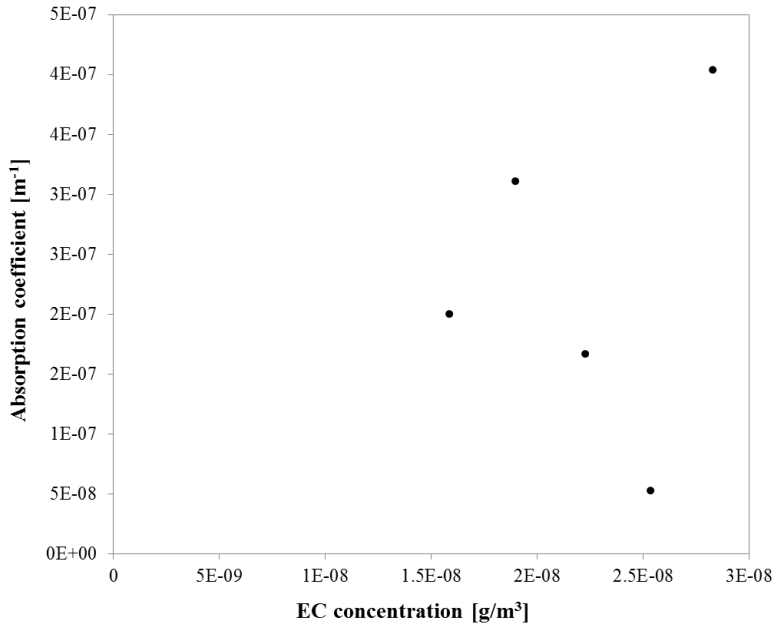

**2009**

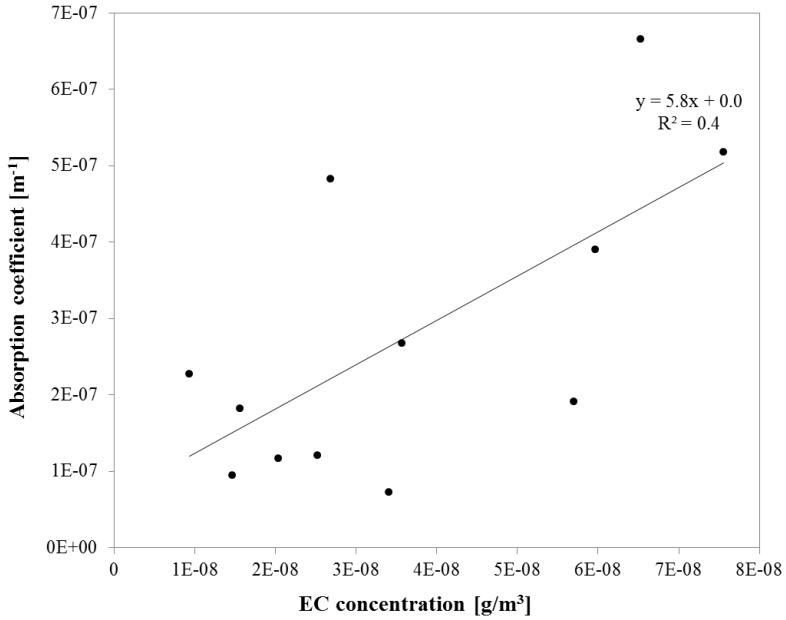
y = 5.8x + 0.0
R² = 0.4
Absorption coefficient [m-1]
EC concentration [g/m3]
7E-07
6E-07
5E-07
4E-07
3E-07
2E-07
1E-07
0E+00
0
1E-08
2E-08
3E-08
4E-08
5E-08
6E-08
7E-08
8E-08

**2011**

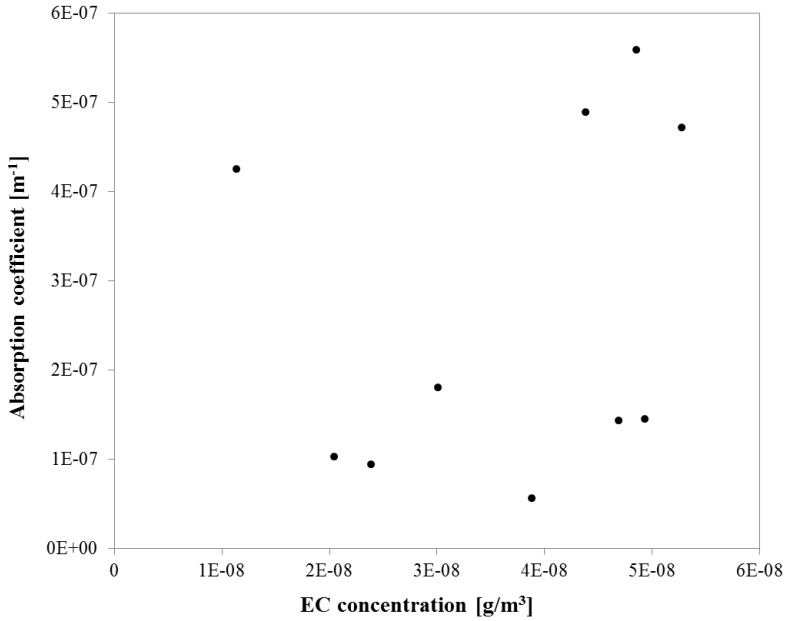
Absorption coefficient [m-1]
EC concentration [g/m3]
6E-07
5E-07
4E-07
3E-07
2E-07
1E-07
0E+00
0
1E-08
2E-08
3E-08
4E-08
5E-08
6E-08

**2012**

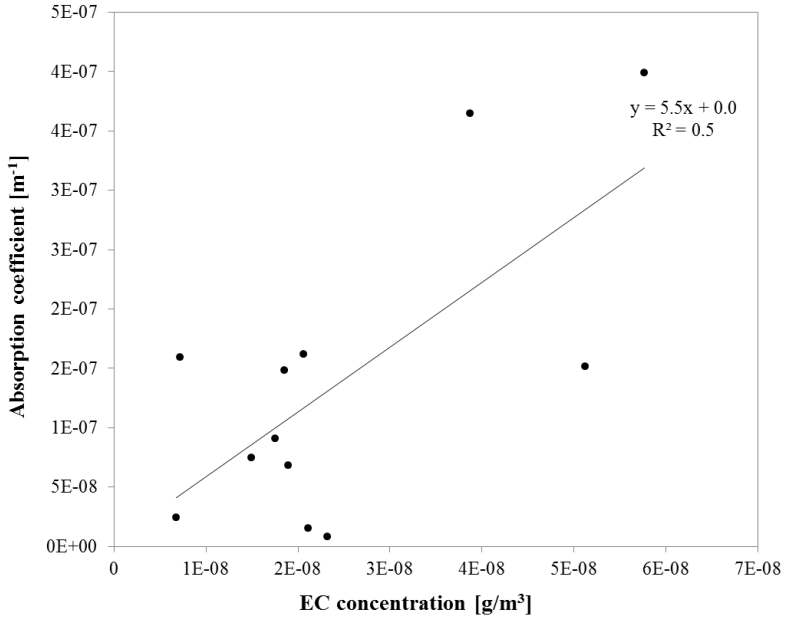
y = 5.5x + 0.0
R² = 0.5
Absorption coefficient [m-1]
EC concentration [g/m3]
5E-07
4E-07
4E-07
3E-07
3E-07
2E-07
2E-07
1E-07
5E-08
0E+00
0
1E-08
2E-08
3E-08
4E-08
5E-08
6E-08
7E-08

**2013**

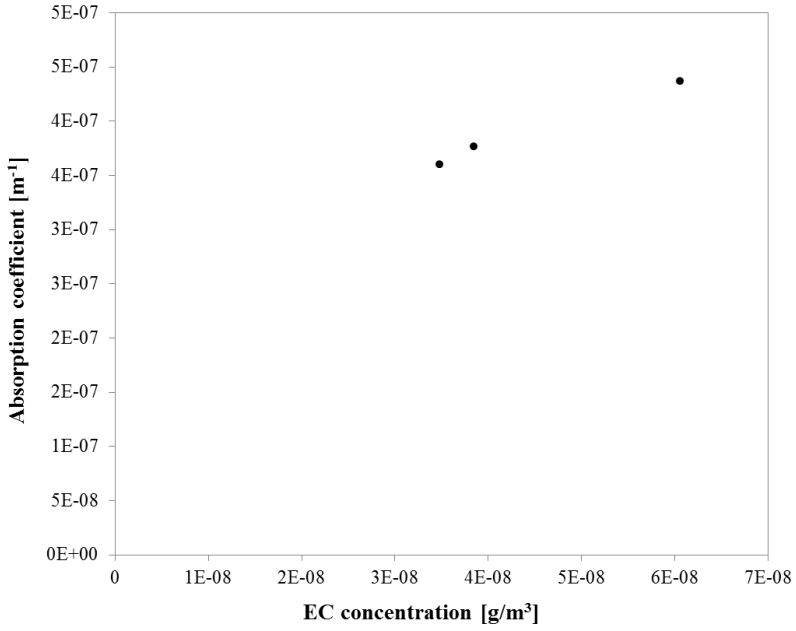
Absorption coefficient [m-1]
EC concentration [g/m3]
5E-07
5E-07
4E-07
4E-07
3E-07
3E-07
2E-07
2E-07
1E-07
5E-08
0E+00
0
1E-08
2E-08
3E-08
4E-08
5E-08
6E-08
7E-08

# Abbreviations

| | |
|---|---|
| **ACTFSLCF** | Arctic Council Task Force on Short-Lived Climate Forcers |
| **AGTP** | Absolute Global Temperature Change Potential |
| **AGWP** | Absolute Global Warming Potential |
| **AMAP** | Arctic Monitoring and Assessment Programme |
| **AU-ENVS** | Aarhus University, Department of Environmental Science |
| **BC** | Black Carbon |
| **BrC** | Brown Carbon |
| **CC** | Carbonate Carbon |
| **COPREM** | Constrained Physical Receptor Model |
| **DEHM** | Danish Eularian Hemispheric Model |
| **EC** | Elemental Carbon |
| **FID** | Flame Ionization Detector |
| **FPS** | Filter Pack Sampler |
| **GAINS** | Greenhouse Gas and Air pollution Interactions and Synergies |
| **GHG** | Green House Gases |
| **GIS** | Greenland Ice Sheet |
| **GTP** | Global Temperature Change Potential |
| **HVS** | High Volume Sampler |
| **IC** | Ion Chromatography |
| **ICP-MS** | Inductively Coupled Plasma Mass Spectrometry |
| **IPCC** | Intergovernmental Panel on Climate Chan |
| **LOSU** | Level of Scientific Understanding |
| **NAO** | North Atlantic Oscillation |
| **OC** | Organic Carbon |
| **PC** | Pyrolytic Carbon |
| **PIXE** | Proton Induced X-ray Emission |
| **PM** | Particulate Matter |
| **$PM_{2.5}$** | Particulate Matter with a diameter < 2.5 μm |
| **$PM_{10}$** | Particulate Matter with a diameter < 10 μm |
| **PMF** | Positive Matrix Factorization |
| **PSAP** | Particle Soot Absorption Photometer |
| **PUF** | Polyurethane Foam |
| **RCP** | Representative Concentration Pathways |
| **RF** | Radiative Forcing |
| **SLCF** | Short-Lived Climate Forcer |
| **WHO** | World Health Organization |